UNIVERSITÉ DE NEUCHÂTEL
FACULTÉ DES SCIENCES

INSTITUT DE GÉOLOGIE
CENTRE D'HYDROGÉOLOGIE

Geochemical modelling of the Soultz-sous-Forêts Hot Dry Rock test site: Coupling fluid-rock interactions to heat and fluid transport

THÈSE

présentée à la Faculté des sciences
de l'Université de Neuchâtel
pour l'obtention du grade de
Docteur ès Science

par

Pierre Durst

Soutenue le 23 mai 2002 devant le jury composé de :

Prof. Pierre Perrochet	Université de Neuchâtel (Suisse)	Directeur
Dr François-David Vuataz	Université de Neuchâtel (Suisse)	Codirecteur
Dr Christian Fouillac	BRGM (France)	Expert
Dr. Bertrand Fritz	CNRS (France)	Expert
Prof. Angelika Kalt	Université de Neuchâtel (Suisse)	Expert
Dr Thomas Kohl	ETH-Zurich	Expert

IMPRIMATUR POUR LA THESE

Geochemical modelling of the Soultz-sous-Forêts Hot Dry Rock test site: Coupling fluid-rock interactions to heat and fluid transport

de M. Pierre Durst

UNIVERSITE DE NEUCHATEL

FACULTE DES SCIENCES

La Faculté des sciences de l'Université de Neuchâtel sur le rapport des membres du jury,

P. Perrochet (directeur de thèse),
F.-D. Vuataz (co-directeur de thèse),
A. Kalt, C. Fouillac (Orléans), T. Kohl (ETH Zürich)
et B. Fritz (Strasbourg)

autorise l'impression de la présente thèse.

Neuchâtel, le 3 juillet 2002

Le doyen:

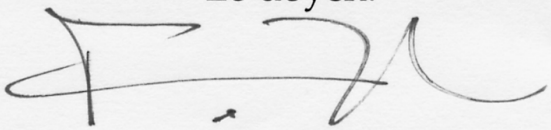

F. Zwahlen

UNIVERSITÉ DE NEUCHÂTEL
FACULTÉ DES SCIENCES

INSTITUT DE GÉOLOGIE
CENTRE D'HYDROGÉOLOGIE

Geochemical modelling of the Soultz-sous-Forêts Hot Dry Rock test site: Coupling fluid-rock interactions to heat and fluid transport

THÈSE

présentée à la Faculté des sciences
de l'Université de Neuchâtel
pour l'obtention du grade de
Docteur ès Science

par

Pierre Durst

Soutenue le 23 mai 2002 devant le jury composé de :

Prof. Pierre Perrochet	Université de Neuchâtel (Suisse)	Directeur
Dr François-David Vuataz	Université de Neuchâtel (Suisse)	Codirecteur
Dr Christian Fouillac	BRGM (France)	Expert
Dr. Bertrand Fritz	CNRS (France)	Expert
Prof. Angelika Kalt	Université de Neuchâtel (Suisse)	Expert
Dr Thomas Kohl	ETH-Zurich	Expert

Abstract

This Ph.D. thesis describes the work performed at the Centre of Hydrogeology of Neuchatel (CHYN) during a project funded by the Swiss Federal Office for Education and Science (no. 98.0008-3 and 00-0453). It represents one of the contributions of the Swiss HDR R&D group to the European Concerted Action for the support of the Hot Dry Rock Geothermal Energy R&D activities 1998-2001 (EC Contract no. JOR3-CT98-0313), located at Soultz-sous-Forêts, Alsace, France. The study carried out at the CHYN was mainly directed towards the geochemical modelling of the Soultz formation brine and the simulation of a future fractured reservoir exploitation. Within the Soultz HDR programme, the main goal of this project is to create a simulation module capable to define and forecast the geochemical evolution of hypersaline fluids flowing in a fissured hot granite. When the future geothermal stimulated reservoir will be built and exploited, it will be necessary to forecast the effects of enhanced flows on the fractures under production/re-injection process. It was decided to create this geochemical module on the basis of an existing code (Chem-TOUGH2), which could be later coupled to the finite element code FRACTure in collaboration with the ETH-Zurich.

The first task of the geochemical modelling was to characterise the state of the fluid-rock system and to determine which are the possible chemical evolutions. The system considered is formed by all mineral phases in contact with the fluid and the most relevant aqueous species. Due to the very high salinity of the Soultz fluid, the activity coefficients have to be calculated by the Pitzer equations. Using the code TEQUIL, a model to calculate the activity coefficient was built for 18 aqueous species at temperatures between 50 and 200°C. Then, the thermodynamic model could be used to estimate the maximum potential for mineral precipitation and/or dissolution, when the fluid is cooled in the heat exchanger from 165 to 65°C, and then injected back into the reservoir: carbonate dissolution appears to be more important than quartz and pyrite precipitation.

After thermodynamics, the next step in water-rock interaction modelling is to determine what really happens. The complete modelling of the reaction rates requires the knowledge of many parameters which are not always available, especially for hot brines. Consequently, the method chosen had to be simplified and was built on one kinetic law for each dissolution or precipitation reaction of the four main minerals considered (calcite, dolomite, quartz and pyrite). The results support those of the thermodynamic modelling, namely that calcite and dolomite dissolution will still be the major process and that quartz and pyrite precipitation will only be a secondary phenomenon.

To develop a geochemical module capable to simulate fluid-rock reactions in the Soultz fractured reservoir, the reactive transport code Chem-TOUGH2 was adapted to the very high salinity fluid. Geochemical subroutines were set up and implemented into Chem-TOUGH2 and tested on a simple case. Then, the geochemical module was extracted and coupled with FRACTure using a sequential non-iterative approach. The new code called FRACHEM calculates thermal-hydraulic processes, chemical reactions, advective transport of the chemical species and variation of porosity and permeability.

The first application of the new code FRACHEM consisted of a 2-D simplified reservoir model, with water injected at 65°C into a single fracture included into a rock matrix initially at a temperature of 165°C during a period of 6.4 years. The results show that at the beginning, calcite and dolomite are rapidly dissolved near the injection point. Then, re-heating induces carbonates precipitation on a wider zone. Finally, permeability evolution mainly shows a high increase near the injection point, due to carbonates dissolution, whereas a small permeability decrease is observed later, due to calcite re-precipitation. In a second application representing the evolution of a model with a similar size to the upper Soultz reservoir, the fluid flowed through two pathways, a direct narrow fracture and a wider but longer one. The results show a 350 % increase of the permeability at the injection point like the previous simulation. The subsequent decrease can reach 60 % if all the re-precipitation is concentrated in the two fractures but should probably not affect significantly the properties of the whole reservoir.

Kurzfassung

Die vorliegende Dissertation wurde am Zentrum für Hydrogeologie der Universität Neuenburg (CHYN) durchgeführt und vom Schweizer Bundesamt für Bildung und Wissenschaft gefördert (BBW Nr. 98.0008-3 und 00-0453). Die Arbeit ist einer der Beiträge der Schweizer Hot Dry Rock (HDR) Gruppe zur Europäischen Konzertierten Aktion zur Förderung der Forschungs- und Entwicklungsaktivitäten zum Thema „Hot Dry Rock Geothermische Energie“ im Zeitraum von 1998 bis 2001 in Soultz-sous-Forêts, Elsass (Frankreich). Die am CHYN durchgeführten Studien zielten hauptsächlich auf eine geochemische Modellierung der salinen Formationswässer in Soultz, sowie auf eine Simulation der Erschließung des zukünftigen geklüfteten Speicherraumes. Innerhalb des Soultz HDR Programmes ist das Hauptziel dieses Projekts die Erstellung eines Simulationsmoduls, welches in der Lage ist, die geochemische Entwicklung hypersaliner Fluide in geklüfteten heißen Graniten zu beschreiben und vorherzusagen. Wenn das zukünftige stimulierte geothermische Reservoir aufgebaut und erschlossen wird, wird es notwendig sein, die Auswirkungen der erhöhten Kluftströmung unter den Bedingungen der Produktion und Reinjektion vorherzusagen. Es wurde beschlossen, dieses geochemische Modul auf der Grundlage eines existierenden Codes (Chem-TOUGH2) zu erstellen und dieses Modul dann in Zusammenarbeit mit der ETH Zürich mit dem Finite Elemente Code FRACTure zu koppeln.

Das erste Ziel der geochemischen Modellierung war die Zustandsbeschreibung des Fluid-Gesteins-Systems und die Bestimmung seiner möglichen chemischen Entwicklung. Das betrachtete System besteht aus den Mineralphasen in Kontakt mit dem Fluid und den wichtigsten darin enthaltenen wässrigen Spezies. Aufgrund der sehr hoch Salinität des Fluids in Soultz mussten die Aktivitätskoeffizienten mit den PITZER-Gleichungen berechnet werden. Mit Hilfe des Programmcodes TEQUIL wurde ein Modell zur Berechnung der Aktivitätskoeffizienten von 18 wässrigen Spezies bei Temperaturen zwischen 50 und 200°C erstellt. Auf dieser Grundlage konnte das thermodynamische Modell dazu verwendet werden, das maximale Potential zur Mineralausfällung und/oder -lösung abzuschätzen, wenn das Fluid im Wärmetauscher von 165 auf 65°C abgekühlt wird und anschließend zurück ins Reservoir injiziert wird: Carbonat-Lösung scheint bedeutender zu sein, als Quartz- und Pyrit-Ausfällung.

Nach der thermodynamischen Modellierung ist der nächste Schritt zum Verständnis der Wasser-Gesteins-Wechselwirkung, zu untersuchen was tatsächlich passiert. Die vollständige kinetische Modellierung der Reaktionsraten erfordert die Kenntnis zahlreicher Parameter, die nicht immer zur Verfügung stehen, insbesondere nicht für heiße Solen. Die gewählte Methode wurde daher vereinfacht und berücksichtigt jeweils nur ein kinetisches Gesetzt für jede Lösungs- oder Fällungsreaktion der vier wesentlichen betrachteten Minerale: Calcit, Dolomit, Quartz und Pyrit. Die Ergebnisse sind mit denjenigen der thermodynamischen Modellierung konsistent; insbesondere ist auch hier die Calcit- und Dolomitlösung der wesentliche Prozess, während Quartz- und Pyritausfällung sekundäre Phänomene sind.

Um ein geochemisches Modul zu entwickeln, welches in der Lage ist, die Fluid-Gesteins-Reaktionen im geklüfteten Speicherraum von Soultz zu simulieren, wurde der Code Chem-TOUGH2 für den reaktiven Stofftransport an die Bedingungen des sehr hoch salinen Fluids angepasst. Geochemische Subroutines wurden aufgestellt, in Chem-TOUGH2 implementiert und an einem einfachen Fall getestet. Anschließend wurde das geochemische Modul extrahiert und mit Hilfe eines sequentiellen, nicht iterativen Ansatzes mit FRACTure gekoppelt. Der neue Code namens FRACHEM berechnet thermo-hydraulische Prozessse, chemische Reaktionen, advektiven Transport der chemischen Spezies und Variationen der Porosität und Permeabilität.

Die erste Anwendung des neuen FRACHEM Code bestand aus einem vereinfachten 2-D Reservoirmodell, wobei Wasser bei 65°C über einen Zeitraum von 6,4 Jahren in eine Einzelkluft injiziert wurde, die von einer Gesteinsmatrix mit einer Anfangstemperatur von 165°C umgeben war. Die Ergebnisse zeigen, dass zu Beginn Calcit und Dolomit in der Nähe des Injektionspunkts schnell gelöst werden. Anschließend induziert die Wiedererwärmung Carbonatausfällung in einem weiteren Bereich. Schließlich zeigt die Entwicklung der Permeabilität eine starke Zunahme durch Calcitlösung im Bereich des Injektionspunktes, während später eine geringe Abnahme aufgrund der Wiederausfällung von Calcit zu beobachten ist. In einer zweiten Anwendung, welche die Entwicklung eines Modells mit ähnlicher Größe wie das obere Soultz-Reservoir repräsentiert, strömt das Fluid durch zwei Fließwege: eine direkte aber enge Kluft und eine längere, weiter geöffnete. Die Ergebnisse zeigen eine Zunahme der Permeabilität um 350 % am Injektionspunkt, ähnlich der vorherigen Simulation. Die nachfolgende Abnahme kann bis zu 60 % betragen, wenn die gesamte Wiederausfällung auf die zwei Klüfte beschränkt ist, beeinträchtigt aber wahrscheinlich nicht nennenswert die Eigenschaften des gesamten Reservoirs.

Résumé

Cette thèse de doctorat décrit le travail effectué au Centre d'Hydrogéologie de Neuchâtel (CHYN) au cours d'un projet financé par l'Office Fédéral Suisse pour l'Éducation et la Science (OFES no. 98.0008-3 et 00-0453). Cela constitue la contribution du groupe suisse de R&D sur le Hot Dry Rock à l'Action Concertée Européenne pour le soutien à l'activité de R&D sur l'énergie géothermique Hot Dry Rock, 1998-2001 (Contrat CE no. JOR3-CT98-0313), située à Soultz-sous-Forêts, Alsace (France). L'étude réalisée au CHYN a été axée principalement sur la modélisation géochimique de la saumure de formation de Soultz et sur la simulation de la future exploitation du réservoir fracturé. Le but premier de ce projet, au sein du programme HDR de Soultz, est de créer un module de simulation capable de définir et de prévoir l'évolution géochimique des fluides hyper salés circulant dans un granite chaud et fracturé. Lorsque le futur réservoir géothermique stimulé sera créé et exploité, il sera nécessaire de prévoir les effets sur les fractures des circulations forcées par le processus de production/réinjection. Il a été décidé de créer ce module géochimique sur la base d'un code existant (Chem-TOUGH2) pouvant par la suite être couplé avec le code en élément finis FRACTure en collaboration avec l'ETH-Zurich.

La première étape de la modélisation géochimique a consisté à caractériser l'état du système fluide-roche et à déterminer les évolutions chimiques possibles. Le système considéré est constitué par l'ensemble des phases minérales en contact avec le fluide et par les espèces aqueuses les plus significatives. La très forte salinité du fluide de Soultz (100 g/l) impose l'usage des équations de Pitzer pour le calcul des coefficients d'activité. À l'aide du code TEQUIL et d'hypothèses raisonnables, un modèle capable de calculer les coefficients d'activité de 18 espèces aqueuses a été construit pour des températures entre 50 et 200°C. Le modèle thermodynamique a alors pu être utilisé pour estimer les maxima potentiels de précipitation ou de dissolution lorsque le fluide refroidi de 165°C à 65°C dans l'échangeur de chaleur est réinjecté dans le réservoir: la dissolution des carbonates apparaît quantitativement plus importante que la précipitation de quartz ou de pyrite.

L'état thermodynamique caractérisé, l'étape suivante dans la modélisation des interactions eau-roche est de déterminer ce qui se passe effectivement. La modélisation cinétique complète des vitesses de réaction requiert la connaissance de nombreux paramètres qui ne sont pas tous disponibles, en particulier pour les saumures chaudes. En conséquence, la méthode retenue a dû être simplifiée et est basée sur une loi cinétique pour chaque réaction de dissolution et de précipitation des quatre minéraux considérés (calcite, dolomite, quartz et pyrite). Les résultats sont en accord avec la modélisation thermodynamique, à savoir que la dissolution de calcite et de dolomite devrait être le phénomène majeur, les précipitations de quartz et de pyrite restant secondaires.

Afin de développer un module géochimique à même de simuler les interactions fluide-roche dans le réservoir fracturé de Soultz, le code de transport réactif Chem-TOUGH2 a été adapté à la très haute salinité du fluide. Des sous-routines géochimiques ont été élaborées et implantées dans Chem-TOUGH2 puis testées sur un cas simple. Le module géochimique a alors été extrait et couplé avec FRACTure selon une approche séquentielle non-iterative. Le nouveau code baptisé FRACHEM peut calculer les processus thermo-hydrauliques, les réactions chimiques, le transport advectif des espèces chimiques ainsi que les variations de porosité et de perméabilité.

La première application du nouveau code FRACHEM a consisté en un modèle 2-D simplifié du réservoir, avec de l'eau injectée à 65°C dans une fracture incluse dans une matrice rocheuse initialement à 165°C pendant 6.4 années. Les résultats montrent qu'au début, les carbonates sont rapidement dissous autour du point d'injection. Le réchauffement induit alors la reprécipitation de la calcite sur une zone plus étendue. Finalement, l'évolution de la perméabilité montre surtout une forte augmentation autour du point d'injection, suivie d'une légère diminution plus loin dans la fracture. Dans une seconde application représentant l'évolution d'un modèle de taille similaire au réservoir supérieur de Soultz, le fluide a circulé suivant deux cheminements, une fracture étroite directe et seconde plus large mais plus longue. Les résultats montrent une augmentation de la perméabilité de 350% au point d'injection comme dans la précédente simulation. La diminution consécutive peut atteindre 60% lorsque toute la reprécipitation est concentrée dans les deux fractures, mais elle ne devrait probablement pas affecter de façon significative les propriétés de l'ensemble du réservoir.

Table of contents

Abstract ... 3
Kurzfassung ... 4
Résumé ... 5
List of Tables ... 8
List of Figures ... 9
Acknowledgements ... 12
1. Introduction
1.1 Hot Dry Rock Research in Switzerland ... 13
1.2 Geothermal energy and Hot Dry Rock technology ... 13
1.3 Directions and goals of the study ... 14
2. Soultz-sous-Forêts Hot Dry Rock test site
2.1 Geological situation of the Soultz project ... 17
2.2 Presentation of the Soultz HDR project ... 18
2.2 Fluid flow in the Rhine graben and in the Soultz reservoir ... 22
2.3 Mineralogical conditions ... 25
2.4 Fluid geochemistry ... 27
2.5 Synthesis ... 38
3. Thermodynamic modelling
3.1 Basis of the thermodynamic modelling ... 39
3.2 Determination of the activity coefficient ... 42
3.3 Modelling of the formation brine ... 46
3.4 Synthesis ... 51
4. Kinetic modelling
4.1 Introduction to water-rock interaction kinetics ... 53
4.2 Calcite ... 55
4.3 Dolomite ... 59
4.4 Quartz ... 62
4.5 Pyrite ... 64
4.6 Effect of dissolution/precipitation processes on the permeability ... 66
4.7 Synthesis ... 70

5. Development of the geochemical module into Chem-TOUGH2

5.1 Presentation of Chem-TOUGH2 code 71

5.2 Implementation of the geochemical model in Chem-TOUGH2 72

5.3 Application of the model to a 1-D fracture 75

5.4 Synthesis 81

6. Building of the coupled code: FRACHEM

6.1 Presentation of FRACTure and coupling strategy 83

6.2 Extraction of the geochemical module for coupling with FRACTure 84

6.3 Synthesis 87

7. Coupled simulation with FRACHEM

7.1 Single fracture model 89

7.2 Two fractures model 96

7.3 Sensitivity and critical parameters 100

7.4 Synthesis 100

8. General discussion, conclusions and recommendations

8.1 General discussion 103

8.2 Conclusions 105

8.3 Recommendations 107

9. References 109

Annexes

List of symbols 117

FRACHEM user's manual 121

Thermodynamic data 127

List of Tables

Table 2.4.1 Simplified qualitative mineralogy of the different facies of the granitic basement at Soultz. 27

Table 2.5.1 Chemical fluid composition in the granite of Soultz fluid. Analyses previous to the 1997 circulation test. 28

Table 2.5.2 Chemical composition of deep fluids in the Buntsandstein of the Rhine Graben..... 29

Table 2.5.3 Compilation of chemical data from five Hot Dry Rock reservoirs. 29

Table 2.5.4 Fluid composition used in modelling. All concentrations are in mmol/l. 36

Table 2.5.5 Fluid composition of the sample KP3-600 analysed by the BRGM and the CGS. All concentrations are in mmol/l. 37

Table 2.5.6 Chemical composition of the fluid from the new reservoir (5000 m). All concentrations are in mmol/l..... 37

Table 3.3.1 Basic data for the modelling of the brine. 47

Table 3.3.2 Composition of the modelled fluid..... 47

Table 3.3.3 Activity coefficients of aqueous species and H_2O activity calculated using TEQUIL. 48

Table 3.3.4 Activity coefficients of HS^-. 48

Table 3.3.5 Coefficients of the equation $\gamma_i = B_0 + B_1.T + B_2.T^2 + B_3.T^3 + B_4.T^4$ 50

Table 4.7.1 Dissolution – precipitation reactions during the cooling – re-heating processes of the fluid circulation in the deep Soultz reservoir. 70

Table 5.3.1 Values of the physical parameters considered for the simulation. 75

Table 7.1.1 Values of the thermal-hydraulic parameters selected for the simulation. 89

Table 7.1.2 Thermal-hydraulic parameters 97

Table 8.1.1 Differences between the Chem-TOUGH2 and FRACHEM codes. 104

List of Figures

Figure 1.3.1 Main steps of the model development. 15
Figure 2.1.1 a) Location of the European HDR research site. b) Borehole network..... 17
Figure 2.1.2 Simplified cross section through the Rhine Graben..... 18
Figure 2.2.1 Conceptual geothermal pilot plant at Soultz. 19
Figure 2.2.2 Circulation experiment between the two deep wells GPK1 and GPK2 at the HDR test site in Soultz in 1997..... 21
Figure 2.3.1 Schematic flow field including the granitic basement. 22
Figure 2.3.2 Temperature logs from the HDR Site in Soultz-sous-Forêts. 23
Figure 2.3.3 E-W profile of the temperature and fluid flow field. 24
Figure 2.4.1: Conceptual model of granitic intrusion in GPK-2. 25
Figure 2.4.2 Characterisation of hydrothermally altered and fractured zones. 26
Figure 2.5.1 Location map of the sampled wells..... 28
Figure 2.5.2 Evolution of the pH of the fluid sampled during the 1997 circulation test..... 30
Figure 2.5.3 Evolution of the Eh of the fluid sampled during the 1997 circulation test..... 31
Figure 2.5.4 Evolution of the dissolved O_2 content of the fluid sampled during the 1997 circulation test..... 31
Figure 2.5.5 Evolution of the conductivity of the fluid sampled during the 1997 circulation test..... 32
Figure 2.5.6 Evolution of the alkalinity of the fluid sampled during the 1997 circulation test..... 32
Figure 2.5.7 Evolution of the chloride concentration in the fluid sampled during the 1997 circulation test..... 33
Figure 2.5.8 Evolution of the sodium concentration in the fluid sampled during the 1997 circulation test..... 33
Figure 2.5.9 Evolution of the potassium concentration in the fluid sampled during the 1997 circulation test..... 34
Figure 2.5.10 Evolution of the calcium concentration in the fluid sampled during the 1997 circulation test..... 34
Figure 2.5.11 Evolution of the magnesium concentration in the fluid sampled during the 1997 circulation test..... 35
Figure 2.5.12 Evolution of the sulphate concentration in the fluid sampled during the 1997 circulation test..... 35
Figure 2.5.13 Evolution of the silica concentration in the fluid sampled during the 1997 circulation test..... 36
Figure 3.2.1. Comparison between saturation indexes (S.I.) calculated with Debye-Huckel (D-H) and Pitzer formalism at three different temperatures..... 45
Figure 3.3.1 Density of the Soulz brine in function of temperature at 40 MPa and along vapour saturation pressure curv. 46

Figure 3.3.2 Schema of the activity coefficient model construction. 49
Figure 4.1.1 Diagram of the two processes controlling the reaction rate. 53
Figure 4.1.2 Schematic representation of the Gibbs free energy change associated with the hydrolysis of a mineral..... 54
Figure 4.2.1 Calcite dissolution rate at 25 and 48 °C in function of H^+ activity from Sjöberg and Rickard (1984)..... 56
Figure 4.2.1 Activation energy evolution in function of pH. 57
Figure 4.2.1 Calcite precipitation rate at 100 °C in function over saturation. 58
Figure 4.3.1 Dissolution rate of dolomite in function of pH at 25, 50 and 80 °C. 59
Figure 4.3.2 Evolution of dolomite dissolution rate in function of inverse temperature. 60
Figure 4.3.3 Dolomite dissolution rate in function of saturation at pH=5 at 65 and 165 °C. 60
Figure 4.3.4 Dolomite precipitation in function of saturation at 65 and 165 °C. 61
Figure 4.4.1 Evolution of quartz dissolution rate in function of pH at 65°C, far from equilibrium. 62
Figure 4.4.2 Evolution of quartz dissolution rate in function of temperature at pH=4.8, far from equilibrium. 63
Figure 4.4.3 Quartz precipitation rate in Soultz fluid from 65 to 165°C. 63
Figure 4.5.1 Pyrite dissolution rate at 65 and 165 °C. 64
Figure 4.5.2 Pyrite precipitation rate in initial Soultz fluid in function of temperature. 66
Figure 4.6.1 Schema of two basic porosity/permeability models. 67
Figure 4.6.2 Evolution of permeability and surface area in function of porosity for the two basic models. 69
Figure 5.2.1 Flow chart of Chem-TOUGH2 with the modifications introduced in this study in italic. 74
Figure 5.3.1 Simulation geometry. 75
Figure 5.3.2 Fluid temperature in function of distance from injection point. 76
Figure 5.3.3 Saturation indexes of the fluid at the beginning of the simulation. 76
Figure 5.3.4 pH evolution with the time in function of the distance from injection point. 77
Figure 5.3.5 Calcite reaction rate in function of the distance from injection point 78
Figure 5.3.6 Dolomite reaction rate in function of the distance from injection point. 78
Figure 5.3.7 Quartz reaction rate in function of the distance from injection point. 79
Figure 5.3.8 Pyrite reaction rate in function of the distance from injection point. 80
Figure 5.3.9 Porosity and permeability in function of the distance from injection 78point in the first 200 m. 80
Figure 5.3.10 Porosity and permeability in the first 10 m function of the elapsed time. 81
Figure 6.2.1 Flowchart of the coupling between FRACTURE and the geochemical module. 86

Figure 7.1.1 Simulation geometry. 89
Figure 7.1.2 Temperature evolution in function of the distance from injection point..... 90
Figure 7.1.3 pH evolution in function of the distance from injection point 91
Figure 7.1.4 Calcite reaction rate in function of the distance from injection point..... 91
Figure 7.1.5 Calcium concentration in function of the distance from injection point..... 92
Figure 7.1.6 Dolomite reaction rate in function of the distance from injection point 93
Figure 7.1.7 Magnesium concentration in function of the distance from injection point. 93
Figure 7.1.8 Quartz reaction rate in function of the distance from injection point. 94
Figure 7.1.9 Pyrite reaction rate in function of the distance from injection point..... 95
Figure 7.1.10 Porosity in function of the distance from injection point..... 95
Figure 7.2.10 Model geometry. 96
Figure 7.2.11 Model discretisation. at different scale. 97
Figure 7.2.12 Calcium and Magnesium evolution in the produced fluid. 98
Figure 7.2.13 Evolution of the porosity in the fractures during the first 12 years..... 99
Figure 8.2.1 Potential reactions during the reservoir exploitation. 106

Acknowledgements

This research project has been entirely financed by the Swiss Federal Office for Education and Science (OFES – BBW). I am willing to thank P. Berlincourt of the OFES for his constant and positive support to this project. I am also willing to thank the Centre of Hydrogeology of Neuchâtel that hosted me during this study.

The help of many persons who contributed to the achievement of this work is gratefully acknowledged herewith.

First, I would like to thank my advisor François-David Vuataz (CHYN, Univ. Neuchâtel) for staying available despite his chronically overbooked timetable and for sharing his encyclopaedic knowledge in geothermics and hydrothermal systems.

The SOCOMINE team at Soultz-sous-Forêts, especially A. Gérard, who provided lots of information, data and encouragement.

Fruitful advice on geochemistry and modelling from B. Fritz and E. Jacquot of the Centre de Géochimie de la Surface (Univ. Louis Pasteur, Strasbourg) helped considerably during the last three years.

I thank M. Azaroual, B. Sanjuan and A. Genter of the BRGM in Orléans for stimulating discussions and for their help in data acquisition.

During a visit to his laboratory, L. Aquilina of the University of Rennes, provided useful ideas on the Soultz fluid geochemistry.

After the World Geothermal Congress 2000 in Japan, I had the opportunity to be received in New Zealand by several laboratories and institutions. S. Simmons (Univ. of Auckland), B. Christenson (Institute of Geological and Nuclear Sciences Limited, Taupo) and S. White (Industrial Research Limited, Lower Hutt) are warmly acknowledged. Special thanks are given to S. White, author of the code Chem-TOUGH, who provided a considerable help for the building of the geochemical model with Chem-TOUGH.

I was also received by Y. Kharaka of the U.S. Geological Survey in Menlo Park, California. His long experience with brine geochemistry brought useful ideas on the modelling method.

Finally, this research would not have been possible without the modelling group of the ETH-Zurich. I would like to thank D. Bächler and T. Kohl for their friendly collaboration and for the common modelling work. L. Rybach, R. Hopkirk, K. Evans and T. Mégel are also thanked for informative discussions and meetings.

My best thanks and gratitude to the members of my PhD jury, P. Perrochet (Univ. Neuchâtel), F.-D. Vuataz (Univ. Neuchâtel), C. Fouillac (BRGM), B. Fritz (CNRS), A. Kalt (Univ. Neuchâtel) and T. Kohl (ETH-Zurich) for the time they gave to the reading and correction of my report as well as for the fruitful discussions during the examination.

In addition, I would like to thank all the people who gave me their support and friendship: all the collaborators of the CHYN, my friends and my family.

1. Introduction

1.1 Hot Dry Rock research in Switzerland

This report represents a Ph.D. thesis which was realised in the framework of the European Concerted Action for the support of the Hot Dry Rock Geothermal Energy R&D activities 1998-2001 (EC Contract no. JOR3-CT98-0313). It represents one of the contributions of the Swiss Hot Dry Rock R&D group to the building and testing of a Hot Dry Rock (HDR) power plant in Soultz-sous-Forêts (Alsace, France). This research was carried out at the Centre of Hydrogeology (CHYN), University of Neuchatel and was funded by the Swiss Federal Office for Education and Science (no. 98.0008-3 and 00.0453).

The Swiss Hot Dry Rock R&D group activities started with the MAGES (Man-made Geothermal Energy Systems) project of IEA (1978-81) focusing mainly on numerical reservoir modelling. Between 1982 and 1991 the Swiss HDR modelling effort was financed by the Swiss National Energy Research Fund (NEFF project 239). The work focussed on field data from the British HDR project at Rosemanowes Quarry near Penryth/Cornwall. The NEFF also financed the Project 359 including results of modelling on Soultz data. From 1993, the Swiss Federal Office for Education and Science (FOES) took over the funding and the work concentrated on the Soultz site, in particular on the non-linear flow behaviour in the fractured granitic reservoir (project no. 93.0100). This work continued in 1996 concentrating on the 1995-97 test results at Soultz (projects no. 95.0673-1 and 95.0673-2). Those phases were conducted by the Research Group Geothermics and Radiometrics, Institute of Geophysics ETH Zurich and Polydynamics Engineering, Männedorf. In 1998 the CHYN team and Mégel GeoWatt, Zurich, joined the project. The results of the 1998-2000 phase are presented in two reports (Baechler et al., 2001; Durst and Vuataz, 2001b)

Started in 1996, a Swiss Hot Dry Rock project called Deep Heat Mining was initiated with its main activities as well as drilling located in the city of Basel. After the selection of a first adequate site in the city of Basel, the objective is to create a deep fractured reservoir and to build a pilot plant delivering electricity and heat. The modular concept of a Deep Heat Mining pilot plant is composed of one injection well and two production wells like the Soultz project. The main difference comes from the presence of a big city with existing heat distribution networks that can take advantage of the excess heat.

1.2 Geothermal energy and Hot Dry Rock technology

Geothermal energy is heat from deep in the Earth. Temperature in the Earth increases with depth, reaching a level of 4,200°C in the core and with more than 99% of the volume beyond 1000°C. The Earth's heat flow conveys some 42 million thermal megawatts to the surface. In areas of magmatic intrusion and volcanism, deep groundwater may be heated and set into upward circulation through fractures and pores in the rock. If these thermal waters reach the surface, hot springs, boiling mud pots, geysers, and fumaroles occur. It is these hydrothermal resources - ground water heated by molten or recently solidified rocks at depth - that are used today for generation of electricity and direct applications of heat. For generation of electricity, hot water at temperatures ranging from about 150 to nearly 370°C is brought to the surface from the underground reservoir through production wells, which may be 300 m to more than 3000 m deep.

Geothermal energy is an important energy source having environmental and economic advantages over fossil and nuclear energy sources. Electricity generated from geothermal steam supplies power without polluting our atmosphere or water, or creating radioactive waste. Clean heat from geothermal water dries vegetables, heats greenhouses, and warms clusters of homes and buildings in district heating systems. Geothermal heat pumps provide highly efficient heating, cooling, and hot water for homes and public buildings. Only a small fraction of our available geothermal resources are being used today. Improvements in technology and widening recognition of geothermal energy true value will lead to a greatly increased amount of this clean, reliable resource being developed in essentially all countries of the world. Geothermal energy is a vital part of a sustainable future.

The number of hydrothermal resources in highly permeable rock formations is limited. However, there are huge land areas under which the rock temperature reaches 200°C at depths around 5 km. But, in general the permeability of these formations is low, so that engineering and new technology will be necessary to generate energy production economically. The principle of HDR technology is to circulate a fluid between an injection well and a production well, along pathways formed by fractures in hot rocks. A deep heat exchanger is then created, and the fluid transfers heat to the surface, where it can be converted to electricity. This process is contained into a closed-loop and no gas or fluid escapes in the atmosphere. The hot fluid produced under pressure at the wellhead flows through a heat exchanger, vaporizing a secondary low-boiling working fluid that drives an electric generator. "Hot Dry Rock" includes now more than "Dry Rock" since formation fluids have been frequently found from deep boreholes drilled in crystalline rocks. Indeed, between fully hydrothermal reservoirs and totally impermeable hot rocks, there is a complete series of low- to medium-permeability rocks which cannot be exploited for geothermal energy production without specific engineering enhancements.

The Soultz HDR project consists of three wells, one for injection and two for production, drilled to 5 km depth. The bottom rock formation is a fractured granite saturated by highly mineralised water and its temperature reaches 200°C. The fluid used for the heat extraction is the formation brine. From injection to production, the fluid will flow through 600 m of altered granite. Then it will be pumped to the surface installations and reinjected at a temperature of about 65°C. This process should be working continuously for years, within a closed loop and without drastic changes of the thermal-hydraulic parameters in the reservoir. This leads to the necessity to forecast the effects of fluid-rock interactions on the fissured reservoir characteristics.

1.3 Directions and goals of the study

The main focus of this study "*Geochemical modelling of the Soultz-sous-Forêts Hot Dry Rock test site: Coupling fluid-rock interactions to heat and fluid transport"* is the geochemical modelling. The goal is to create a simulation module capable to define and forecast the geochemical evolution of fluids flowing under various temperatures in a fissured hot granite, the dissolution and precipitation occurring as well as their effect on the permeability. This module will then be coupled to a thermal-hydraulic code. This part of the work has been performed in collaboration with D. Baechler also realising a Ph.D. thesis at ETH-Zurich on thermal-hydraulic modelling.

The fluid-rock interactions in the Soultz reservoir have already been the subject of previous study (Genter, 1990; Azaroual, 1994; Jacquot, 2000). However the coupled thermal-chemical-hydraulic simulation of the whole Soultz system was still missing.

Geochemical modelling of hypersaline brines at high temperature is rather new, and basic experimental data are still missing or under acquisition by several laboratories worldwide. Moreover, most of the research carried out in this field concerns either cold brines (sea water, closed basins under high evaporation, underground salt dissolution, etc.) or hot dilute fluids (hydrothermal fluids, geothermal reservoirs, etc.). Indeed, thermodynamic and kinetic modelling of fluids with a salinity larger than seawater and temperature over 150°C is rarely encountered in the scientific literature. Finally, physical and chemical problems linked to the geochemical equilibrium calculations are not straightforward and have to be overcome.

Another problem curbing the simulation experiments was the absence of complete and sound chemical analyses of the Soultz fluid. Only limited sets of fluid and gas chemical data were available in the literature, and the fluid samples collected during the 1997 flow test were analysed only 1.5 years after, which involved problems for the precision and quality of the analytical results linked to this long delay.

It was decided to create the geochemical module on the basis of an existing code, which could be later coupled to the finite element code FRACTure, developed by Th. Kohl at ETH-Zurich (Kohl and Hopkirk, 1995). After having reviewed in detail several geochemical codes, it was decided to use Chem-TOUGH2 as a basis to create the simulation module. As stated in the 1998 proposal, at the end of this double research project, the geochemical processes simulation module should work in a coupled way with FRACTure, the thermal-hydraulic-mechanical model, in order to provide 2-D

simulation of the HDR Soultz reservoir behaviour. This leads to an additional constraint as the geochemical module should remain sober in terms of computing time. The steps leading to the creation of a new thermal-chemical-hydraulic code named FRACHEM are summarized in Figure 1.3.1.

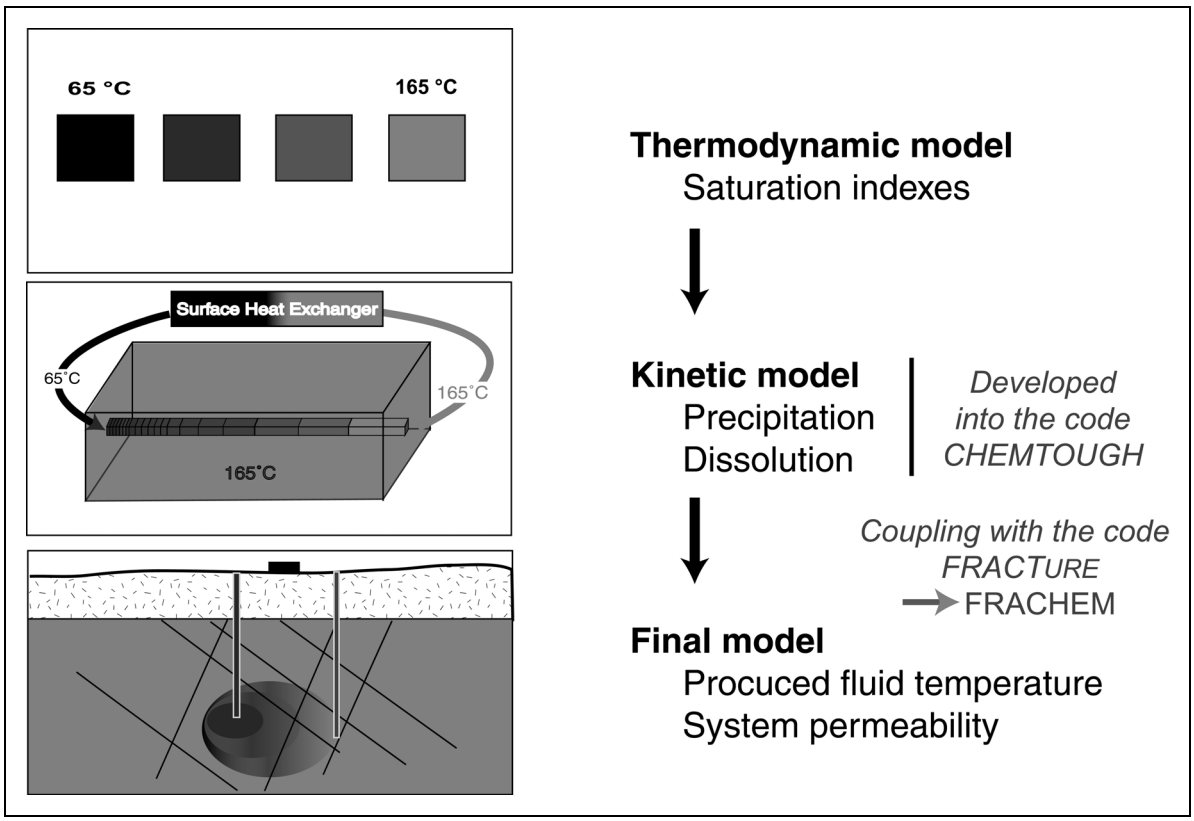

Figure 1.3.1 Main steps of the model development.

This report articulates in three main parts:

- The first part consists of chapter 2, which details the situation of the Soultz system, its geological and thermal-hydraulic environment as well as the characterisation of the fluid and the mineral phases.
- The second part details the building of the conceptual geochemical model. It includes chapter 3 on thermodynamic modelling: determination of the activity coefficient, mass balance calculations, equilibrium calculations, determination of an average Soultz fluid composition. Follows chapter 4 on kinetic modelling: dissolution and precipitation of major minerals relevant to the water-rock interaction processes, effects of dissolution/precipitation on rock permeability.
- The third part describes the numerical work. The implementation of the geochemical code in Chem-TOUGH2 and application of the model to a 1-D fracture composes the chapter 5. Chapter 6 concerns the extraction of geochemical modules and the coupling with FRACTure. Chapter 7 describes the application of the newly built FRACHEM code to two simple cases (single fracture and two fractures models)

2. Soultz-sous-Forêt Hot Dry Rock test site

2.1 Geological situation of the Soultz project

The European HDR research site is situated at Soultz-sous-Forêts (northern Alsace, France) on the western edge of the Rhine Graben, about 50 km north of Strasbourg (Figure 2.1.1 a). The site is in the former Pechelbronn oil field and was selected because of the high heat flow anomaly observed from a large number of oil wells. The surface expression of this anomaly is tightly confined and suggests the existence of deep convective cells.

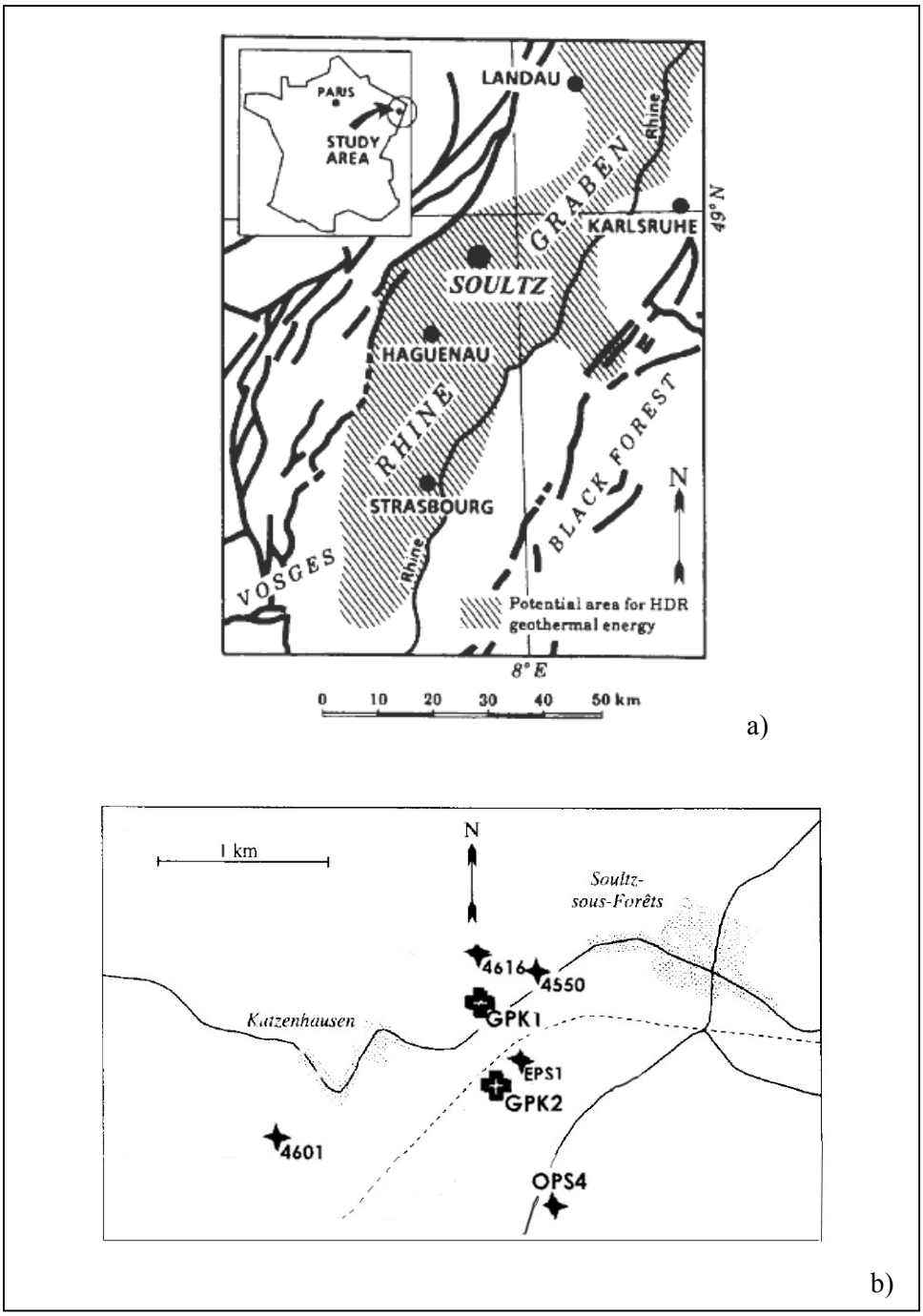

Figure 2.1.1 a) Location of the European HDR research site. b) Borehole network (Genter and Traineau, 1996).

The Figure 2.1.1 b shows the different boreholes drilled at Soultz. 4550 (1500 m), 4601 (1600 m) and 4616 (1400 m) are old oil wells, EPS1 (2227 m) was the first exploration well of the HDR project,

OPS4 (1537 m) is an observation well drilled in 2000 GPK1 (3590 m) was used as an injection well during the precedent phase and is now intended to be an observation well and GPK2, after being used as a production well has been deepened to 5000 m and is intended to be the injection well of the pilot plant.

The Rhine Graben runs along 300 km from the Jura to the South to the Taunus Massif to the North. He is bordered by the Vosges to the West and the Black Forest and the Odenwald to the East. The Figure 2.1.2 shows the structure of the Rhine Graben constituted of step faults. In the northern part of the graben these faults are subvertical and N-S trending. The sites is located 5 km from the main Rhine fault constituting the western border of the graben.

This structure induces a great variation of the thickness of the sediment cover that goes to more than 4 km. At the Soultz site, the crystalline basement is covered by 1400 m of Triassic and Tertiary sediments.

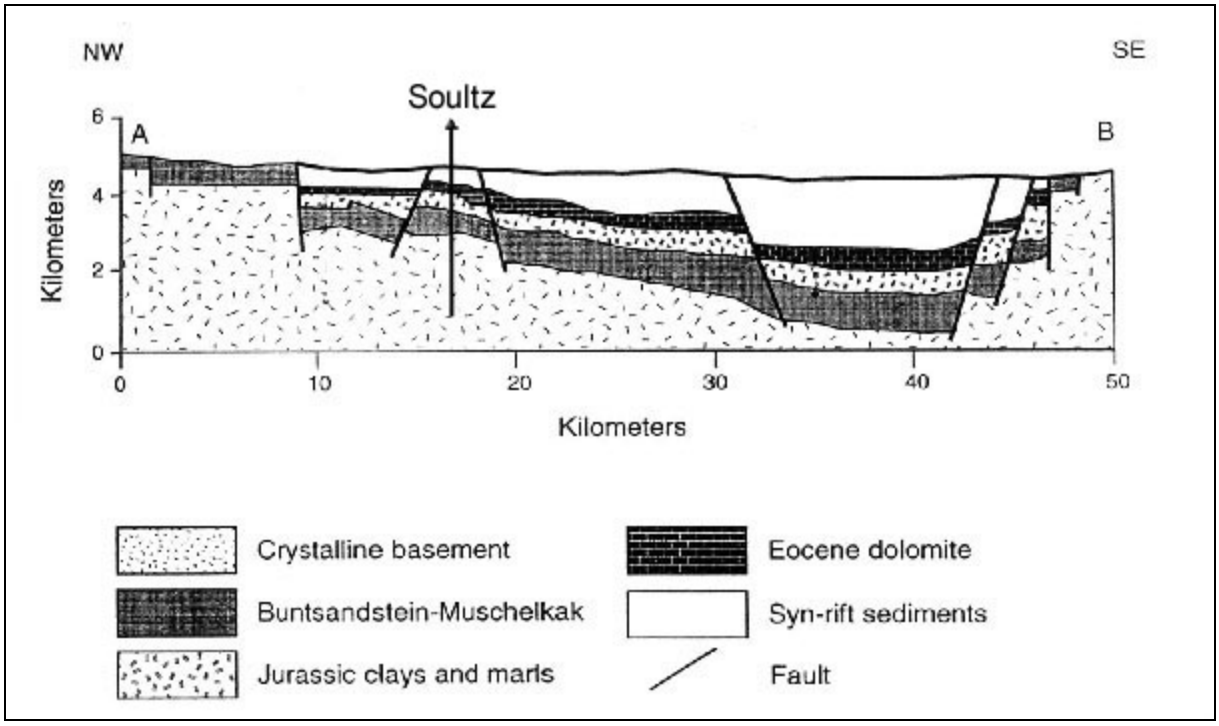

Figure 2.1.2 Simplified cross section through the Rhine Graben (Komninou and Yardley, 1997).

2.2 Presentation of the Soultz HDR project

The Hot Dry Rock (HDR) / Hot Fractured rock (HFR) concept aims at using the vast amount of heat stored in the Earth's crust but which is not accessible by conventional geothermal technology which requires large, hot, natural aquifers to extract the heat. In HDR/HFR systems, a well is drilled into high-temperature (>180°C) fractured basement rock that underlies most of Europe. Then it is stimulated to enhance the natural permeability of the fracture network to create a reservoir or heat exchanger into which additional wells are drilled. Water (if possible formation fluid) circulated through the fracture network in the hot rock gathers heat, which can be extracted at the surface via the wells to generate electricity and for direct use (Fig. 2.2.1).

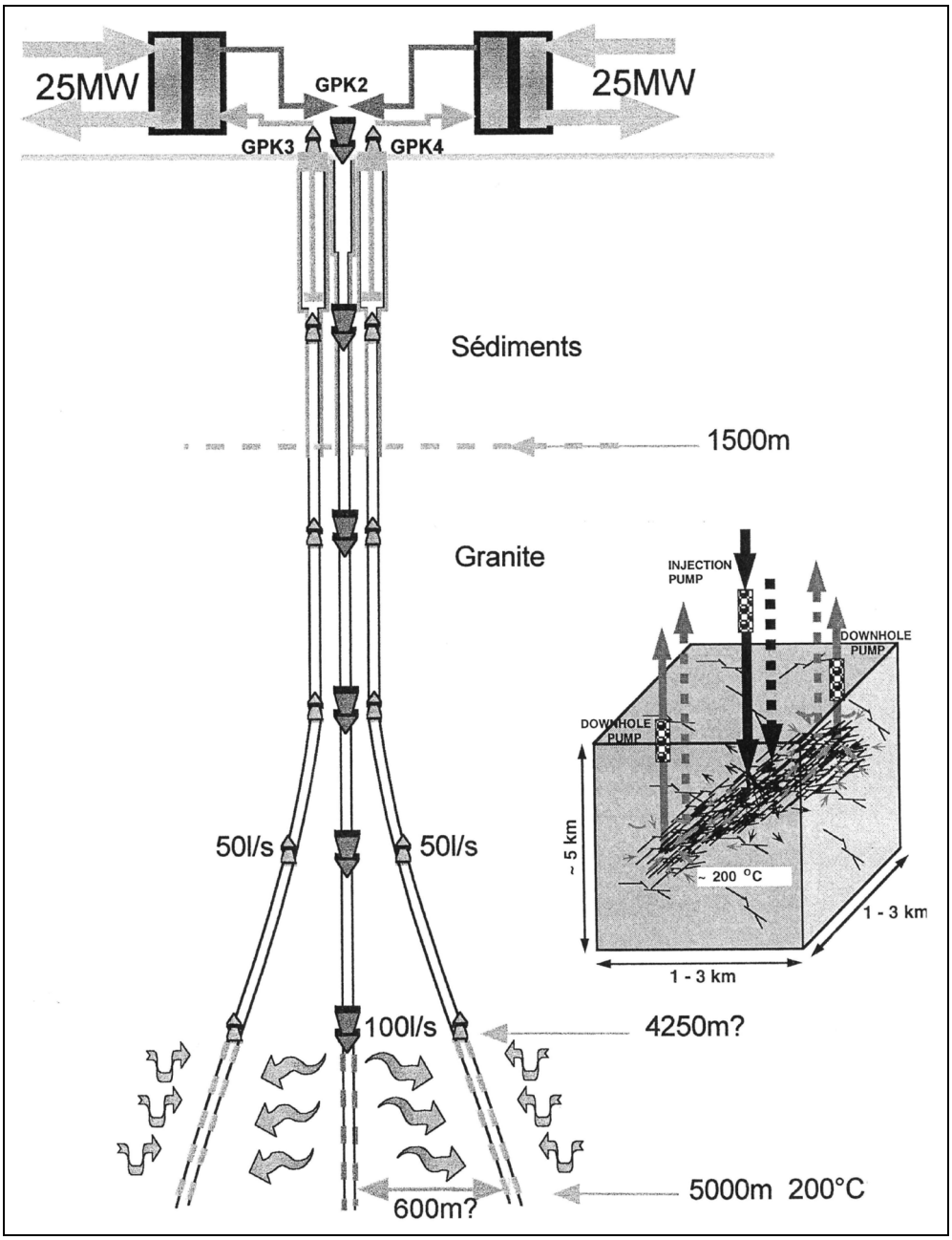

Figure 2.2.1 Conceptual geothermal pilot plant at Soultz. Installed electric power production will reach 6 MWe and thermal power production will range between 40 and 70 MWth (Baria et al. 1998).

The European HDR project started in 1987 and has been funded by France, Germany and the European Commission (EC). A number of organisations from other countries such as Italy, Sweden, United Kingdom and Switzerland are also involved. Until 2001 the project has been administered and co-ordinated by the company Socomine managed by a core team of three senior staff (British, French and German), who were based permanently on site and provided a link between the funding agencies and the research organisations (Baria et al., 2000). Recently the Industrial Consortium (EEIG) "Heat Mining" has taken up the management of the project with the new contract signed with the European Commision for the period 2001-2004.

During the initial phase (1987–1989), a well (GPK1) was drilled to 2000 m depth in order to penetrate the crystalline basement at 1377 m depth and obtain basic data. The bottom hole temperature was 140.3°C. The temperature gradient and the heat flow values are high in the sedimentary cover (10.5°C/100 m; 176 mW/m^2) and quasi-normal in the granite basement (2.8°C/100 m; 82 mW/m^2). A

number of geophysical measurements were carried out to assess the rock mass conditions at 2000 m depth (Bresee, 1992).

During 1989-1991, an attempt was made to drill a continuous cored well (EPS1) to 3500 m, re-opening an old oil well located about 400 m SSE of GPK1. The coring started at about 900 m but it proved to be difficult to control the deviation. The well was terminated at the depth of 2280 m, at which point the deviation had exceeded 25°. The continuous coring nevertheless gave very useful information on the joint network and mineralogy, and provided the basis for subsequent interpretation of cuttings and geophysical logs.

During 1992-1993 the existing well GPK1 was extended, essentially vertically, from 2000 m to 3590 m depth. Geophysical and other scientific measurements were carried out during and after drilling. Following the drilling of the well, large scale hydraulic tests were carried out to characterise the rock mass. Supporting activities during the injections included microseismic monitoring, production logging, fluid sampling, etc. (Baria et al., 1995).

Following this stage, GPK1 was put on production (June / July 1994) to assess the productivity and the injection properties following the massive injections in 1993 (Baria et al., 1995). The existing information available (stress, joints, thermal modes and seismicity) was then used to target a second deep well GPK2 to a depth of around 3890 m approximately 450 m south of GPK1.

In 1995 and subsequently 1996, GPK2 was stimulated with a maximum flow of 78 l/s to improve the injectivity as a function of flowrate (Gérard et al., 1977). During the 1996 injection a total of 28,000 m^3 of fluid was injected between 3200 m and 3600 m in three flow steps (24, 45 and 78 l/s) with a maximum wellhead pressure of 13 MPa for 78 l/s.

In 1997 a circulation test was carried out at the European HDR Project in Soultz-sous-Forêts which showed that it was possible to circulate at around 25 l/s between two deep wells in the depth range of 3000-3500 m and a separation of about 450 m. The test lasted for about 4 months and produced excellent results, but it was observed that although the heat produced was sufficient for space heating (140-150ºC, 10 MWth), the temperature was not sufficiently high for electricity generation at an economic rate (Fig. 2.2.2).

Both the funding agencies and the industrial consortium felt that heat production by HDR at around 200ºC was more attractive for electricity generation and therefore it was decided to extend an existing deep well GPK2 to a depth of around 5000 m to access the required temperature. Scientific investigation was carried out to characterise the rock mass at great depth and assess if they would be as favourable as found for the successful circulation test at 3000-3500 m in 1997.

Further development of this technology required that the past successful experience at Soultz is replicated at higher temperatures and larger flow rates in order to further improve the efficiency and economy of the technology. Following the successful circulation experiment in 1997 at Soultz, it was decided to re-enter and deepen the well GPK2 from 3876 m to 5000 m (Baumgärtner et al., 1998). Temperatures of around 200°C were anticipated at this depth. The well GPK2 at the European HDR site was successfully re-entered and deepened from 3876 m to 5084 m depth and fully completed in 104 days (mid February to the end of May 1999).

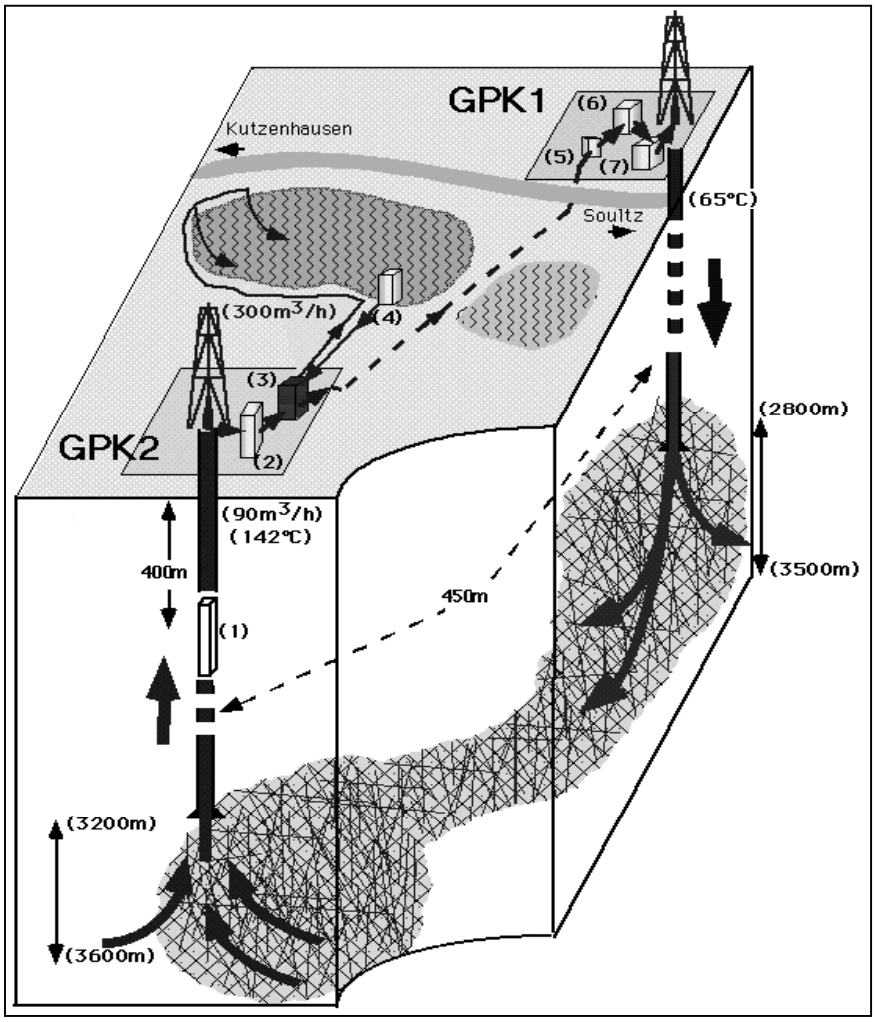

Fig. 2.2.2 Circulation experiment between the two deep wells GPK1 and GPK2 at the HDR test site in Soultz in 1997 (Gérard et al.,. 1999). 1: submersible pump, 2: pre-filter, 3: heat exchanger, 4: pumps for cooling circuit, 5: corrosion test chambers, 6: filter battery, 7: re-injection pump.

The programme of re-entry included pulling of the existing 3211 m long internal 9 5/8" by 7" casing string, fishing of a submersible pump and some 150 m of 2 3/8" tubing, sealing of a major loss zone and reaming open from 6 1/4" to 8 1/2" in granite (3211 – 3876 m). The well was extended to 5048 m in 8 1/2" hole size and again completed with a floating 9 5/8" by 7" casing string. The casing shoe is at 4431 m. A bottom hole core was taken at 5048 - 5051 m depth and the core recovery was approximately 40%. A pilot hole in 6 1/4" was drilled from 5051 - 5084 m for in situ stress measurements (Baumgärtner et al., 2000).

Several geophysical logs were performed after the deepening of GPK2 and the bottom hole temperature reaches 200°C. Carried out in 2000, hydraulic stimulation tests demonstrated that at a depth of 4500-5000 m, it was possible to develop a huge reservoir with moderate efforts.

The next phase programme plans to drill two deviated wells at a depth of 5000 m where the granite temperature reaches 200°C and to stimulate a new large fractured reservoir. Hydraulic, thermal and geochemical measurements as well as modelling of coupled processes will help to characterise this reservoir before the long-term flow tests and the exploitation of a first geothermal pilot power plant.

2.3 Temperature and fluid flow in the Rhine graben and in the Soultz reservoir

Soultz-sous-Forêts is the centre of the largest anomaly of surface heat flow density in central Europe. With a background value of 80 mW m^{-2} for the Rhine Graben, heat flow density exceeds 140 mW m^{-2} at the Soultz site. This anomaly is located about 70 km north of the Kaiserstuhl volcano which is associated with a minimum in crustal thickness and a maximum of mantle He-isotope concentrations in the upper Rhine Graben. The surface heat flow density anomaly at Soultz is not a signal associated with processes at great depth (e.g., rifting) but the result of a redistribution of heat by advection due to fluid flow in the upper crust (Pribnow and Clauser, 2000).

The heat and fluid flow of the Rhine graben has been investigated by several authors, using various models based on temperature observations, fluids chemical and isotopic composition, fracture analysis as well as hydraulic testing in Soultz. From these models, it appears that the system is mostly recharged by meteoric water in the Vosges massif, infiltrating down to the bottom part of the graben where the sedimentary cover reaches a thickness of 5 km. On the other hand, infiltration in the Black Forest along the fractures bordering the graben contributes very little to the deep flow system. The fluid flows from the deeper eastern part of the graben towards the Soultz horst where the basement is closest to the surface (Aquilina et al., 2000). On the western border of the graben, there is mixing of the evolved saline fluids with surface waters infiltrated in the Vosges. Large scale exchange of saline fluids occurs between the Buntsandstein and the upper part of the crystalline basement in a succession of convection cells. This process can develop because the viscosity of the fluid decreases with increasing temperature (Fig. 2.3.1). Thus, the water is forced to flow beneath the deepest part of the graben filling. Rising from great depths, these fluids carry enough heat to produce the observed heat flow density anomaly at Soultz.

Figure 2.3.1 Schematic flow field including the granitic basement (Aquilina et al., 2000). The

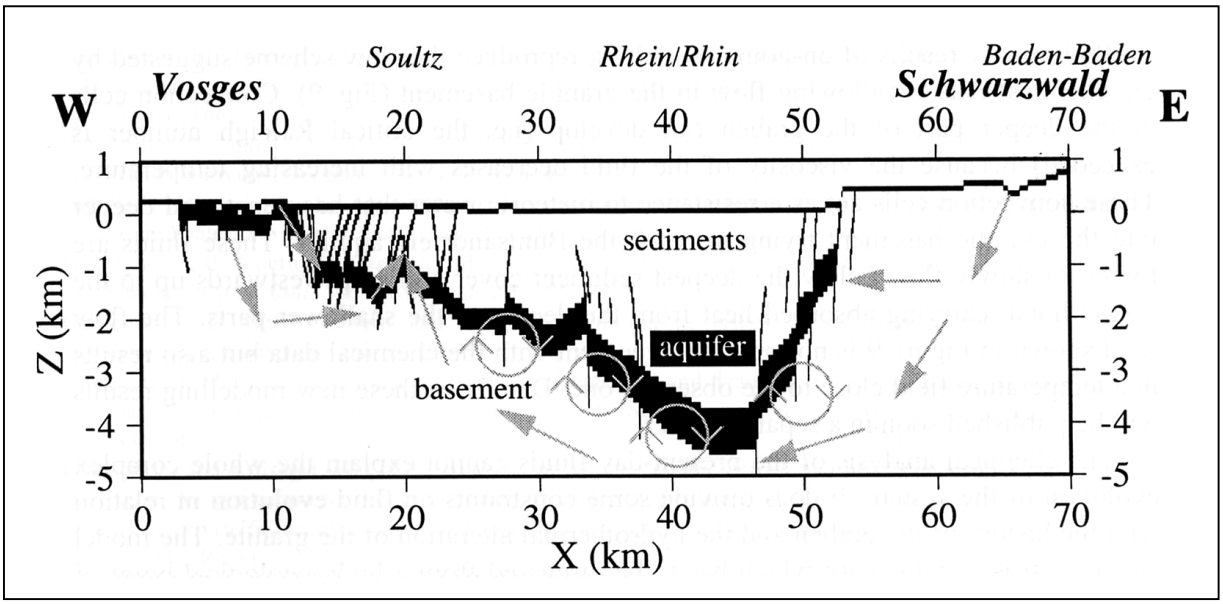

arrows indicate the direction of flow but are not related to the velocity. The numerical model is 15 km deep.

The flow scheme shown is in good agreement with both the observed temperatures (Figure 2.3.2) and the results of chemical pore fluid analyses. The concept of rising water in the granitic basement at the HDR site is also in agreement with the temperatures measured in the Soultz boreholes. The temperature gradient of 100 °C/km in the top sediments drops to 10 °C/km in the drilled granitic section (1.4 to 3.8 km). The thermal anomaly detected at the surface of the Soultz area is limited in depth to the thickness of the sediment cover (1.4 km).

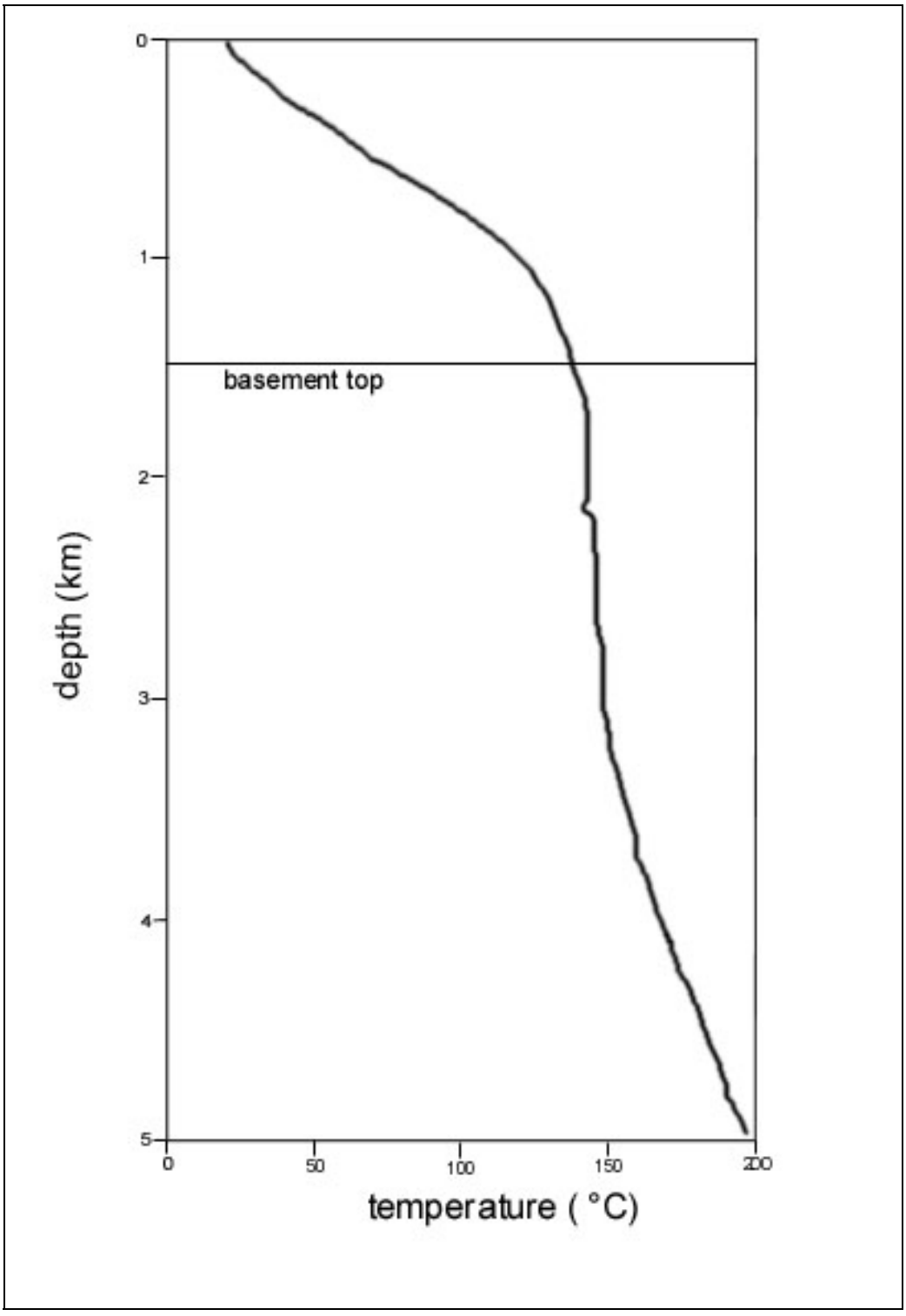

Figure 2.3.2 Temperature log from GPK2 well in Soultz-sous-Forêts (Schellschmidt and Pribnow, 2001).

Below the top of the basement, the low temperature gradient can be explained by an upward fluid circulation. A simulation of the thermal and fluid flow performed by Baechler and Kohl (2001) atribute this upflow to a convection cell taking place between 3700 and 1000 m (Figure 2.3.3). The maximum fluid velocities near the two major faults exceed several cm.year^{-1}.

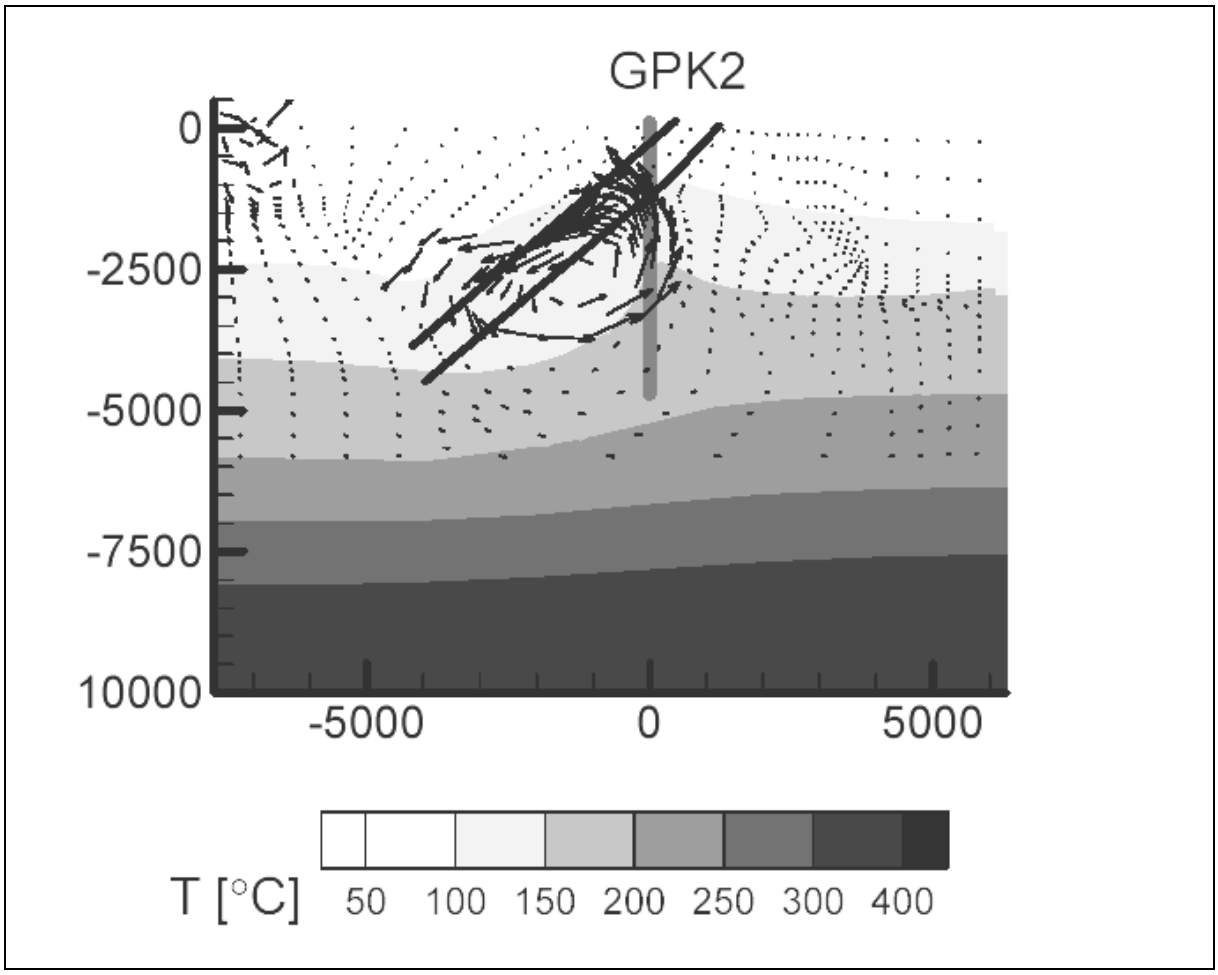

Figure 2.3.3 E-W profile of the temperature and fluid flow field (Baechler et al., 2001). The flow velocities in the central model domain have been scaled down by a factor of 20 in order to represent even smaller components. Black lines represent the two Kutzenhausen and Soultz faults.

As results from hydraulic experiments, two flow regimes are considered: (1) flow in the artificially stimulated volumes of enhanced permeability around the open hole sections of GPK1 and GPK2, and (2) channelled flow along natural fault zones. A detailed analysis of the hydraulic experiments has identified hydraulically active sections in both holes. These results, in combination with geometrical analyses, show that there is no direct connection of GPK1 and GPK2 through a natural fault zone. All channelled pathways form indirect connections, resulting from the intercept of fault zones. This indicates that the two boreholes are connected to two different regional fault systems (Pribnow and Clauser, 2000).

The stimulated areas have been created around the open-hole sections of the boreholes with the hydro-fracturing technique. As these areas of increased permeability overlap, they form a direct connection between the holes which can be treated as an equivalent porous medium.

The investigated Soultz HDR reservoir between 2000 and 3800 m is clearly dominated by large fault zones. Both, the unperturbed steady state temperature field and the hydraulic perturbations can only be explained quantitatively by accounting for strong hydraulic heterogeneities. Models assuming unfractured rock can be clearly discarded for the Soultz reservoir, even under ambient (i.e. not hydraulically stimulated) conditions (Kohl et al., 2000). The combined investigations of the temperature field and of the hydraulic experiments require the existence of high permeable features. The non-Darcian flow regime linked to the hydraulic behaviour in fractured rock is due to the fact that the Graben faults extend vertically from surface to the reservoir depth. Moreover, the lateral extension of these fractures over large distances provides their huge storage capacity. The models for the

ambient thermal-hydraulic fields predict a less developed connection to the surface but a high permeable zone limited to the Buntsandstein and topmost granitic units. On the basis of the newly deepened GPK2 measurements, this model predicts especially a lower natural permeability of the rock matrix at greater depth.

2.4 Mineralogical conditions

Petrological investigations of the granite massif were carried out in Soultz-sous-Forêts since the drilling of the first well GPK1. Later, drill cuttings and cores of wells EPS1 and GPK2 were also studied in great detail. The crystalline rock encountered below 1400 m is a porphyritic granite with abundant K-feldspar large crystals, biotite, hornblende and accessory minerals such as apatite, titanite and magnetite (Traineau et al., 1991). Variation in mineralogical content is mostly dependant on the abundance of the large K-feldspar crystals. There are also some fine-grained, biotite-rich xenoliths, one to several centimetres in size, with mineralogical composition of diorite to meladiorite. The analyses of the cuttings and core samples from the deepening of GPK2 show a new facies appearing at 4860 m. This facies correspond to a fine–grained two-mica granite interpreted as a newer granitic intrusion (Baria et al., 2002). The conceptual geological model is schematised in Figure 2.4.1.

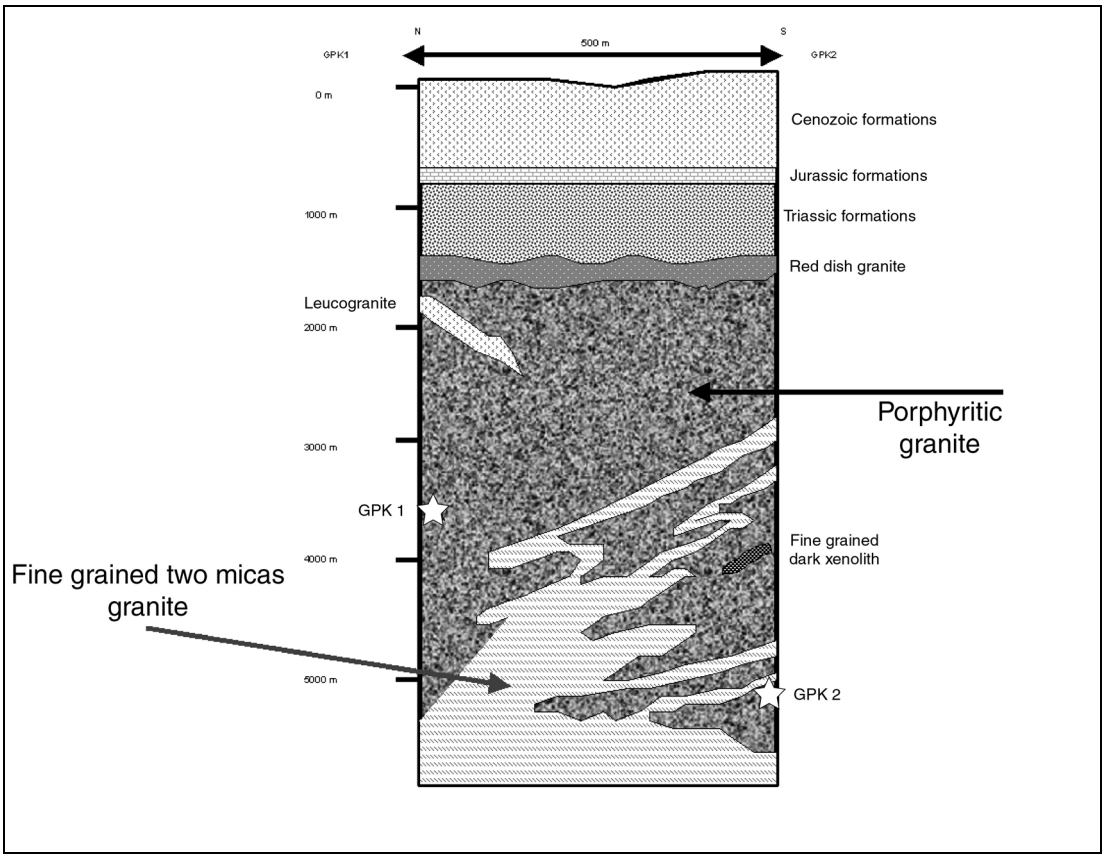

Fig. 2.4.1: Conceptual model of granitic intrusion in GPK-2. The bottom of the wells GPK-1 and GPK-2 is marked as a white star (Baria et al., 2002).

On the Soultz HDR site, the granitic basement high fracturation degree is in relation with the graben tectonics. These fractures have allowed fluid circulations over long time periods so that hydrothermalism is responsible of major petrographic transformations undergone by the granite.

Analysis of the petrography and fluid inclusions of the granite revealed several alteration phases (Traineau et al., 1991; Ledésert 1993). The granite underwent an earlier pervasive alteration stage which is widespread in the massif as shown by the core study (Genter 1989). Transformation of

primary minerals (biotite, hornblende, plagioclase) has given way to secondary propylitic assemblages, where chlorite is the most common phase. Later, vein alteration related to water-rock interactions developed in the fracture system. The most common products are white mica or regular illite-smectite mixed layers, carbonates, iron oxides and locally quartz (Fig. 2.4.2).

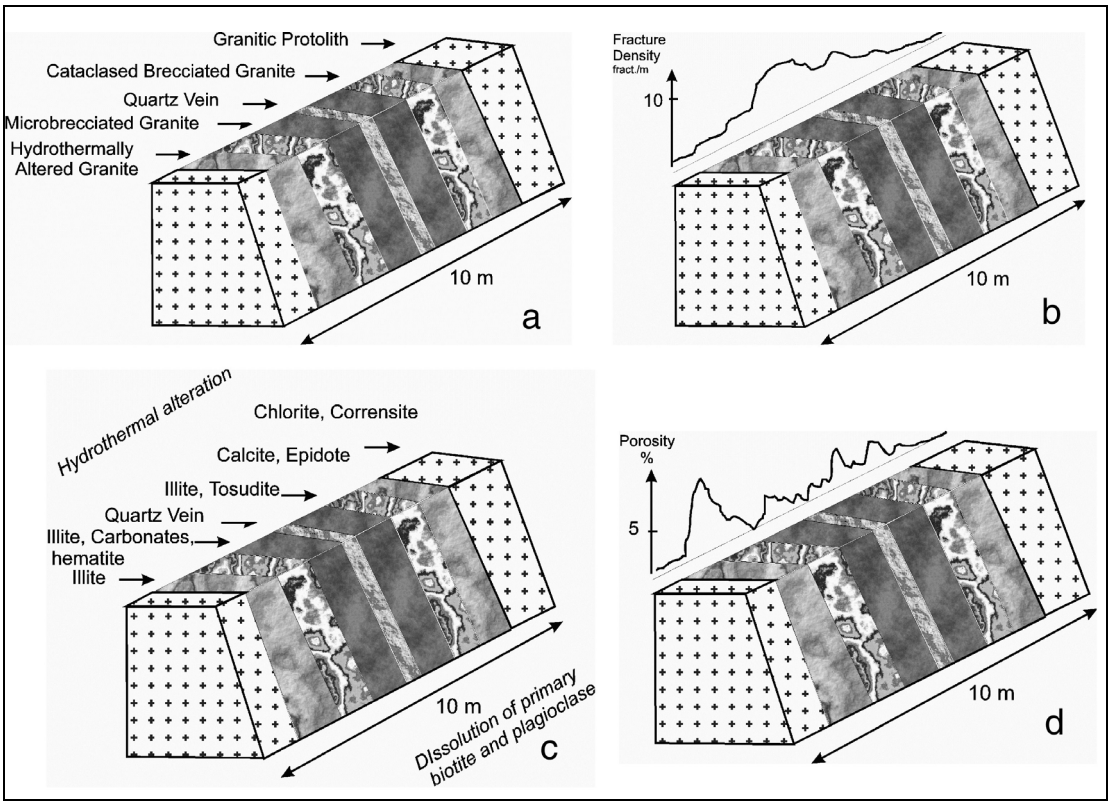

Figure 2.4.2 Characterisation of hydrothermally altered and fractured zones (Genter et al., 1998). (a) Conceptual lithofacies granite zonation of hydrothermally altered and fractured zone. (b) Fracture density distribution. (c) Conceptual spatial hydrothermal alteration sequence of a fractured zone. (d) Porosity profile.

Three mineralogical assemblages can be deciphered. (1) The first facies is the healthy granite in which the fracturation density is close to zero. Consequently, this facies only plays a minor role in the rock fluid storage capacity and in the fluid-rock interaction processes. (2) The second facies is composed of hydrothermalised granite blocks partly cemented by alteration products which consist essentially of clay minerals and carbonates. This facies is the most porous so that it contains the majority of the formation fluid and it plays a major role in the present fluid-rock interaction processes. (3) The third facies is the most altered, because the fracturation density is the highest and the initial granite has been totally crushed. In this case, alteration processes are more complete and the only remaining minerals from the initial granite (mainly quartz) are fully cemented by clays, carbonates and secondary quartz veins, so that the resulting porosity is quite low. However the density of open fractures indicates that most of the fluid will circulate through this facies. A synthetic and qualitative description of the minerals encountered in the three facies is presented in Table 2.4.1.

Table 2.4.1 Simplified qualitative mineralogy of the different facies of the granitic basement at Soultz (Jacquot 2000).

Facies 1 Healthy granite		Facies 2 Hydrothermalised granite		Facies 3 Vein alteration	
Mineral	**Volume %**	**Mineral**	**Volume %**	**Mineral**	**Volume %**
Quartz	24.2 %	Quartz,	4.09 %	Quartz.	43.9 %
K-feldspar	23.6 %	K-feldspar,.	13.9 %	Illite	40.2 %
Plagioclase	42.5 %	Chlorite	4.8 %	Smectite	9.6 %
Biotite	4.2 %	Illite	24.6 %	Calcite	4.3 %
Hornblende	3.1 %	Smectite	9.7 %	Dolomite	0.7 %
Chlorite	2.0 %	Calcite	3.3 %	Pyrite	1.0 %
Calcite	0.3 %	Dolomite	0.8 %	Galena	0.3 %
		Pyrite	0.7 %		
		Galena	1.3 %		

2.5 Fluid geochemistry

The most critical point for fluid-rock interactions modelling is probably a good definition of the fluid. Ideally analyses should provide for reservoir conditions data for elemental fluid composition and gas phase composition as well as physico-chemical parameters like pH and Eh. Unfortunately not all of these informations are available for the deep reservoir. There are multiple causes for this lack of data. First, drilling operations, the hydraulic fracturation and injection tests disturb the fluid chemistry, which may need a consequent production volume before regaining its original state. Second, the sampling of deep fluids is technically difficult. Wellhead sampling gives a fluid that has undergone transformation, like degassing, during the upflow, whereas downhole sampling at high pressure and temperature often fail to really take a representative sample, which still has to be analysed before chemical modification. Third, most of the analyses are performed on cooled samples which can have precipitated some minerals or constituted colloids. Fourth, the high salinity of the fluid requires the need of a dilution for some analytical methods which enhances the error percentage of the result for minor elements. Last, the requirements of the general project planning are sometimes in contradiction with the best possible geochemical survey.

The present geochemical study is mostly based on the data from the 1997 circulation test. Nevertheless, a brief overview of previous analyses from Soultz boreholes and other deep fluids from the Rhine Graben, as well as from other Hot Dry Rock projects was carried out in order to help the comprehension of the Soultz geochemistry. Furthermore, the first chemical data from the 5000 m-depth reservoir are also included in this chapter.

2.5.1 Geochemical context of the Soultz Project

Pauwels et al. (1993) and Aquilina et al. (1997) compiled the chemical data of the Soultz fluid (Table 2.5.1). EPS1 sample comes from EPS1 wellhead, KS228 from GPK1 wellhead and KP-3500 from a downhole sampling (3500 m) in GPK1. These three analyses show a very similar fluid with a total dissolved solids close to 100 g/l, indicating an homogeneous fluid composition in the granite between 3500 m and the top of the crystalline basement (about 1400 m).

Table 2.5.1 Chemical fluid composition in the granite of Soultz fluid. Analyses previous to the 1997 circulation test. All concentrations are in mmol/l. Depth: depth origin of the fluid. T: fluid temperature at depth. TDS: Total Dissolved Solids. Alk.: total alkalinity. na: data not analysed or not available.

Well	Sample	Depth m	T °C	TDS g/l	pH	Cl	Na	K	Ca	Mg	SO_4	SiO_2	Fe	Alk. meq/l
EPS1	EPS1	2200	150	101	5.2	1686	1231	85.9	199	5.02	2.41	1.92	7.16	na
GPK1	KS228	1815	137	99	5.82	1650	1226	84.9	167	6.17	2.19	1.62	4.15	10.6
GPK1	KP-3500	3500	165	101	5.03	1720	1213	71.8	182	4.61	2.02	3.50	na	7.50

Aquilina et al. (2000) showed that the fluids originate from a brine in Triassic sediments at the border of the Rhine Graben, diluted by a mature meteoric water that dissolves micas and sulphates in the Triassic Buntsandstein and in the granitic basement. Then, the fluids percolate into fractured granites, dissolving plagioclases and precipitating secondary minerals in veins such as quartz, illite, montmorillonite, calcite, dolomite and pyrite.

Pauwels et al. (1993) also included chemical data from four other deep fluids in the Rhine Graben (Table 2.5.2). Cronenbourg is located in Strasbourg, Bühl and Bruchsal on the eastern edge of the graben and the Soultz sample comes from an old oil well (Figure 2.5.1). These four fluids originate from the Buntsandstein formation. Aquilina et al. (2000) used these data along with isotopic data, to show that deep fluids in the Rhine Graben are a mix between a Bühl-type brine and paleometeoric water. The crystalline fluid in Soultz reservoir seems to have the same origin, but is more influenced by subsequent water-rock interactions.

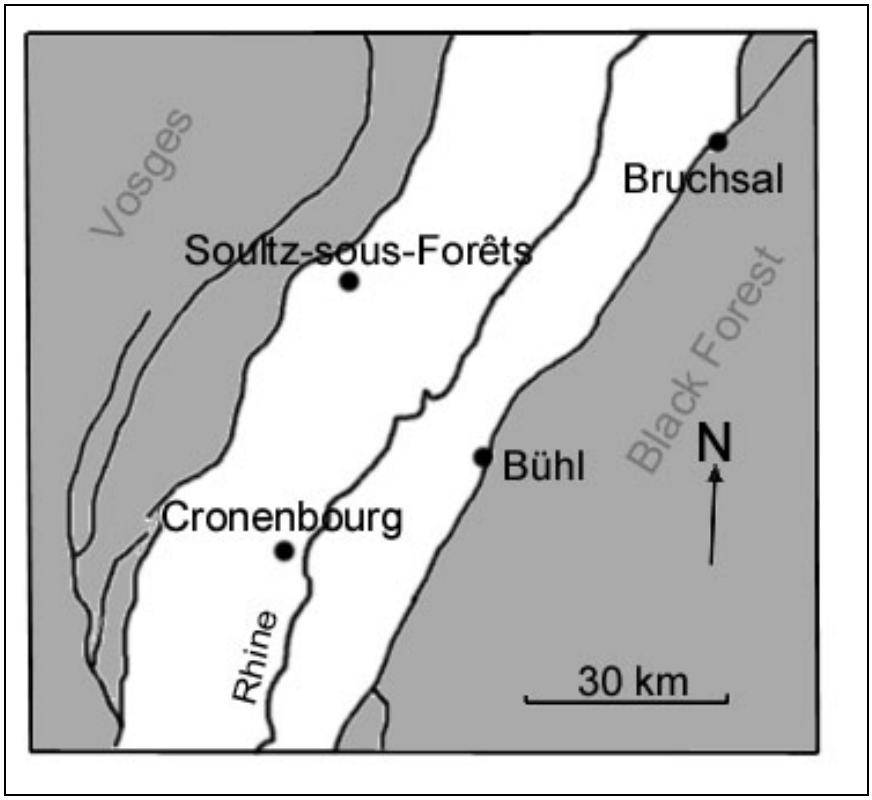

Figure 2.5.1 Location map of the sampled wells.

Table 2.5.2 Chemical composition of deep fluids in the Buntsandstein of the Rhine Graben. All concentrations are in mmol/l. Depth: depth origin of the fluid. T: fluid temperature at depth.

Location	Depth m	T °C	TDS g/l	Cl	Na	K	Ca	Mg	SO_4	SiO_2	Fe	Alk. meq/l
Soultz	1403	116	103	1717	1209	88.3	209	5.76	2.44	1.83	4.92	
Cronenbourg	2870	140	104	1748	1370	103	120	5.18	4.89	2.38	na	2.2
Bruchsal	1800	114	120	2121	1657	56.2	193	19.8	3.94	0.696	1.39	7.7
Bühl	2655	115	207	3399	2779	12.8	291	78.1	15.5	na	0.644	na

The Table 2.5.3 presents data from five other Hot Dry Rock projects coming from Althaus (1982), Dietrich (1982), Stenger (1982) Winchester (1993), Matsunaga et al. (1995), Kiho and Mambo (1995), and Richards et al. (1992).

Table 2.5.3 Compilation of chemical data from five Hot Dry Rock reservoirs. na: data not available.

HDR SITES	Bad Urach	Fenton Hill	Hijiori	Ogachi	Rosemanowes
Well depth (m)	3325	4010	2303	1100	2780
Sampling date	1978	27-Jul-1992	Nov. 1991	1993	15-Aug-1988
Production test	None	3.5 months	3 months	22 days	5.5 months
Injected fluid	None	Fresh water closed loop	Fresh water	Fresh water	Fresh water
Rock temp. (°C)	143	327	250-270	170-230	99.8
Fluid temp. (°C)	143	182	167	108	99.8
pH	4.2	na	na	na	8.8 (at 25°C)
TDS (g/l)	na (~ 2.5)	3.434	1.4	1.25	0.419
Na (mmol/l)	24.3	39.1	13	13	4.38
K (mmol/l)	4.09	2.28	$3.3 \cdot 10^{-1}$	0.45	$8.72 \cdot 10^{-2}$
Ca (mmol/l)	3.75	0.449	0.9	0.1	0.344
Mg (mmol/l)	1.85E-2	$4.11.10^{-3}$	na	na	$3.29 \cdot 10^{-3}$
Cl (mmol/l)	Large amount	26.9	5.3	1.4	2.06
SO_4 (mmol/l)	Present	3.93	$5.2 \cdot 10^{-1}$	1.6	0.775
HCO_3 (mmol/l)	na	9.64	1.8	9.2	1.21
SiO_2 (mmol/l)	2.61	7.06	4	2.7	1.09
Fe (mmol/l)	1.98	$1.43 \cdot 10^{-2}$	na	na	$3.94 \cdot 10^{-4}$

All these projects present significant differences with Soultz, above all in the fact that the circulation fluid is partially or totally composed of fresh water instead of formation fluid. The only element in the same concentration range as in Soultz fluid is silica. Durst and Vuataz (2000) used geochemical modelling to show that all the fluids are slightly oversaturated in regard to quartz, the oversaturation increasing with the difference between production fluid and reservoir temperatures. The silica concentration in the production fluid is mostly governed by the maximum oversaturation possible in regard to quartz. A heavy oversaturation in regard to iron oxides and oxi-hydroxides for the Fenton

Hill and Rosemanowes fluids indicates that the reservoir conditions are probably more acidic and reducing than those given by surface observations.

2.5.2 Analysis of the data from the 1997 circulation test

The 1997 circulation test lasted from July 12 to November 16. The chemical data come from three sources. First, the field monitoring performed just after sampling, with analysis measurements at temperatures between 19 and 52°C. This monitoring includes pH, Eh, O_2 content and electrical conductivity, as well as alkalinity. Ca and Cl are obtained by titration and SiO_2 by colorimetry. Fluid samples were regularly taken for more complete analyses. Unfortunately, these samples were analysed only one and a half year after the end of the circulation test. The samples were then analysed both by the Bureau de Recherches Géologiques et Minières (BRGM) and the Centre de Géochimie de la Surface de Strasbourg (CGS). The cation values come from acidified samples.

The evolution of the pH shows a stabilisation between 5 and 5.3 (Figure 2.5.2). However, fluid cooling and some CO_2 degassing during the sampling lead to an increase of the pH before recording measurement. A measurement performed directly in the surface circuit after the heat exchanger gave a pH value of 4.8 at 60-65°C.

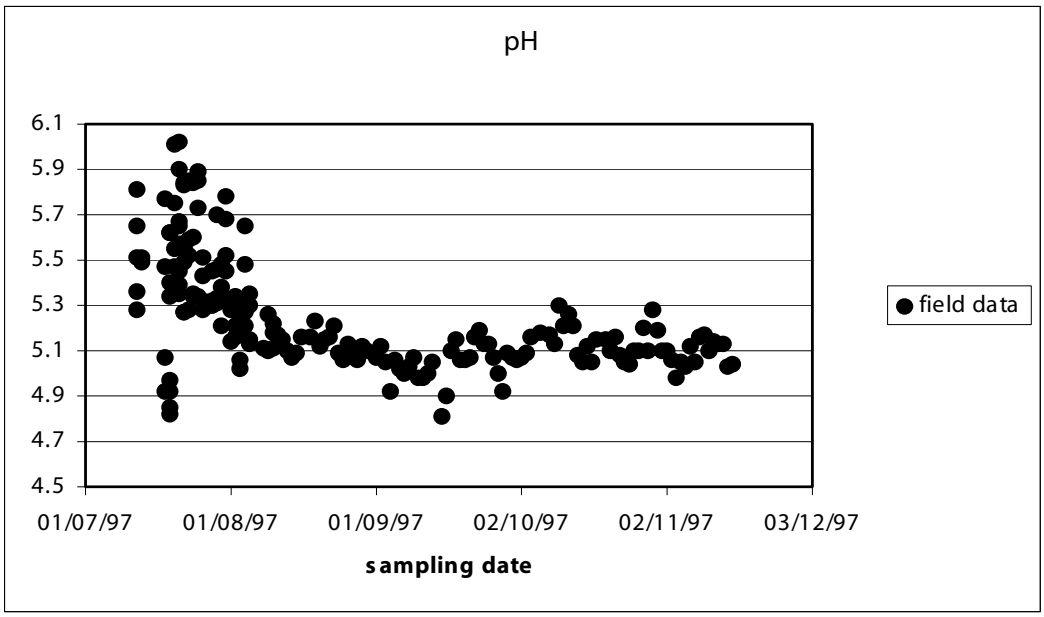

Figure 2.5.2 Evolution of the pH of the fluid sampled during the 1997 circulation test.

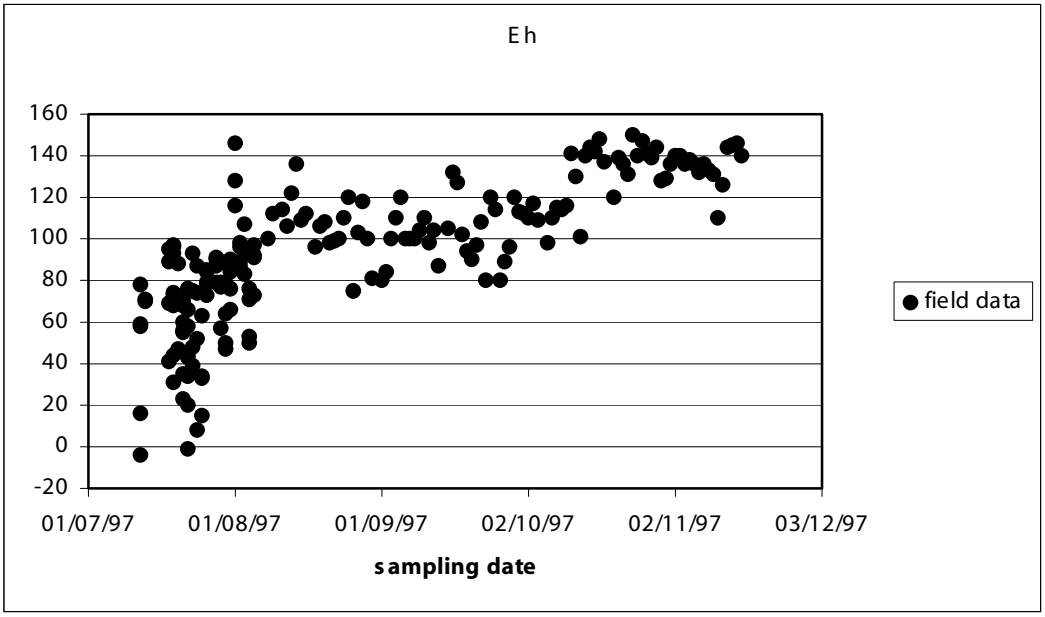

Figure 2.5.3 Evolution of the Eh of the fluid sampled during the 1997 circulation test.

Despite the evolution of the measured redox potential (Eh) toward a more or less stable value between 120 and 150 mV, it is improbable that it reflects the condition in the reservoir (Figure 2.5..3). The redox potential can be subject to rapid changes during upflow and sampling due to interaction with the casing, cooling and degassing. As an illustration, the gas analyses on samples taken between 1845 and 3500 m show an H_2 content ranging from 0.25% to 7.2%, whereas wellhead samples range from 20.1% to 46.3%.

The dissolved oxygen content (O_2) reached quickly a very low value and the few values higher than the detection limit after September 1997 probably came from O_2 introduced during sampling (Figure 2.5.4).

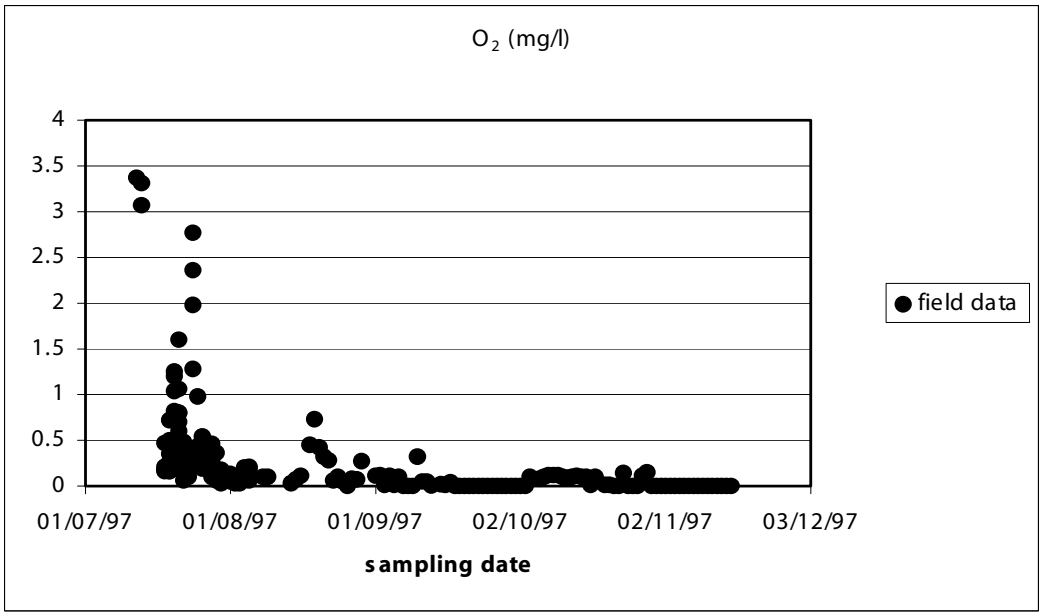

Figure 2.5.4 Evolution of the dissolved O_2 content of the fluid sampled during the 1997 circulation test.

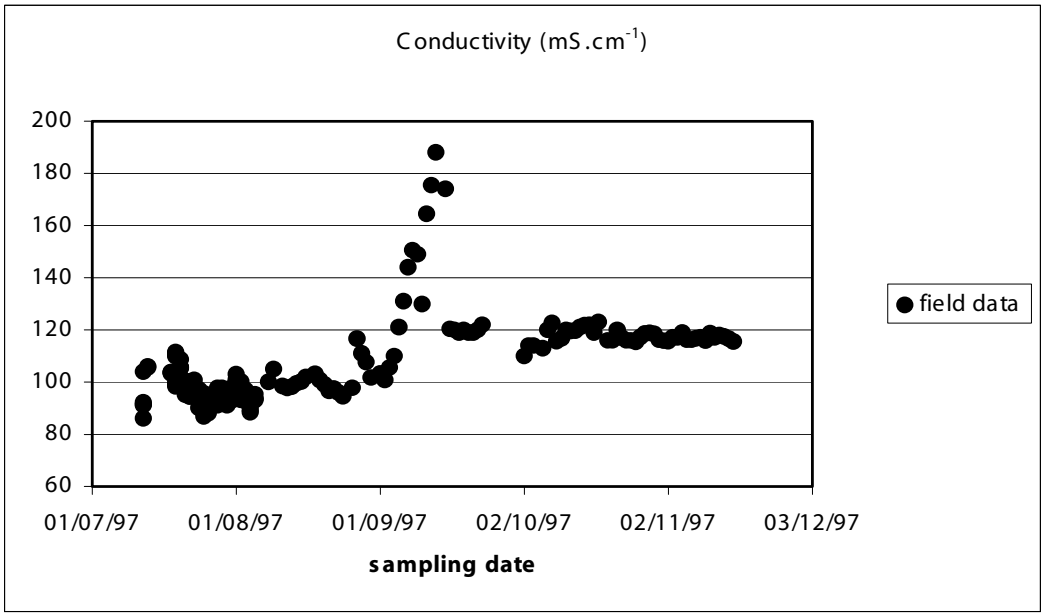

Figure 2.5.5 Evolution of the conductivity of the fluid sampled during the 1997 circulation test.

The conductivity of the fluid seems to reflect the evolution of the salinity except for the first half of September (Figure 2.5.5). The cause of this increase is unknown, but it began by coincidence after the cleaning of the heat exchanger in August 27 and ended with the next cleaning in September 16.

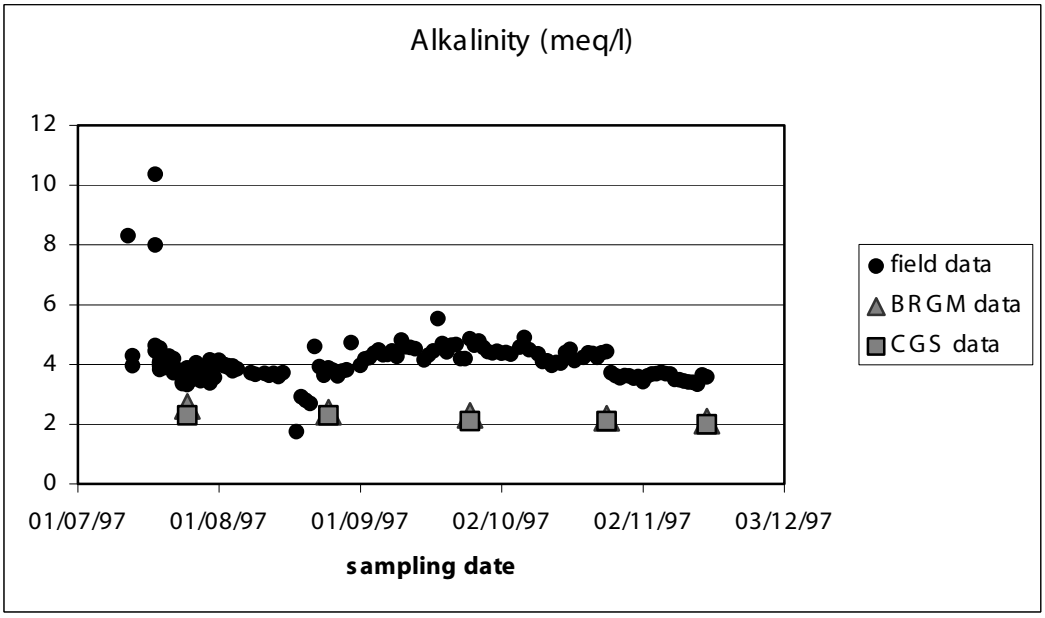

Figure 2.5.6 Evolution of the alkalinity of the fluid sampled during the 1997 circulation test.

After the first two weeks of circulation, the alkalinity measured in situ fluctuated around 4 meq/l (Figure 2.5.6). The variations are still abnormally high, given the stability of pH and Ca concentration. This seems to indicate a sampling problem probably due to CO_2 degassing. The alkalinity values analysed at the BRGM and CGS laboratories one and a half year after the sampling are not really pertinent.

The chloride concentration given by field titration reached a plateau around 1500 mmol/l (Figure 2.5.7). The concentration obtained by ionic chromatography in CGS and BRGM are slightly higher, respectively 1564 and 1608 mmol/l for the last sample.

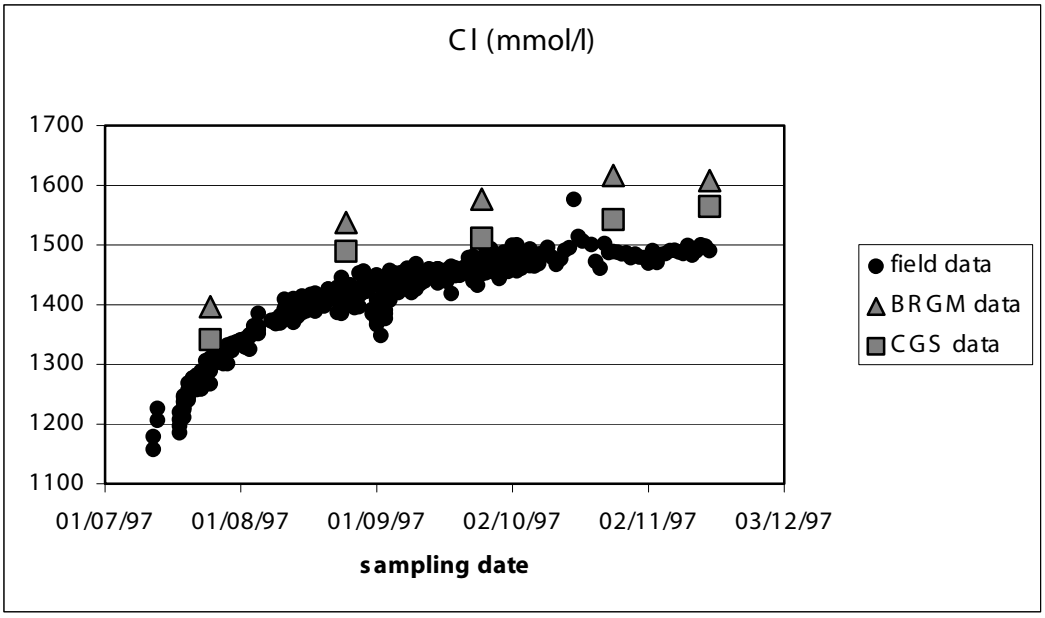

Figure 2.5.7 Evolution of the chloride concentration in the fluid sampled during the 1997 circulation test.

The Na concentration rose during the test from around 950 to 1063 mmol/l (CGS analyses) and 1100 mmol/l (BRGM analyses) (Figure 2.5.8).

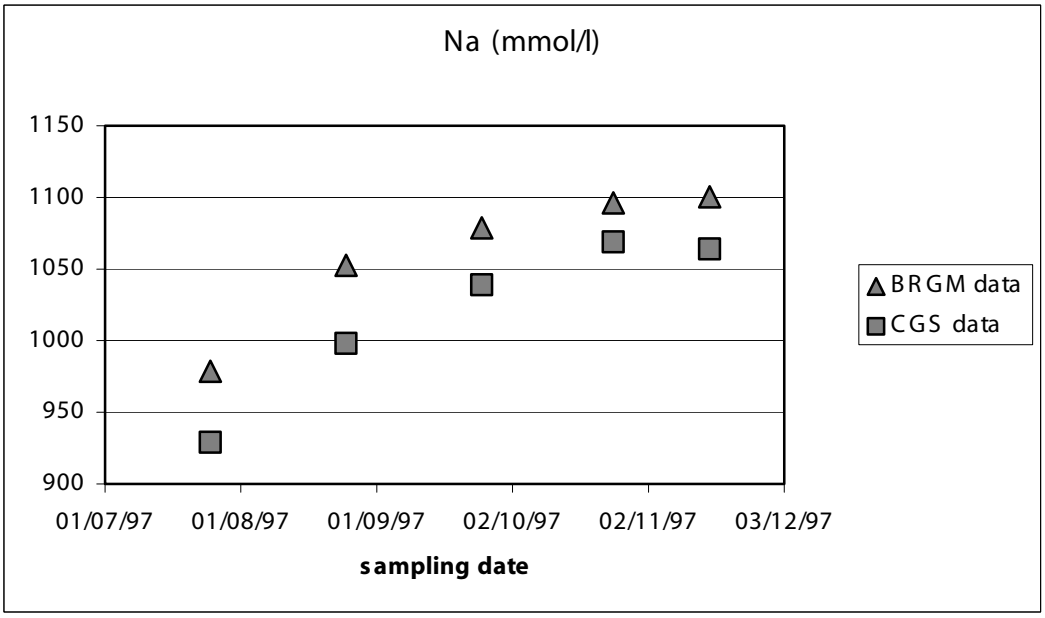

Figure 2.5.8 Evolution of the sodium concentration in the fluid sampled during the 1997 circulation test.

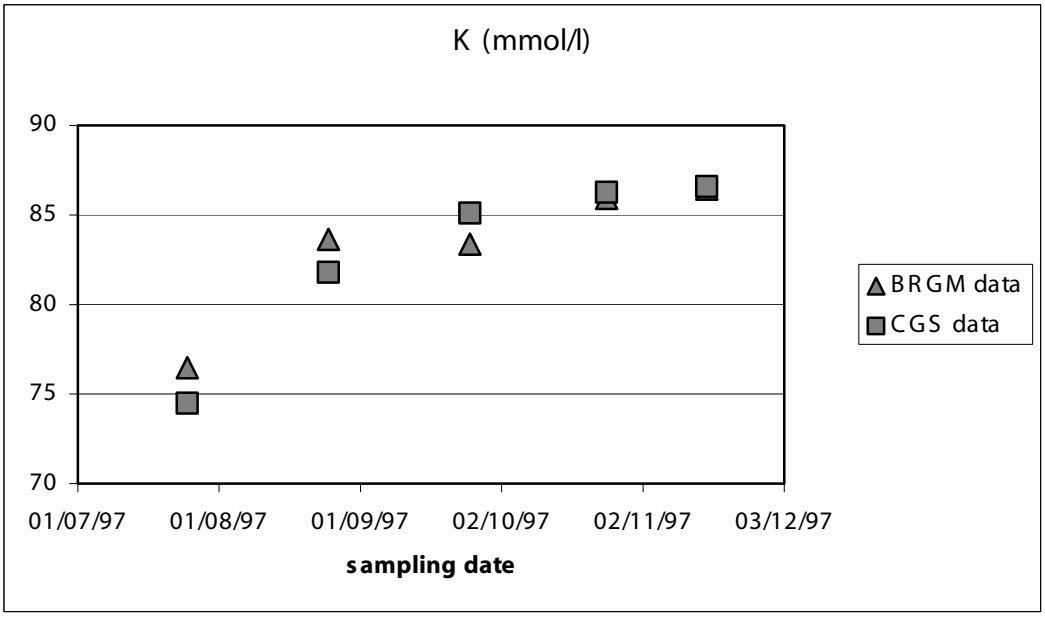

Figure 2.5.9 Evolution of the potassium concentration in the fluid sampled during the 1997 circulation test.

Considering the CGS and BRGM analyses, the potassium concentration started from 74, respectively 76 mmol/l and reached 87, respectively 86 mmol/l by the end of the test (Figure 2.5.9).

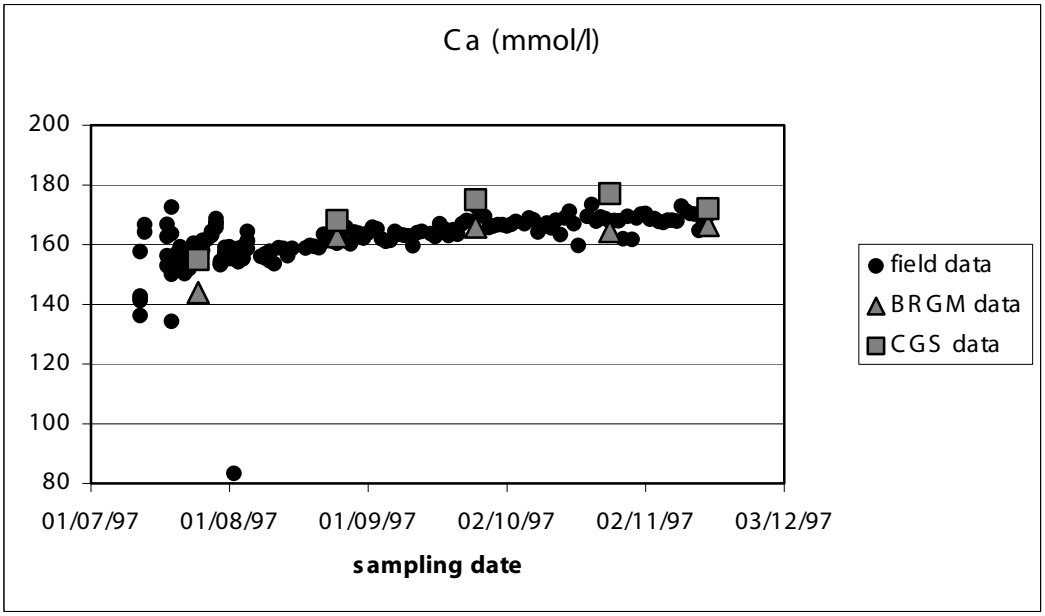

Figure 2.5.10 Evolution of the calcium concentration in the fluid sampled during the 1997 circulation test.

The three data sets show a slight evolution of the calcium concentration toward a stabilisation (Figure 2.5.10). Field titrations and CGS results range from 155 to 172 mmol/l and BRGM analyses from 144 to 166 mmol/l

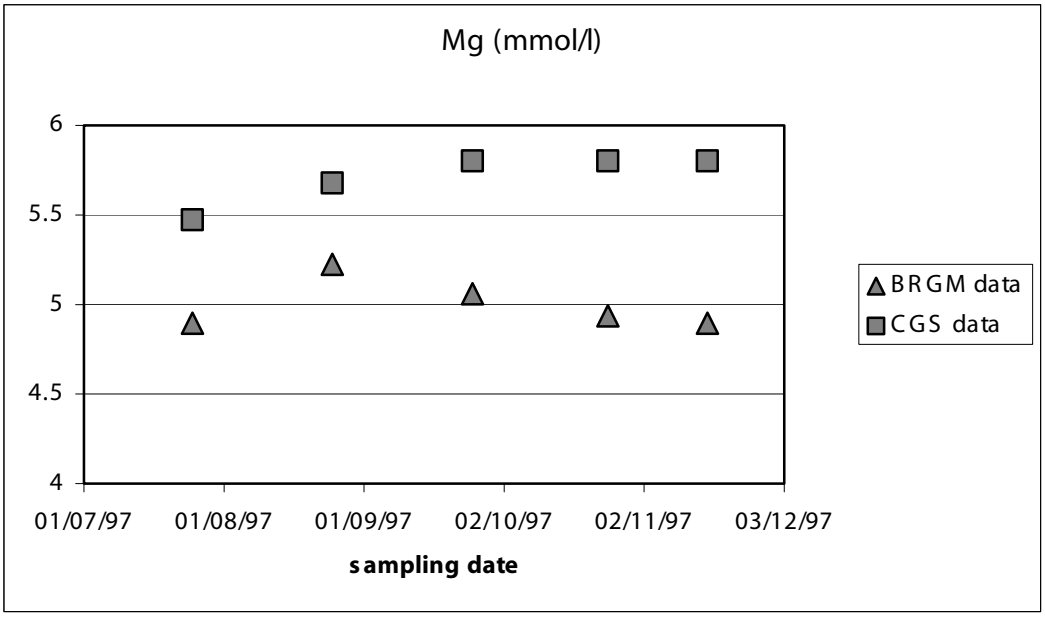

Figure 2.5.11 Evolution of the magnesium concentration in the fluid sampled during the 1997 circulation test.

The magnesium concentration was more stable than calcium concentration and ended at 5.8 mmol/l (CGS data) and 4.9 mmol/l (BRGM data) (Figure 2.5.11).

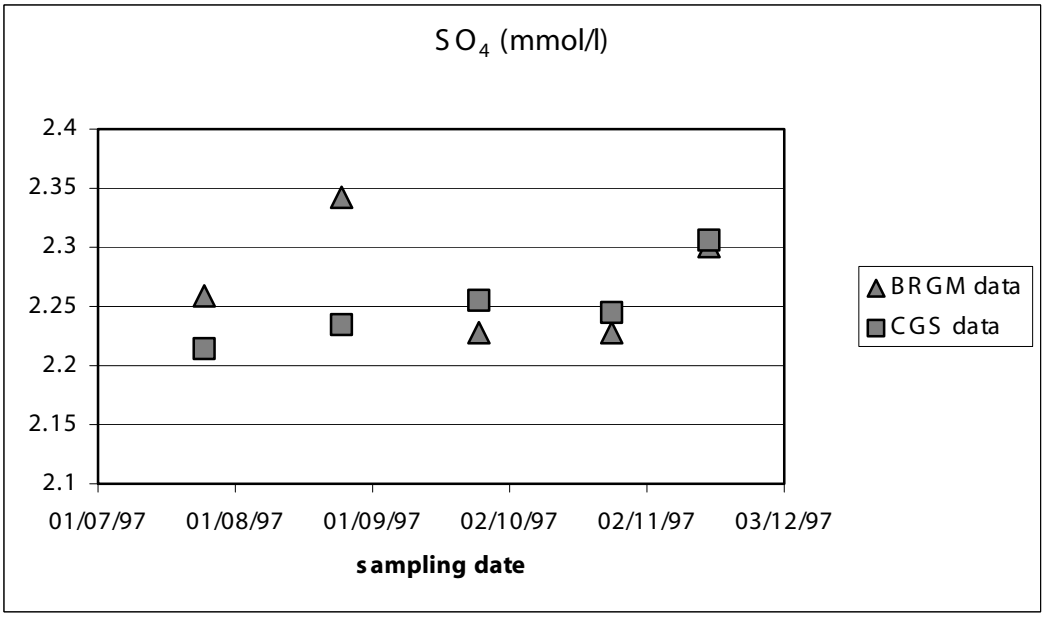

Figure 2.5.12 Evolution of the sulphate concentration in the fluid sampled during the 1997 circulation test.

Like magnesium concentration, the sulphate content did not vary much (Figure 2.5.12). The BRGM data show some fluctuations, but in both datasets the concentration ends at 2.30 mmol/l.

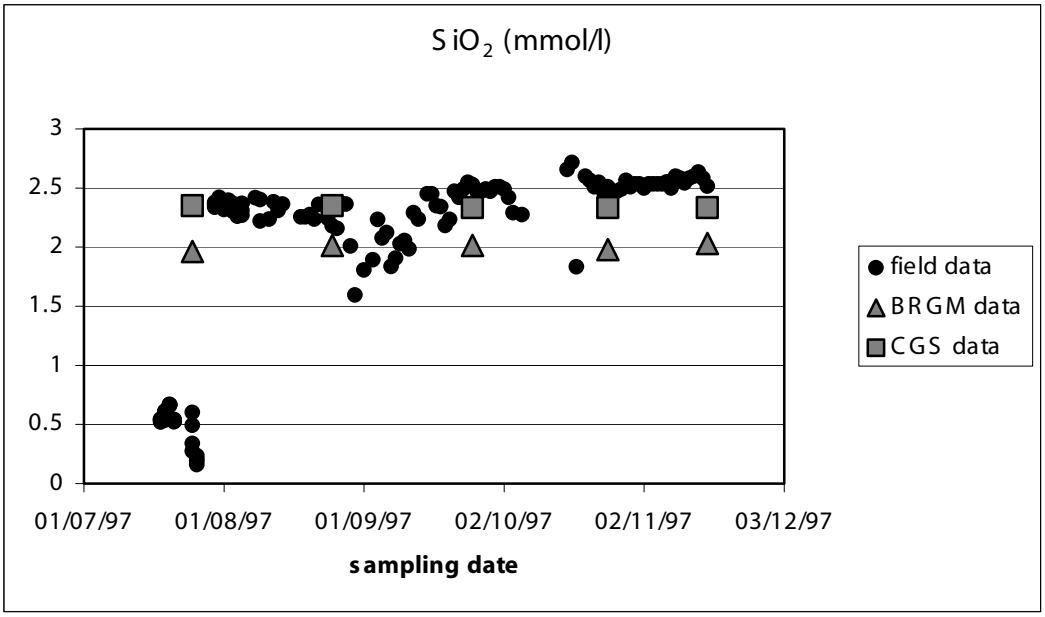

Figure 2.5.13 Evolution of the silica concentration in the fluid sampled during the 1997 circulation test.

The field silica data of the first 15 days reflect a problem in the analytical procedure (Figure 2.5.13). The next measurements show a slight increase from 2.3 to 2.6 mmol/l until the end of the test. The concentration fall after August 27 can also be observed on chloride data and follows a cleaning of the heat exchanger. The analyses from CGS and BRGM are more stable and start respectively at 2.35 and 1.97 mmol/l for ending at 2.33 and 2.03 mmol/l.

The values used as a starting point for the modelling of the fluid come from the sample KP3-97-600 taken on November 16, 1997 and analysed at the CGS (Table 2.5.4). This choice was guided by the fact that the last sample from the test should be more representative of the original reservoir fluid and that the CGS analyses are closed to the field analyses.

The complete analysis of the same sample realized by both the BRGM and the CGS is summarized in Table 2.5.5.

Table 2.5.4 Fluid composition used in modelling. All concentrations are in mmol/l.

Sample	Date	Cl	Na	K	Ca	Mg	SO_4	SiO_2	Fe	F
KP3-600	16/11/97	1564	1064	86.6	172	5.81	2.3	2.33	0.54	0.21

Table 2.5.5 Fluid composition of the sample KP3-600 from GPK2 well, analysed by the BRGM and the CGS. All concentrations are in mmol/l.

Major elements			Trace elements		
	BRGM	**CGS**		**BRGM**	**CGS**
Cl	1608	1564	**Ba**	$7.28 \cdot 10^{-3}$	
Na	1100	1064	**As**	$1.47 \cdot 10^{-1}$	
K	86.4	86.6	**Rb**	$2.64 \cdot 10^{-1}$	
Ca	166	172	**Cs**	$9.86 \cdot 10^{-2}$	
Mg	4.90	5.81	**Al**	$2.97 \cdot 10^{-3}$	$1.48 \cdot 10^{-2}$
SO_4	2.30	2.31	**Ni**	$1.31 \cdot 10^{-3}$	
SiO_2	2.03	2.33	**Cu**	$2.52 \cdot 10^{-4}$	
Br	2.89		**Co**	$1.53 \cdot 10^{-4}$	
B	2.71		**Cr**	$8.27 \cdot 10^{-4}$	
Sr	5.25		**Cd**	$8.90 \cdot 10^{-5}$	
Li	25.2		**Zn**	$3.49 \cdot 10^{-2}$	
Fe		$5.4 \cdot 10^{-1}$	**Ag**	$< 4.63 \cdot 10^{-5}$	
F		$2.1 \cdot 10^{-1}$	**Ti**	$9.44 \cdot 10^{-4}$	
Mn	$2.97 \cdot 10^{-1}$	$2.37 \cdot 10^{-1}$	**Pb**	$1.25 \cdot 10^{-3}$	$< 5 \cdot 10^{-4}$
			PO_4		$8.00 \cdot 10^{-3}$

2.5.3 First geochemical analyses of the new reservoir fluid at 5000 m

The former production well GPK-2 has been deepened to 5000 m, where the reservoir temperature reaches 200°C. The open hole part of the well (4431 to 5048 m) presents a producing zone. A 40-day production test was carried out and the fluid was sampled and analysed by the BRGM (Table 2.5.6). The composition of this fluid is close to that of the upper reservoir (3600 m) except for silica (6.8 mmol/l), iron (2.6 mmol/l), magnesium (3.2 mmol/l) and sulphate (1.6 mmol/l). The silica and iron concentration rise should come from the higher solubility of quartz and pyrite at 200°C and the sulphate decrease should reflect the lower solubility of sulphates minerals at this high temperature.

Table 2.5.6 Chemical composition of the fluid from the new reservoir (5000 m) sampled in GPK2. All concentrations are in mmol/l.

Date	**Sampling location**	**pH**	**Cl**	**Na**	**K**	**Ca**	**Mg**	**SO_4**	**SiO_2**	**Fe**	**TDS g/l**	**Alk. meq/l**
05/11/99	Wellhead	6.09	1733	1392	62.6	120	2.30	2.63	3.91	2.56	102	8
26/11/99	Wellhead	5.43	1631	1166	73.6	165	3.08	1.74	6.81	1.73	94.8	6.6
29/11/99	Wellhead	5.41	1626	1140	74.4	165	3.16	1.75	6.53	1.93	94.1	6.3
3/12/99	Wellhead	5.46	1651	1148	73.4	169	3.20	1.73	6.06	2.61	95.4	7.7
2/12/99	650 m	5.45	1665	1192	93.3	169	4.03	1.62	na	1.71	97.2	na
2/12/99	650 m	5.51	1651	na	na	na	na	1.61	na	na	na	na
2/12/99	700 m	5.72	na	1196	96.6	172	4.07	na	na	na	na	na

2.6 Synthesis

Since the 1980's, numerous research projects have been completed, linked to the Soultz-sous-Forêts geothermal programme. Among them, topics such as tectonics, geothermal gradient, heat flow, fluid flow within the Rhine graben, fluid and rock geochemistry, water-rock interaction and petrography were studied. They provide now a wealth of data and interpretation, leading to a sound knowledge of the Rhine graben history and its geological, thermal and hydraulic processes.

Results of the thermal-hydraulic modelling show the presence of large-scale exchange of saline fluids between the Buntsandstein (Lower Triassic) and the upper part of the crystalline basement in a series of small convection cells. Below the Hot Dry Rock experiments zone (3 to 5 km), there is a slow but pervasive seepage of fluids from the bottom of the graben up to the Soultz area. This extensive fluid flow transfers heat, but small amounts of water, and consequently, the effect on the composition of the deep saline fluids is limited.

Hydrothermal alteration of the fractured granite strongly modified the petrophysical and mineralogical conditions of the rock, where fluid flow is observed at depth. Indeed, the formation fluid in fractures is not in contact with fresh granite, but with hydrothermalised granite blocks partly cemented by alteration products.

Representative fluid samples are difficult to collect from deep wells, especially if they are not under a prolonged production period. Discrete sampling at wellheads after a limited production test may be difficult to interpret (cooling, degassing, transient chemical conditions), but the same problems can occur with downhole sampling. During the only long-term circulation test carried out in the reservoir at 3.0-3.5 km, numerous samples have been collected and measured, but the chemical analyses were carried out 1.5 years after, which left analytical uncertainties. Other samples from previous tests were treated rapidly, but they may not be most representative of the thermal and hydraulic deep reservoir conditions. Nevertheless, all these fluid samples collected from the wells in the fractured granite (2 to 5 km) show the existence of a sodium chloride (Na-Cl) brine with a total salinity of about 100 g/l. A great similarity is observed between the fluids circulating in fractured and altered granite, and those sampled in the Triassic formation.

During the 1997 circulation test, physico-chemical parameters were monitored (pH, Eh, O_2 and conductivity) and a few chemical analyses performed (Alkalinity, Cl, Ca and SiO_2), allowing to estimate when the conditions reached the equilibrium. At the end of this 4-month test, one could deduce that wellhead samples and measurements were more or less at equilibrium, except for temperature. Therefore, the analysis of the last collected sample has been considered as representative of the deep reservoir and has been used during the present study for geochemical modelling.

After the deepening of well GPK2, the open hole section from 4431 to 5048 m was put to production and fluid and gas samples were collected. Wellhead- and depth- (650 –700 m) samples were collected, and the analyses of the conservative parameters (Na, K, Ca, Cl) show similar results compared to the shallower reservoir.

After the creation of the deep reservoir and the construction of the pilot power plant, only the first long-term production period of at least one year will allow to verify if fluids of different composition will intermix with the hot fractured granite reservoir of Soultz-sous-Forêts.

3. Thermodynamic modelling

3.1 Basis of the thermodynamic modelling

The first step of the geochemical modelling consists in characterising the state of the fluid-rock system and to determine which are the possible chemical evolutions. This is done by considering the fluid-rock system, as a thermodynamic system formed by mineral, fluid and gaseous species. The thermodynamic laws will then be used to calculate the direction in which the system can potentially evolve.

3.1.1 Thermodynamic bases of the modelling

The system considered is constituted of all mineral phases in contact with the fluid, all gases present and all aqueous species. These species include of course H_2O but also all species that can be formed by the elements present in the fluid: simple ions like H^+, Ca^{++} or Fe^{++} and complex species like $Fe(OH)^+$, CO_3^{--} or $CaHCO_3^+$.

The free energy of the system can be expressed as:

$$G = \sum_{i=1}^{N} q_i \mu_i \qquad \text{Eq. 3.1.1}$$

where: G is the Gibbs free energy (J)

q_i is the quantity of component i in the system (mol)

μ_i is the chemical potential of component i ($J.mol^{-1}$)

N is the number of components of the system.

A reaction can spontaneously occur if it involves a diminution of the system free energy.

Each chemical reaction such as " $CaMg(CO_3)_2 + 2H_2O \rightarrow Ca^{++} + Mg^{++} + 2HCO_3^- + 2OH^-$ " can be written as:

$$\sum_{j=1}^{Re} \nu_j r_j \rightarrow \sum_{i=1}^{Pr} \nu_i p_i \qquad \text{Eq. 3.1.2}$$

where: r_j is the reactant j

p_i is the product i

ν_i is the stoechiometric coefficients of components i

Re and Pr are the total number of reactants, respectively products, in the reaction.

The variation of free energy corresponding to the reaction involving ν_j moles of component r_j at constant temperature and pressure will be:

$$\Delta G = RT \ln\left[\frac{Q}{K}\right] \qquad \text{Eq. 3.1.3}$$

where: ΔG is the variation of free energy ($J.mol^{-1}$)

R is the ideal gas constant (8.31451 $J.mol^{-1}.K^{-1}$)

T is the temperature of the system (K)

Q is the ionic activity product (dimensionless)

K is the equilibrium constant of the reaction (dimensionless).

The ionic activity product is defined as:

$$Q = \frac{\prod_{i=1}^{\mathrm{Pr}} a_i^{\nu_i}}{\prod_{j=1}^{\mathrm{Re}} a_j^{\nu_j}} \qquad \text{Eq. 3.1.4}$$

where a_i is the activity of component i calculated as:

$$a_i = \gamma_i m_i \qquad \text{Eq. 3.1.5}$$

where: γ_i is the activity coefficient of component i

m_i is the molality of component i in the system (mol.kg^{-1}).

The equilibrium constant is defined as:

$$K = \exp\left[-\frac{\Delta G^0}{RT}\right] \qquad \text{Eq. 3.1.6}$$

where ΔG^0 is the standard free energy variation associated to the reaction (J.mol^{-1}). ΔG^0 can be calculated from the standard formation free energy of each reaction component (Eq. 3.1.7).

$$\Delta G^0 = \sum_{i=1}^{\mathrm{Pr}} G_{fi}^0 - \sum_{j=1}^{\mathrm{Re}} G_{fj}^0 \qquad \text{Eq. 3.1.7}$$

3.1.2 Equilibrium in solution

The reactions in the aqueous phase can be considered reversible and almost instantaneous. The only notable exceptions will be some redox reactions which can be slow. Consequently, these reactions will be treated in the chapter of kinetic modelling. Considering this assumption, the aqueous system will remain in an equilibrium state. Expressed differently, this means that its free energy will remain minimal and this can be mathematically expressed as:

$$\begin{cases} \Delta G_1 = 0 \\ \vdots \\ \Delta G_k = 0 \\ \vdots \\ \Delta G_N = 0 \end{cases} \qquad \text{Eq. 3.1.8}$$

which is equivalent to:

$$\begin{cases} \log Q_1 - \log K_1 = 0 \\ \vdots \\ \log Q_k - \log K_k = 0 \\ \vdots \\ \log Q_N - \log K_N = 0 \end{cases} \qquad \text{Eq. 3.1.9}$$

where ΔG_k is the variation of free energy for the reaction k (J.mol^{-1})

Q_k is the ionic activity product of the reaction k (dimensionless)

K_k is the equilibrium constant of the reaction k (dimensionless)

The reactions are considered instantaneous, so the flux of element entering or leaving the system is equal to zero. The other constraints in the system are the preservation of the total quantity of each element and the conservation of the electrical neutrality. For example, if the carbon is present in the system under the species: CO_2, CO_3^{--}, HCO_3^- and H_2CO_3, the variation of the molality of these species should remain constant.

$$Ct_i = \sum_{j=1}^{Sp} \tau_{ji} m_j \qquad \text{Eq. 3.1.10}$$

where: Ct_i is the total concentration of element i ($mol.kg^{-1}$)

τ_{ji} is the quantity of element i contained in species j (mol)

Sp is number of species in the system.

The electrical neutrality is expressed as:

$$\sum_{i=1}^{Sp} m_i z_i = 0 \qquad \text{Eq. 3.1.11}$$

where z_i is the charge of the species i.

The equation system describing the aqueous system is obtained by combining equation 3.1.8 with equations 3.1.4, 3.1.6, 3.1.9, 3.1.10 and 3.1.11. For a system with N equations and El elements, this will give:

$$\begin{cases} \sum_{i=1}^{\mathrm{Pr}_1} \nu_{i1}\left(\log\gamma_{i1} - \log m_{i1}\right) - \sum_{j=1}^{\mathrm{Re}_1} \nu_{j1}\left(\log\gamma_{j1} - \log m_{j1}\right) - \log K_1 = 0 \\ \vdots \\ \sum_{i=1}^{\mathrm{Pr}_k} \nu_{ik}\left(\log\gamma_{ik} - \log m_{ik}\right) - \sum_{j=1}^{\mathrm{Re}_k} \nu_{jk}\left(\log\gamma_{jk} - \log m_{jk}\right) - \log K_k = 0 \\ \vdots \\ \sum_{i=1}^{\mathrm{Pr}_N} \nu_{iN}\left(\log\gamma_{iN} - \log m_{iN}\right) - \sum_{j=1}^{\mathrm{Re}_N} \nu_{jN}\left(\log\gamma_{jN} - \log m_{jN}\right) - \log K_N = 0 \\ Ct_1 - \sum_{j=1}^{Sp} \tau_{j1} m_j = 0 \\ \vdots \\ Ct_k - \sum_{j=1}^{Sp} \tau_{jk} m_j = 0 \\ \vdots \\ Ct_{El} - \sum_{j=1}^{Sp} \tau_{jEl} m_j = 0 \\ \sum_{i=1}^{Sp} m_i z_i = 0 \end{cases} \qquad \text{Eq. 3.1.12}$$

where: γ_{ik} is the activity coefficient of component i from reaction k

m_{ik} is the molality of component i from reaction k in the system ($mol.kg^{-1}$)

ν_{ji} is the stoechiometric coefficients of components i from reaction k.

The resolution of this system provides the repartition of the elements between the different aqueous species, also named the speciation. The knowledge of the speciation allows the calculation of the pH as $pH = -\log a_{H^+}$, as well as the alkalinity. The alkalinity of a solution correspond to the quantity of added H^+ ions needed, from which each new acid addition will cause an equivalent diminution of the pH. For example, 1 mole of CO_3^{--} can absorb 2 mole of H^+ with the reactions

$CO_3^{--} + 2H^+ \rightarrow HCO_3^- + H^+ \rightarrow H_2CO_3$

3.1.3 Fluid-mineral equilibrium

The reactions between the aqueous and mineral phases can be described by the same way. For a mineral dissolution reaction:

$$xMin + \sum_{j=1}^{R} \nu_j r_j \rightarrow \sum_{i=1}^{P} \nu_i p_i \quad \text{(if Min is a pure phase, its activity can be assumed equal to 1)}$$

When speaking of fluid-rock system, $\log \frac{Q}{K}$ is also named the saturation index (SI) of the solution in regard to the mineral. Then the equation 3.1.3 says that when:

- SI<0 the solution is undersaturated in regard to this mineral. The fluid can potentially dissolve this mineral
- SI=0 the solution is in equilibrium in regard to this mineral. No reaction should occur.
- SI>0 the solution is oversaturated in regard to this mineral. The fluid can potentially precipitate this mineral.

However, from a realistic point of view, the reactions between the aqueous phase and mineral phases can not be considered instantaneous and even not spontaneous as the activation energy may require for example a saturation index significantly higher than zero for making the precipitation possible.

3.2 Determination of the activity coefficient

The calculation of the solution speciation and the saturation indexes, as shown in the preceding chapter, requires the knowledge of the thermodynamic activity of the chemical species.

3.2.1 Debye-Hückel theory

The activity of aqueous species in solution depends on its molality but is also affected by the interaction forces between the electrolytes. In the Debye-Hückel theory the influence of the species on each other is quantified by a unique parameter, the ionic strength of the solution expressed as:

$$I = \frac{1}{2} \sum_i m_i z_i^2 \qquad \text{Eq. 3.2.1}$$

The activity coefficient can then be calculated as:

$$\log \gamma_i = \frac{A(T) z_i^2 \sqrt{I}}{1 + a_i^{\,0} B(T) \sqrt{I}} \qquad \text{Eq. 3.2.2}$$

where: A(T) and B(T) are empirical coefficients dependent on the temperature

$a_i^{\,0}$ is an empirical parameter related to the ionic radius of the specie.

This equation is only valid for solution with ionic strength below 0.1 and has been extended by Davies (1962) and Helgeson (1969, 1981) for higher ionic strengths. These extended equations are the most commonly used in geochemical modelling. The Helgeson's one, also called the B-dot Equation is written for electrolytes:

$$\log \gamma_i = \frac{A(T) z_i^2 \sqrt{I}}{1 + a_i^{\,0} B(T) \sqrt{I}} + \dot{B}(T) I \qquad \text{Eq. 3.2.3}$$

where $\dot{B}(T)$ is an empirical coefficient dependent on the temperature.

The activity coefficient of neutral species are set to that of aqueous CO_2 in pure sodium chloride

solution of equal ionic strength.

The activity of the water is expressed as:

$$\log a_w = \frac{1}{\Omega}\left(-\frac{\sum m}{2.303} + \frac{2}{3} A(T) I^{\frac{3}{2}} \sigma\left(4B(T)\sqrt{I}\right) - \dot{B}(T) I^2 \right) \qquad \text{Eq. 3.2.4}$$

where: Ω is the number of mole of water in 1 kg of fluid (≈55.5)

σ is defined by: $\sigma(x) = \frac{3}{x^3}\left(1 + x - \frac{1}{1+x} - 2\ln(1+x)\right)$ Eq. 3.2.5

Nevertheless, equations 3.2.3 and 3.2.4 are only valid for fluid with ionic strengths below 0.8 and the Soultz fluid has an ionic strength around 1.6.

3.2.2 Pitzer theory

A method for the calculation of the activity coefficients in brines has been proposed by Pitzer (1973, 1975). It consists of semi-empirical equations dealing with the interaction between specific electrolytes.

The application of Pitzer equations to an electrolyte solution gives:

$$\ln \gamma_i = \underbrace{\left(\frac{z_i^2}{2}\right) f'(I,T)}_{\text{Debye-Hückel type term}} + \underbrace{2\sum_j \lambda_{ij}(I,T) m_j}_{2^{\text{nd}}\text{ order virial expansion}} + \underbrace{\sum_{j,k}\left(\left(\frac{z_i^2}{2}\right)\lambda'_{jk}(I,T) + 3\mu_{ijk}(T)\right) m_j m_k}_{3^{\text{rd}}\text{ order virial expansion}} \qquad \text{Eq. 3.2.6}$$

and

$$\ln a_w = \left(-\frac{\sum m}{\Omega} - \frac{1}{\Omega}\left(If'(I,T) - f(I,T)\right) + \frac{1}{\Omega}\left(\sum_{i,j}\left(\lambda_{ij}(I,T) + \lambda'_{jk}(I,T)\right) m_i m_j + 2\sum_{i,j,k} \mu_{ijk}(T) m_i m_j m_k \right) \right) \qquad \text{Eq. 3.2.7}$$

with:

$$f(I) = -\left(\frac{9.212AI}{3a^0 B}\right)\ln\left(1 + a^0 B\sqrt{I}\right) \qquad \text{Eq. 3.2.8}$$

$$f'(i) = {df(I)}/{dI}$$

λ_{ij} are second order interaction coefficients dependent on ionic strength and temperature

$$\lambda'(I,T) = {d\lambda(I,T)}/{dI}$$

μ_{ijk} are third order interaction coefficients dependent on temperature

a^0 is the solute hard-core diameter dependent on temperature and pressure.

Harvie et al. (1984), Moller (1988), Greenberg and Moller (1989) and Moller et al. (1998) developed Pitzer's equations for solutions of electrolytes and neutral species in order to model the

Na-K-H-Ca-Cl-SO_4-HCO_3-CO_3-CO_2-H_2-H_4SiO_4 system from 0°C to 250°C. These developments give for water activity:

$$\ln a_w = -\frac{\sum m}{\Omega} - \frac{2}{\Omega}\left(\begin{array}{l} \frac{If'-f}{2} + \sum_c \sum_a m_c m_a \left(B^{\phi}_{ca} + ZC_{ca}\right) \\ + \sum_c \sum_{c'>c} m_c m_{c'} \left(\Phi^{\phi}_{cc'} + \sum_a m_a \Psi_{aa'c}\right) \\ + \sum_a \sum_{a'>a} m_a m_{a'} \left(\Phi^{\phi}_{aa'} + \sum_c m_c \Psi_{cc'a}\right) \\ + \sum_n \sum_c m_n m_c \lambda_{nc} + \sum_n \sum_a m_n m_a \lambda_{na} + \sum_n \sum_c \sum_a m_n m_c m_a \zeta_{nca} \end{array}\right) \quad \text{Eq. 3.2.9}$$

where: a are anions indexes , c cations indexes and n neutral species indexes

$$Z = \sum_i |z_i| m_i \quad \text{Eq. 3.2.10}$$

B_{ij}^{ϕ}, C_{ij}, Φ_{ij}^{ϕ}, Ψ_{ijk} and λ_{ij} are parameters dependent on ionic strength and temperature

ζ_{ijk} is a parameter dependent on temperature.

For a cation M, the activity coefficient can be calculated as:

$$\ln \gamma_M = \left(\begin{array}{l} z_M^2 F + \sum_a m_a \left(2B_{Ma} + ZC_{Ma}\right) \\ + \sum_c m_c \left(2\Phi_{Mc} + \sum_a m_a \Psi_{Mca}\right) + \sum_a \sum_{a'>a} m_a m_{a'} \Psi_{Maa'} \\ + |z_M| \sum_c \sum_a m_c m_a C_{ca} + 2\sum_n m_n \lambda_{nM} + \sum_n \sum_a m_n m_a \zeta_{naM} \end{array}\right) \quad \text{Eq. 3.2.11}$$

with:

$$F = \frac{f'}{2} + \sum_c \sum_a m_c m_a B'_{ca} + \sum_c \sum_{c'>c} m_c m_{c'} \Phi'_{cc'} + \sum_a \sum_{a'>a} m_a m_{a'} \Phi'_{aa'} \quad \text{Eq. 3.2.12}$$

The equation for an anion A is similar, but the equation for neutral species is:

$$\ln \gamma_N = 2\sum_c m_c \lambda_{Nc} + 2\sum_a m_a \lambda_{Na} + \sum_c \sum_a m_c m_a \zeta_{Nca} \quad \text{Eq. 3.2.13}$$

It should be noted that this model does not calculate the entire speciation in the fluid. The number of aqueous species explicitly described in the model is reduced and the effect of the speciation is included in the activity coefficient calculation. For an example, NaOH is not present in the model and the effect of the speciation between NaOH and Na^+ is taken into account in the calculation of Na^+ activity coefficient. This means that combinations of Debye-Hückel's model and Pitzer's model should be made with precaution. The only chemical variables that can be compared without risks are the saturation indexes.

3.2.3 Specific modelling of the Soultz system

In order to highlight the differences between the two models, a parallel modelling of the speciation in solution for a Soultz type brine was carried out at different temperatures with the codes PHREEQC for the Debye-Hückel concept (Parkhurst, 1995) and TEQUIL for the concept of Pitzer (Duan et al.,

1996). The results show that the difference of the saturation indexes foreseen by these models can be really significant as displayed in Figure 3.2.1 (Durst and Vuataz, 2000).

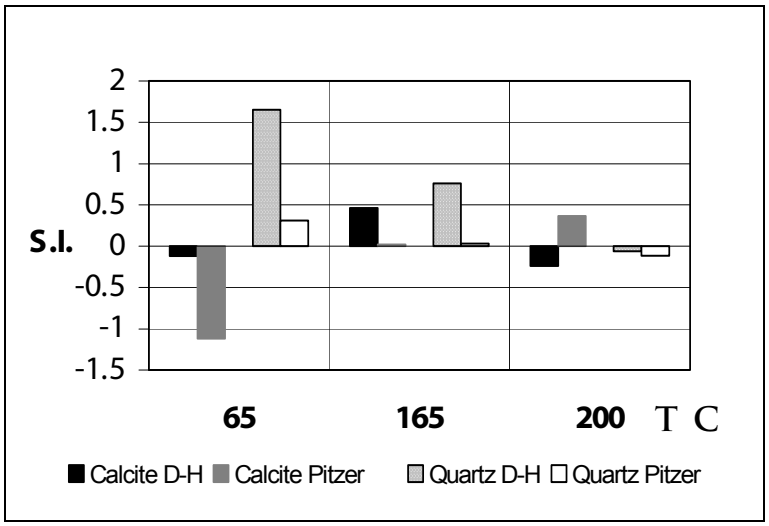

Figure 3.2.1. Comparison between saturation indexes (S.I.) calculated with Debye-Huckel (D-H) and Pitzer formalism at three different temperatures.

The S.I. value of zero for calcite calculated with Pitzer formalism at 165°C comes from the definition of the fluid that was set in equilibrium with the rock at this reservoir temperature.

The application of the Pitzer specific interaction model for the Soultz system has been first studied by Azaroual (1994) who highlighted the need of this approach but also stressed its difficulties. Unfortunately, the use of Pitzer equations brings new problems. Firstly, they increase the complexity of the code and decrease the performances of the model. Secondly, the equations parameters are unknown for aluminium, and for some species like Mg^{++} and Fe^{++}, they are not available at high temperatures (165°C and above). For simplification of the model, some specifications have been worked out for the Soultz system:

- The fluid used is the natural formation fluid.
- No boiling, degassing or condensation takes place in the system.
- There is no mixing with a different type of fluid.
- The fluid-rock interactions do not modify the major species concentration (chlorine and sodium).

Given those assumptions, the only variable parameter having a significant influence on Pitzer's equations and thus on activity coefficients is temperature. This allows the use of a two-step method for the thermodynamic model. First, the activity coefficient of each species is determined at different temperatures for a mean Soultz fluid composition, as discussed in the next chapter.

$$\gamma_i = B_{i0} + B_{i1}T + B_{i2}T^2 + B_{i3}T^3 + B_{i4}T^4 \qquad \text{Eq. 3.2.14}$$

where B_{i0} to B_{i4} are coefficients calculated for each species.

Second, the activity of each aqueous species can be calculated as a simple function of temperature and molality.

$$a_i = \gamma_i(T)m_i \qquad \text{Eq. 3.2.15}$$

This method allows a simple and fast calculation of the activity of aqueous species as well as the speciation, because the activity coefficient does not depend any more on the ionic strength or on the composition of the fluid. Nevertheless this method is really specific to the Soultz system. A variation of the type of fluid modelled will require a new calculation of the B_i parameters and anyway this method will not be suitable in any system where one of the above assumptions does not hold.

3.3 Modelling of the formation brine

3.3.1 Composition of the fluid

The variability of temperature and pressure in the system calls for the utilisation of a concentration unit independent of those parameters that will be the molality in mmol.kg^{-1}. In order to convert the analyses data, the density of the fluid has been calculated in function of pressure and temperature using the relation developed by Batzle and Wang (1992). The density of the Soultz fluid is assumed to be equal to its sodium chloride solution equivalent.

$$\rho_w = 1 + 10^{-6}\begin{pmatrix} -80T - 3.3T^2 + 0.00175T^3 + 489P - 2TP + 0.016T^2P \\ -1.3\cdot 10^{-5}T^3P - 0.333P^2 - 0.002TP^2 \end{pmatrix} \quad \text{Eq. 3.3.1}$$

$$\rho_b = \rho_w + S\left(0.668 + 0.44S + 10^{-6}\cdot\begin{pmatrix} 300P - 2400PS + \\ T(80 + 3T - 3300S - 13P + 47PS) \end{pmatrix}\right) \quad \text{Eq. 3.3.2}$$

Where: ρ_w is the density of water in g.cm^{-3}

ρ_b is the density of the brine in g.cm^3

T is the temperature in °C

P is the pressure in MPa

S is the weight fraction of NaCl

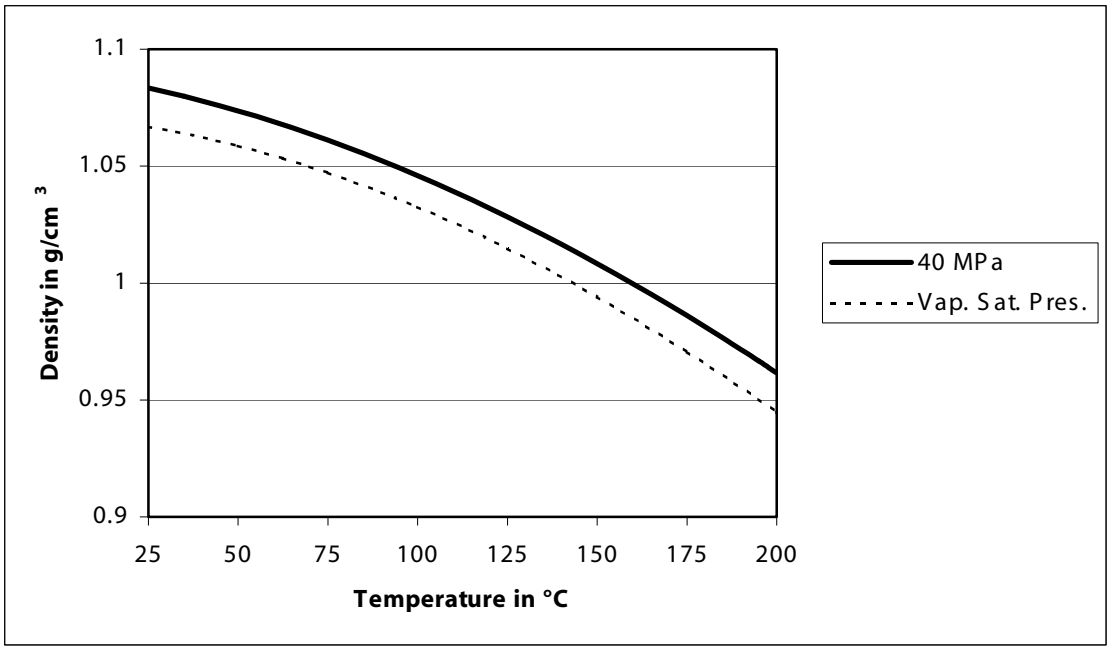

Figure 3.3.1 Density of the Soulz brine in function of temperature at 40 MPa and along vapour saturation pressure curve.

The fluid density at laboratory condition (25°C, 1 bar) is 1.071 g.cm^{-3} and reaches 0.995 g.cm^{-3} for reservoir conditions of 165°C and 40 MPa (Figure 3.3.1).

The modelling of the fluid is based on the reliable data from the 1997 circulation test (Table 3.3.1).

Table 3.3.1 Basic data for the modelling of the brine.

	Na^+	K^+	Ca^{++}	Mg^{++}	Fe^{++}	SiO_2	Cl^-	SO_4^{--}

Composition (mmol.kg^{-1})	**Na^+**	**K^+**	**Ca^{++}**	**Mg^{++}**	**Fe^{++}**	**SiO_2**	**Cl^-**	**SO_4^{--}**
Physicochemical parameters	993	80.8	160	5.42	0.501	2.17	1460	2.19
	T (°C)		**Pressure (MPa)**		**pH**		**Redox**	
	165		40		~ 4.8		Negative	
Mineral phases in equilibrium	Calcite		Dolomite		Pyrite		Quartz	

The first step was the calculation of the amount of carbon dissolved in the fluid. This was done using the assumption that the fluid is in equilibrium in regard to calcite at 165°C with a pH of 4.8. The modelling performed with TEQUIL gives a total dissolved carbon (TDC) of 40.1 mmol.kg^{-1} and for 95% under the form of aqueous CO_2. This value is still dependent on the pH assumption, the TDC would be 25.7 mmol.kg^{-1} for a pH of 4.9 and 61.4 mmol.kg^{-1} for a pH of 4.7.

This modelling also showed that the concentration of sulphate measured (2.19 mmol.kg^{-1}) leads to a high oversaturation of the fluid in regard to anhydrite at 165°C. This mineral has only been observed in one rock sample, therefore the fluid should be at the best in equilibrium in regard to anhydrite. The equilibrium concentration at this temperature is 1.47 mmol.kg^{-1}. Knowing the presence of pyrite in the mineral phase, the negative redox potential of the fluid and the precipitation of galena in the surface installation, the difference observed (0.72 mmol.kg^{-1}) should represent the dissolved sulphides. The concentration of the reservoir fluid in all the elements taken into account in the model is yet characterized (Table 3.3.2).

Table 3.3.2 Composition of the modelled fluid.

	Na^+	**K^+**	**Ca^{++}**	**Mg^{++}**	**Fe^{++}**	**SiO_2**	**Cl^-**	**SO_4^{--}**	**HS^-**	**C**
	993	80.8	160	5.42	0.501	2.17	1460	1.47	0.72	40.1

At the time of this study, no reliable theoretical model existed for the speciation and activity of aluminium, especially in hot brines. For this reason, the aluminium was not included in the thermodynamic model. This prevents the modelling of K-feldspar and clays. Although Jacquot (2000) showed that these minerals are not susceptible to play a significant role in term of volume variation, the clays could influence the chemical composition of the fluid by ion exchange or dissolution/precipitation processes in proportion that cannot be estimated.

3.3.2 Calculation of the activity coefficients

The activity coefficient model described in chapter 3.2 requires the calculation of the γ for an average fluid at different temperatures. For H, O, Na, K, Ca, Si, C, Cl and SO_4 species, this was done with TEQUIL at 50, 80, 110, 140, 170 and 200 °C (Table 3.3.3). This calculation was performed with the composition given in Table 3.3.2 without allowing any mineral or gas precipitation or dissolution. A simulation of a temperature decrease from 165°C to 65°C in presence of calcite shows that 1 kilogram of fluid could dissolve $2.77.10^{-3}$ moles of calcite. A comparison simulating the same cooling in the absence of minerals showed that the difference between the two solutions at 65°C does not produce activity coefficient (γ) variations greater than 3%, confirming the method chosen for γ calculation.

Table 3.3.3 Activity coefficients of aqueous species and H_2O activity calculated using TEQUIL.

Temperature	**50 °C**	**80 °C**	**110 °C**	**140 °C**	**170 °C**	**200 °C**
aH_2O	0.9551	0.9554	0.9561	0.9570	0.9583	0.9599

γNa^+	$7.78 \cdot 10^{-1}$	$7.01 \cdot 10^{-1}$	$7.47 \cdot 10^{-1}$	$7.01 \cdot 10^{-1}$	$6.41 \cdot 10^{-1}$	$5.73 \cdot 10^{-1}$
γK^+	$6.92 \cdot 10^{-1}$	$6.34 \cdot 10^{-1}$	$6.70 \cdot 10^{-1}$	$6.34 \cdot 10^{-1}$	$5.86 \cdot 10^{-1}$	$5.30 \cdot 10^{-1}$
γCa^{++}	$2.79 \cdot 10^{-1}$	$1.79 \cdot 10^{-1}$	$2.17 \cdot 10^{-1}$	$1.79 \cdot 10^{-1}$	$1.41 \cdot 10^{-1}$	$1.04 \cdot 10^{-1}$
$\gamma Ca(HCO_3)^+$	$4.93 \cdot 10^{-1}$	$4.16 \cdot 10^{-1}$	$4.49 \cdot 10^{-1}$	$4.16 \cdot 10^{-1}$	$3.78 \cdot 10^{-1}$	$3.36 \cdot 10^{-1}$
γH^+	1.02	$8.41 \cdot 10^{-1}$	$9.06 \cdot 10^{-1}$	$8.41 \cdot 10^{-1}$	$7.73 \cdot 10^{-1}$	$7.00 \cdot 10^{-1}$
γCl^-	$5.60 \cdot 10^{-1}$	$4.54 \cdot 10^{-1}$	$4.94 \cdot 10^{-1}$	$4.54 \cdot 10^{-1}$	$4.11 \cdot 10^{-1}$	$3.65 \cdot 10^{-1}$
γOH^-	$3.94 \cdot 10^{-1}$	$2.83 \cdot 10^{-1}$	$3.27 \cdot 10^{-1}$	$2.83 \cdot 10^{-1}$	$2.37 \cdot 10^{-1}$	$1.92 \cdot 10^{-1}$
γHCO_3^-	$3.57 \cdot 10^{-1}$	$2.55 \cdot 10^{-1}$	$2.95 \cdot 10^{-1}$	$2.55 \cdot 10^{-1}$	$2.12 \cdot 10^{-1}$	$1.71 \cdot 10^{-1}$
γCO_3^{--}	$2.76 \cdot 10^{-2}$	$9.38 \cdot 10^{-3}$	$1.44 \cdot 10^{-2}$	$9.38 \cdot 10^{-3}$	$5.66 \cdot 10^{-3}$	$3.12 \cdot 10^{-3}$
γSO_4^{--}	$4.31 \cdot 10^{-2}$	$1.66 \cdot 10^{-2}$	$2.47 \cdot 10^{-2}$	$1.66 \cdot 10^{-2}$	$9.88 \cdot 10^{-3}$	$5.59 \cdot 10^{-3}$
$\gamma CaCO_3(aq)$	1.00	1.00	1.00	1.00	1.00	1.00
$\gamma CO_2(aq)$	1.34	1.31	1.32	1.31	1.30	1.30
γH_4SiO_4	1.23	1.16	1.18	1.16	1.14	1.12
$\gamma CaSO_4(aq)$	1.00	1.00	1.00	1.00	1.00	1.00

The calculation of activity coefficients for Mg^{++} at 25°C and 60°C was performed with EQ3nr, using the Harvie, Moller and Weare database. The result gave a γMg^{++} of $3.25 \cdot 10^{-1}$ at 25°C and $2.47 \cdot 10^{-1}$ at 60°C. The equilibrium of the fluid in regard to dolomite at 165 °C gave a γMg^{++} of $1.72.10^{-1}$ at 165°C.

The activity coefficients for HS^- were calculated from 25 to 200°C based on data from Barrett and Anderson (1988) on the solubility of galena in NaCl solution. These data were obtained in a molal solution of NaCl with pH=4 and a dissolved sulphide concentration of 1 $mmol.kg^{-1}$ (Table 3.3.4).

Table 3.3.4 Activity coefficients of HS^-.

Temperature	**25°C**	**50°C**	**100°C**	**150°C**	**200°C**
γHS^-	$1.30 \cdot 10^{-4}$	$1.09 \cdot 10^{-4}$	$1.08 \cdot 10^{-4}$	$5.82 \cdot 10^{-5}$	$1.47 \cdot 10^{-5}$

The calculation of activity coefficients for Fe^{++} at 25°C and 60°C was performed with EQ3nr, using the Pitzer database. The result gave a γFe^{++} of $2.96 \cdot 10^{-1}$ at 25 °C and $2.39 \cdot 10^{-1}$ at 60 °C. The equilibrium of the fluid in regard to dolomite at 16 °C gave a γFe of $1.28.10^{-1}$ at this temperature.

The Figure 3.3.2 schematises the different steps performed for obtaining the activity coefficient model.

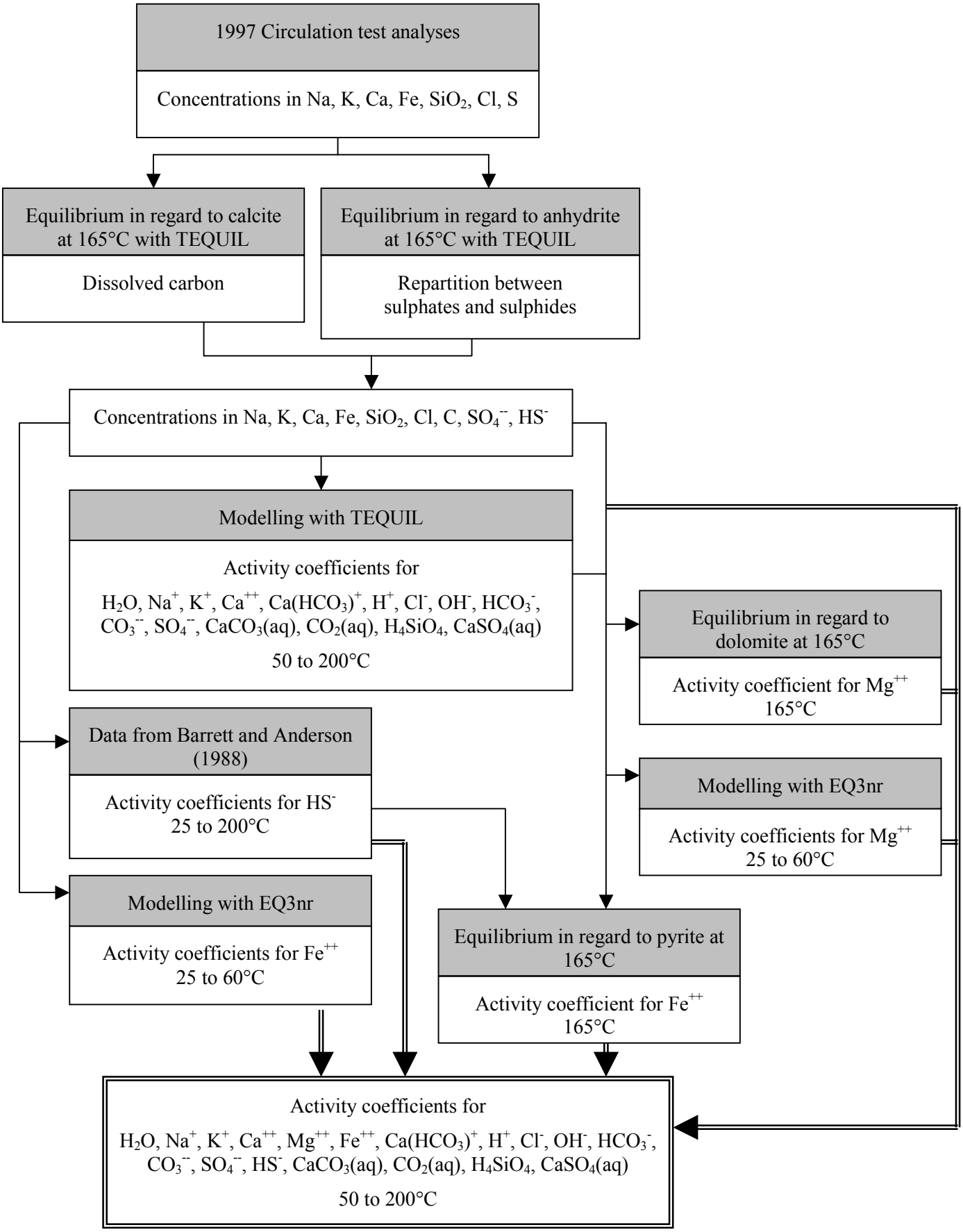

Figure 3.3.2 Schema of the activity coefficient model construction

A polynomial interpolation of the values obtained was performed in order to obtain the coefficient used in equation 3.2.14 (Table 3.3.5).

Table 3.3.5 Coefficients of the equation $\gamma_i = B_0 + B_1 T + B_2 T^2 + B_3 T^3 + B_4 T^4$.

	B_0	B_1	B_2	B_3	B_4
aH2O	0.955608	$-0.268621 \cdot 10^{-04}$	$0.389146 \cdot 10^{-06}$	$-0.125171 \cdot 10^{-08}$	$0.257202 \cdot 10^{-11}$
γNa+	0.955608	$-0.268621 \cdot 10^{-04}$	$0.389146 \cdot 10^{-06}$	$-0.125171 \cdot 10^{-08}$	$0.257202 \cdot 10^{-11}$
γK+	$0.148302 \cdot 10^{+01}$	$-0.316001 \cdot 10^{-01}$	$0.419182 \cdot 10^{-03}$	$-0.229938 \cdot 10^{-05}$	$0.437243 \cdot 10^{-08}$
γCa++	$0.137038 \cdot 10^{+01}$	$-0.424256 \cdot 10^{-01}$	$0.543639 \cdot 10^{-03}$	$-0.292164 \cdot 10^{-05}$	$0.552984 \cdot 10^{-08}$
γH+	$0.294133 \cdot 10^{+01}$	$-0.744534 \cdot 10^{-01}$	$0.949630 \cdot 10^{-03}$	$-0.508025 \cdot 10^{-05}$	$0.956790 \cdot 10^{-08}$
γCl-	$0.171669 \cdot 10^{+01}$	$-0.449296 \cdot 10^{-01}$	$0.574913 \cdot 10^{-03}$	$-0.308265 \cdot 10^{-05}$	$0.581276 \cdot 10^{-08}$
γCO2(aq)	$0.167784 \cdot 10^{+01}$	$-0.131991 \cdot 10^{-01}$	$0.170756 \cdot 10^{-03}$	$-0.931070 \cdot 10^{-06}$	$0.180041 \cdot 10^{-08}$
γSO4--	0.313601	$-0.104143 \cdot 10^{-01}$	$0.131810 \cdot 10^{-03}$	$-0.703870 \cdot 10^{-06}$	$0.133359 \cdot 10^{-08}$
γH4SiO4	$0.193092 \cdot 10^{+01}$	$-0.268539 \cdot 10^{-01}$	$0.337269 \cdot 10^{-03}$	$-0.178498 \cdot 10^{-05}$	$0.334362 \cdot 10^{-08}$
γFE++	0.342837	$-0.197551 \cdot 10^{-02}$	$0.408163 \cdot 10^{-05}$	0	0
γMG++	0.396939	$-0.314796 \cdot 10^{-02}$	$0.108163 \cdot 10^{-04}$	0	0
γHS-	$0.210969 \cdot 10^{-03}$	$-0.507186 \cdot 10^{-05}$	$0.877067 \cdot 10^{-07}$	$-0.609429 \cdot 10^{-09}$	$0.136579 \cdot 10^{-11}$
γCO3--	0.205858	$-0.681574 \cdot 10^{-02}$	$0.854205 \cdot 10^{-04}$	$-0.452599 \cdot 10^{-06}$	$0.852881 \cdot 10^{-09}$
γOH-	$0.163025 \cdot 10^{+01}$	$-0.481896 \cdot 10^{-01}$	$0.619779 \cdot 10^{-03}$	$-0.333916 \cdot 10^{-05}$	$0.632716 \cdot 10^{-08}$
γCa(HCO3)+	$0.137701 \cdot 10^{+01}$	$-0.345803 \cdot 10^{-01}$	$0.446597 \cdot 10^{-03}$	$-0.240895 \cdot 10^{-05}$	$0.455247 \cdot 10^{-08}$
γHCO3-	$0.149635 \cdot 10^{+01}$	$-0.444200 \cdot 10^{-01}$	$0.571479 \cdot 10^{-03}$	$-0.308008 \cdot 10^{-05}$	$0.583848 \cdot 10^{-08}$
γCaCO3(aq)	$0.100000 \cdot 10^{+01}$	0	0	0	0
γCASO4(AQ)	$0.100000 \cdot 10^{+01}$	0	0	0	0

3.3.3 Calculation of the reaction potential of the system

The thermodynamic model can be used to estimate the maximum precipitation or dissolution that might potentially occur when the 165°C fluid is cooled down to 65°C and reinjected in the reservoir. This was done with ChemTough for calcite, dolomite, quartz, and pyrite, allowing only one mineral reaction in each simulation. Lead is not included in the thermodynamic model but an estimation based on galena solubility showed that with the concentration of sulphides available in the fluid, most of Pb can potentially precipitate during cooling.

As a result, each kg of cooled fluid can potentially dissolve 590 mg of calcite and 535 mg of dolomite and can precipitate 98 mg of quartz, 29 mg of pyrite and 0.354 mg of galena. The extrapolation of these values for on year of production in the condition of the 1997 circulation test (25kg.s^{-1}) gave a dissolution of 460'000 kg (170m^3) of calcite and 420'000 kg (155m^3) of dolomite as well as a precipitation of 80'000 kg (30 m^3) of quartz, 22'000 kg (4m^3) of pyrite and 260 kg (0.04 m^3) of galena near the bottom of the injection well. On the basis of this thermodynamic simulation, it appeared that the dissolution of carbonates (325 m^3) seems significantly more important than the precipitation processes (34 m^3), presumably leading to an increase of injectivity. This result should be taken only as an indication of the maximum order of magnitude of the fluid-rock interaction processes. It should be reminded that, from the tracer test carried out during the 1997 production test, the mass of fluid contained within the reservoir has been estimated to $1.04 \cdot 10^6$ tons (Jacquot, 1998).

3.4 Synthesis

The system considered is formed by all mineral phases in contact with the fluid and the most relevant aqueous species. The reactions between the aqueous phase and mineral phases can not be considered instantaneous and even not spontaneous, as the activation energy may require for example a saturation index significantly higher than zero for making the precipitation possible.

Due to the very high salinity of the Soultz fluid, with an ionic strength of 1.6, the determination of the activity coefficient should theoretically not be calculated using the Debye-Hückel theory, limited to an ionic strength smaller than 0.8. On the other hand, the Pitzer theory allows to calculate activity coefficients for brines. Comparative tests at different temperatures showed significant variations of the saturation indexes of calcite and quartz. The use of the Pitzer equations increases the complexity of the code and some parameters of the equations are unknown for aluminium or not available at high temperatures. After simplification of the model, temperature remains the only variable parameter having influence on the activity coefficient and a two-step method allows to calculate the activity of the aqueous species as well as the speciation for the Soultz fluid composition. Starting from the most reliable data of the 1997 circulation test, the amount of dissolved carbon and sulphide are calculated with the code TEQUIL, a model based on the Pitzer theory. Then, considering that the fluid at depth is in equilibrium with calcite, dolomite, pyrite and quartz, all the activity coefficients have been computed.

Finally, the thermodynamic model can be used to estimate the maximum potential for mineral precipitation and/or dissolution, when the fluid is cooled in the heat exchanger from 165 to 65°C and then reinjected into the reservoir. As a result, it appears that the dissolution of carbonates is significantly more important than the precipitation of quartz and sulphide.

4. Kinetic modelling

4.1 Introduction to water-rock interaction kinetics

The thermodynamic model is able to provide the saturation indexes of the fluid in regard to all mineral phases that can potentially play a role in the system. The next step in water-rock interaction modelling is to determine what will really happen. The thermodynamic disequilibria are the drive of the chemical reactions and the kinetic model should look at the mechanisms involved in these reactions in order to predict which reactions actually occur and what will be their rate (Helgeson et al., 1969). The understanding of reaction kinetics is at a much lower level than that of equilibrium chemistry even though rapid progress is being made.

According to Berner (1978), there are two processes that can control the reaction rates (Figure 4.1.1). In systems with low or no fluid flow, the reaction rate depends mainly on the diffusion of aqueous species through the fluid layer close to the mineral surface. In systems with more fluid circulation, the reaction is controlled by the surface reaction rate. The respective importance of the two processes in function of the fluid flow varies in function of their respective rate that can change by several order of magnitude between different reactions. The forced fluid flow in the Soultz system leads to a surface reaction control for minerals with a low reaction rate, like quartz. For carbonates, the exact reaction rate probably depends on the fluid flow. However, as the fine simulation of the flow in the porous space will not be carried out, an average flow will be assumed in the model.

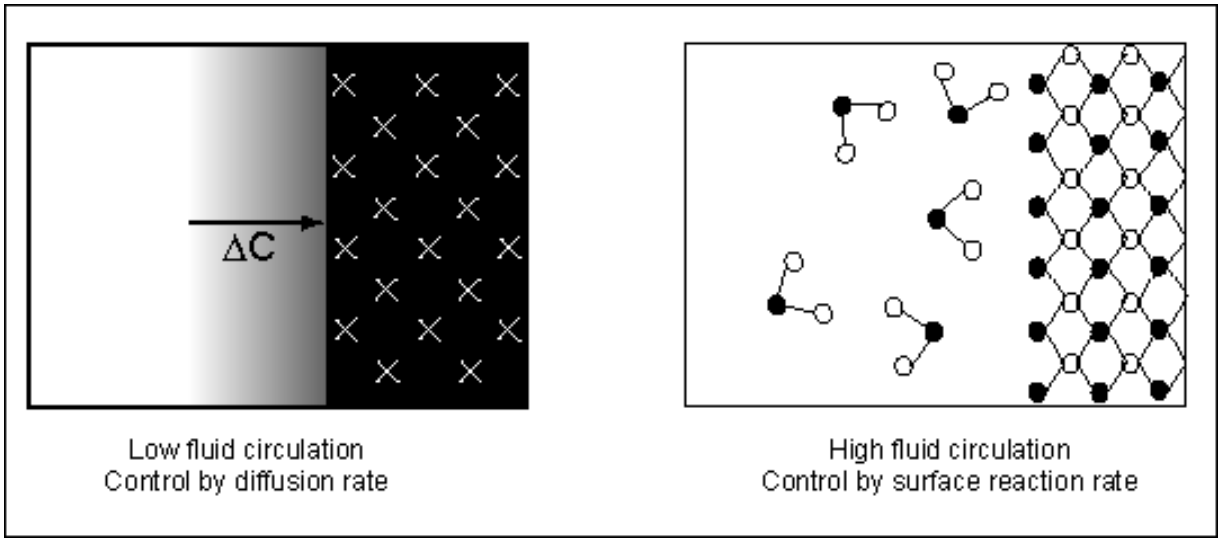

Figure 4.1.1 Diagram of the two processes controlling the reaction rate.

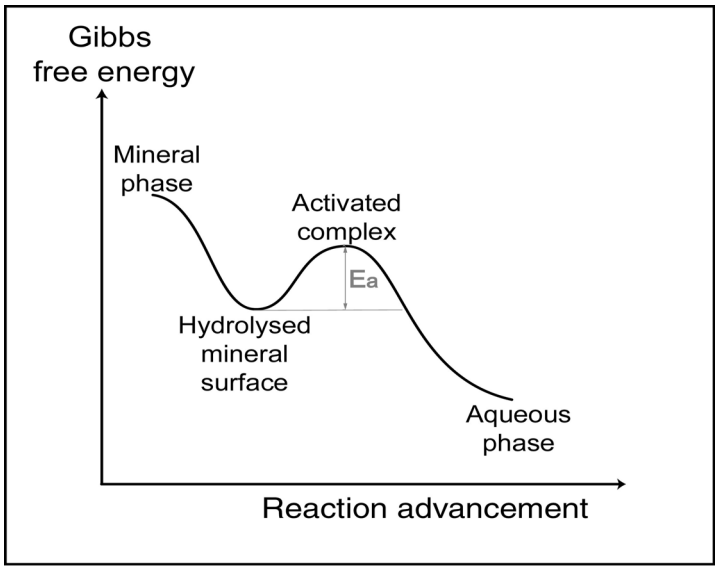

Figure 4.1.2 Schematic representation of the Gibbs free energy change associated with the hydrolysis of a mineral.

The kinetic mechanisms as described by Lasaga (1981) and Aagaard and Helgeson (1982) are based on the Transition state theory (Figure 4.1.2). It involves the formation of an activated complex with a higher Gibbs free energy. The amount of energy needed for the formation of this activated complex is called activation energy E_a. The mathematic formulation of the Transition state theory comes to the general formula for reaction rate as:

$$v = k_c s\left(1-\left(\frac{Q}{K}\right)^p\right)^o \qquad \text{Eq. 4.1.1}$$

for dissolution, and:

$$v = k_c s\left(\left(\frac{Q}{K}\right)^p - 1\right)^o \qquad \text{Eq. 4.1.2}$$

for precipitation, where:

- v is the reaction rate in $mol.s^{-1}$
- k_c is the kinetic constant of the reaction in $mol.m^{-2}.s^{-1}$
- s is the reaction surface area in m^2
- o, p are empirical exponential factors.

k_c can be expressed as:

$$k_c = k_{c0} f\left(a_i^*\right)\exp\left(\frac{-E_a}{RT}\right) \qquad \text{Eq. 4.1.3}$$

where:
- k_{c0} is an constant independent of the conditions in $mol.m^{-2}.s^{-1}$
- $f(a^*_i)$ is a function of the activity of the species involved in the creation and the destruction of the activated complex
- E_a is the activation energy in $J.mol^{-1}$.
- R is the universal gas constant ($8.3144\ J.mol^{-1}.K^{-1}$)
- T is the temperature in °K

The complete modelling of the reaction rates will require the knowledge of a great number of parameters. First, the precipitation or dissolution of a mineral can involve different reaction mechanisms in function of the conditions (pH, temperature, fluid flow...), therefore the appropriate one has to be determined. Second, the parameters n, m, k_0, f and E_a have to be known for each reaction. Third, the variables s, a^*_i and Q/K has to be furnished by the model. The thermodynamic model will provide a^*_i and Q/K and an estimation of s will be discussed in the chapter on coupled modelling, but the parameters for the complete kinetic equation do not always exist, especially for hot brines. Anyway, the equation can be reduced to:

$$v = k_{c0} s f\left(a_i^*\right) g(T) h\left(\frac{Q}{K}\right) \qquad \text{Eq. 4.1.4}$$

where:

- $f(a^*_i)$ is a term accounting on the catalysing or inhibiting effect of the aqueous species (including H^+)
- g(T) is a term accounting on the temperature effect
- h(Q/K) is a term accounting on the distance from thermodynamic equilibrium.

The method chosen in the present study is to build one kinetic law for each dissolution or precipitation reaction. These laws were constructed from data found in published experiments, conducted if possible in NaCl brines.

The work of Jacquot (2000) shows that the carbonates seem to be the most reactive minerals in the Soultz HDR system, but sulphur minerals were not considered in his modelling attempts. The primary goal of the kinetic model will be to simulate precipitation and dissolution of quartz, calcite, dolomite and pyrite. Nevertheless other minerals like feldspar, anhydrite and hematite should later be incorporated in the model, at least to confirm that they do not play an important role. The kinetic modelling of clays has been postponed due to the lack of available parameters and the complexity of the model including variable composition minerals.

4.2 Calcite

4.2.1 Calcite dissolution

Sjöberg and Rickard (1984) showed that far from equilibrium the calcite dissolution rate is controlled by two processes, the surface reaction and the diffusion of H^+ to the mineral surface. According to this study, in the Soultz conditions, the two processes coexist with a predominance of surface reaction. The previous authors used rotating apparatus with a rotational speed from 300 rpm to 5000 rpm. Giving the type of circulation expected in the Soultz reservoir, the values obtained for 300 rpm seem more appropriate (Figure 4.2.1).

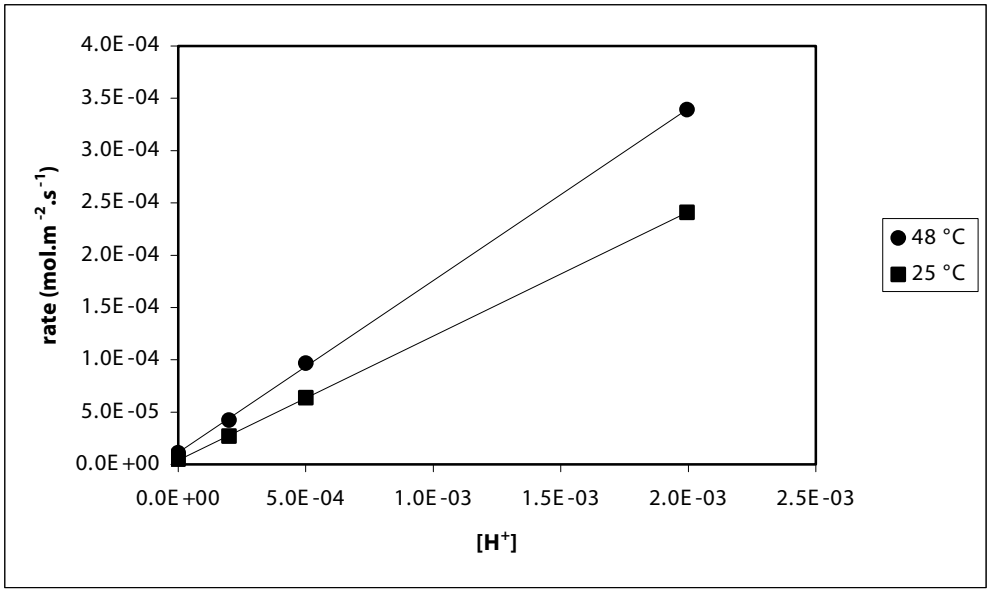

Figure 4.2.1 Calcite dissolution rate at 25 and 48°C in function of H^+ activity from Sjöberg and Rickard (1984).

At a given temperature, the rate can be expressed as a linear function of the activity of H^+. This gives at 48°C (321.15°K):

$$rate_{321.15,a_{H^+}} = 1.643 \cdot 10^{-1} a_{H^+} + 1.11 \cdot 10^{-5} \qquad \text{Eq. 4.2.1}$$

The temperature dependency of the dissolution rate varies with the pH due to the respective proportion of diffusion and surface reaction. The temperature dependent part of the dissolution rate can not be a pure Arrhenius law but must include this pH effect in the form of:

$$g(T, a_{H^+}) = A \exp\left(\frac{-E_A(a_{H^+})}{RT}\right) \qquad \text{Eq. 4.2.2}$$

where: E_A is the activation energy in $J.mol^{-1}$

A is the Arrhenius preexponential factor

R is the universal gas constant (8.3144 $J.mol^{-1}.K^{-1}$)

T is the temperature in °K.

The rate at any temperature and pH will be:

$$rate_{T,a_{H^+}} = (1.643 \cdot 10^{-1} a_{H^+} + 1.11 \cdot 10^{-5}) A \exp\left(\frac{-A'(a_{H^+})}{T}\right), \quad A' = \frac{E_A}{R} \qquad \text{Eq. 4.2.3}$$

A'(a_{H^+}) can be estimated by comparison of the rates obtained at different temperatures.

$$\frac{rate_{T,a_{H^+}}}{rate_{321.15,a_{H^+}}} = \exp\left(\frac{-A'(a_{H^+})}{321.15} - \frac{A'(a_{H^+})}{T}\right) \qquad \text{Eq. 4.2.4}$$

$$A'(a_{H^+}) = \ln\left(\frac{rate_{T,a_{H^+}}}{rate_{321.15,a_{H^+}}}\right)\frac{1}{\frac{1}{321.15}-\frac{1}{T}} \qquad \text{Eq. 4.2.5}$$

The application of Eq. 4.2.5 to the rate obtained at 25 and 48°C show a linear relation between A' and pH (Figure 4.2.2).

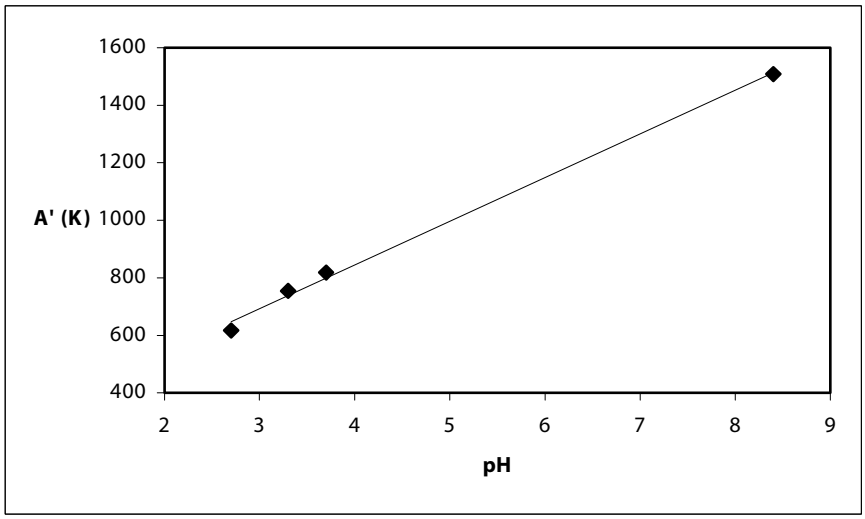

Figure 4.2.2 Activation energy evolution in function of pH.

This relation can be written in function of a_{H^+}:

$$A'(a_{H^+}) = -65.98\ln(a_{H^+}) + 237.1 \qquad \text{Eq. 4.2.6}$$

The equations 4.2.1 and 4.2.2 also impose that:

$$g(321.15, a_{H^+}) = A\left(\frac{-A'(a_{H^+})}{321.15}\right) = 1 \text{ or } A = \left(\frac{A'(a_{H^+})}{321.15}\right)\frac{T}{321.15} \qquad \text{Eq. 4.2.7}$$

The combination of the equations 4.2.3, 4.2.6 and 4.2.7 leads to the calcite dissolution equation:

$$v = \left[\begin{array}{l}\left(1.643\cdot10^{-1}a_{H^+} + 1.11\cdot10^{-5}\right)s\dfrac{T}{321.15} \\ \exp\left(\dfrac{(T-321.15)(-65.98\ln(a_{H^+})+237.1)}{321.15.T}\right)\end{array}\right]\left(1-\frac{Q}{K}\right) \qquad \text{Eq. 4.2.8}$$

In the Soultz system, the rate obtained should lead to a strong calcite dissolution concentrated in the vicinity of the injection point. The lack of data at higher temperature is not likely to cause a significant error due to the fact that most dissolution will occur at temperature close to 65°C. The critical imprecision should comes from the turbulent flows, which can induce some variations in the ratio between surface reactions and H^+ diffusion.

4.2.2 Calcite precipitation

The calcite precipitation law is based on the study from Shiraki and Brantley (1995) on near equilibrium kinetics at 100°C. This fits the Soultz conditions where calcite precipitation should occur

during a progressive heating between 65° and 165°C. The precipitation is dominated by spiral growth for Q/K<1.72 and by surface nucleation at higher oversaturation. The precipitation rate will be (Figure 4.2.3):

$$rate_{100°C} = 10^{-5}\left(\frac{Q}{K} - 1\right)^{1.93} \quad \text{for } \frac{Q}{K} < 1.72 \qquad \text{Eq. 4.2.9}$$

$$rate_{100°C} = 5.25 10^{-4} \exp\left(\frac{-2.36}{\ln\left(\frac{Q}{K}\right)}\right) \quad \text{for } \frac{Q}{K} > 1.72 \qquad \text{Eq. 4.2.10}$$

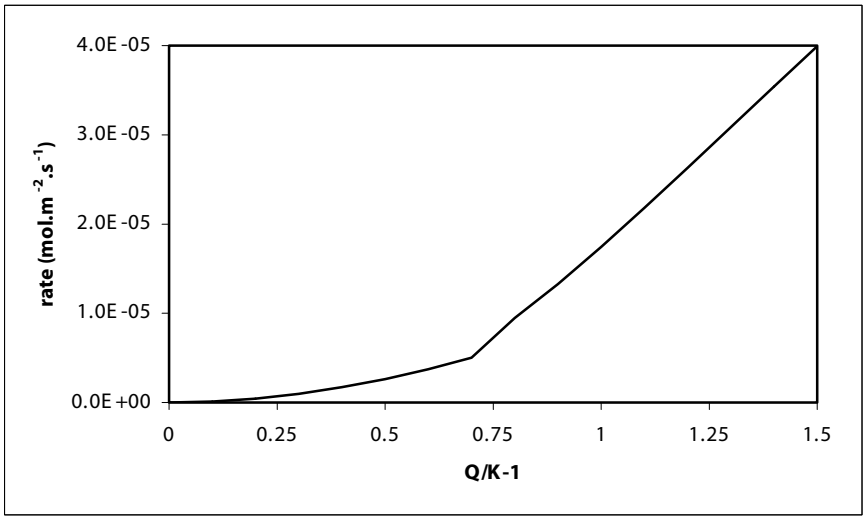

Figure 4.2.3 Calcite precipitation rate at 100 °C in function over saturation.

At higher oversaturation and for low fluid flow, the rate can be controlled by diffusion processes but due to the progressive reheating such conditions are not likely to happen.

Zhang and Dawe (2000) showed a inhibitor effect of the magnesium concentration on calcite precipitation. This effect is not really quantified but it does not seems to be significant for the Ca^{2+}/Mg^{2+} ratio of the Soultz fluid.

The temperature effect is assumed to be dependent on the Arrhenius law for spiral grow (Jacquot 2000):

$$rate_T = rate_{100°C} A \exp\left(\frac{-A_E}{RT}\right) \qquad \text{Eq. 4.2.11}$$

with $A_E = 41.84$ kJ.mol^{-1} this gives:

$$A = 1927T \qquad \text{Eq. 4.2.12}$$

The combination of equations 4.2.9, 4.2.10, 4.2.11 and 4.2.12 gives:

$$\begin{cases} v = 1.9310^{-2} T \exp\left(\frac{-41840}{RT}\right) s\left(\frac{Q}{K}-1\right)^{1.93} & \text{for } \frac{Q}{K} < 1.72 \\ v = 1.011 T \exp\left(\frac{-41840}{RT}\right) s \exp\left(\frac{2.36}{\ln\left(\frac{Q}{K}\right)}\right) & \text{for } \frac{Q}{K} > 1.72 \end{cases} \quad \text{Eq. 4.2.13}$$

In the Soultz system, the re-precipitation rate of calcite will be one or two orders of magnitude less than the dissolution rate. So, if the dissolution is likely to occur near the injection point, the precipitation can potentially take place in a more wider zone. However, the competition between transport, reactions and temperature change does not allow any extrapolation of the calcite deposition behaviour without numerical simulation.

4.3 Dolomite

4.3.1 Dolomite dissolution

The dolomite dissolution law is based on the work of Gautelier et al. (1999). The experiment were performed with pH from –0.39 to 4.44 and temperatures from 25 to 80°C. The results are summarized in Figure 4.3.1.

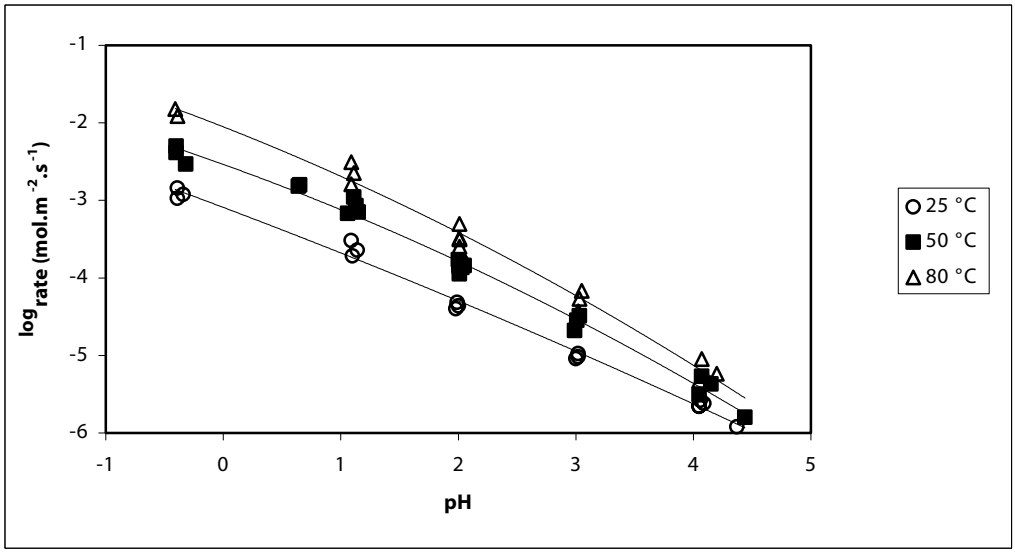

Figure 4.3.1 Dissolution rate of dolomite in function of pH at 25, 50 and 80°C.

The fitting of these plots gives:

$$\log_{rate_{25°C}} = -0.0153\,pH^2 - 0.5723\,pH - 3.0904 \quad \text{Eq. 4.3.1}$$

$$\log_{rate_{50°C}} = -0.0404\,pH^2 - 0.5444\,pH - 2.5358 \quad \text{Eq. 4.3.2}$$

$$\log_{rate_{80°C}} = -0.0436\,pH^2 - 0.5948\,pH - 2.0509 \quad \text{Eq. 4.3.3}$$

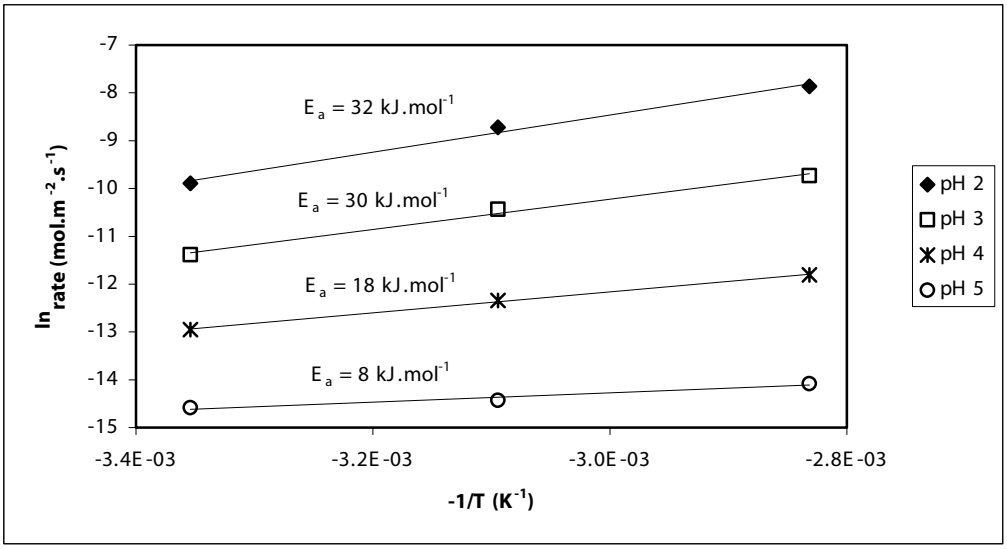

Figure 4.3.2 Evolution of dolomite dissolution rate in function of inverse temperature.

The desired equation should have the form of :

$$rate_T = f(pH)\,A\exp\left(\frac{-E_a}{RT}\right) \qquad \text{Eq. 4.3.4}$$

The equations 4.3.1, 4.3.2 and 4.4.3 allow the calculation of the rate evolution with temperature at constant pH (Figure 4.3.2). From this figure, it is possible to calculate E_a and A:

$$E_a = 49480 - 8080\,pH \quad J.mol^{-1} \qquad \text{Eq. 4.3.5}$$

$$A = 2.104\cdot10^{7}\exp(-2.754\,pH) \qquad \text{Eq 4.3.6}$$

Consequently the dolomite dissolution equation will be:

$$v = \left\{\begin{matrix} 10\text{^}\left(-0.0436\,pH^2 - 0.5948\,pH - 2.0509\right)s \\ 2.104\cdot10^{7}\exp(-2.754\,pH)\exp\left(\frac{972\,pH - 5951}{T}\right)\end{matrix}\right\}\left(1-\frac{Q}{K}\right) \qquad \text{Eq. 4.3.7}$$

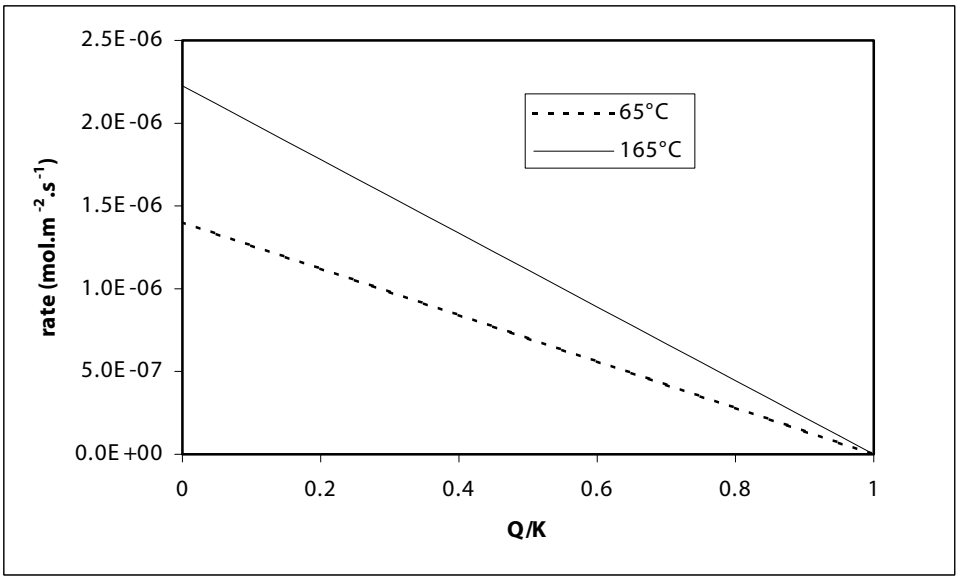

Figure 4.3.3 Dolomite dissolution rate in function of saturation at pH=5 at 65 and 165°C.

The rate obtained (Figure 4.3.3) are two orders of magnitude below the calcite dissolution rate. Although the reaction is still quick, the dolomite dissolution zone can probably extends farther than the calcite's one.

4.3.2 Dolomite precipitation

The dolomite precipitation law comes from the study of Arvidson and Mackenzie (1999). Their experiment were performed with temperatures ranging from 100 to 200°C and pH from 4.8 to 7, and they combined their data with those available in the literature. The accuracy of the rates determined in dolomite precipitation experiments is always questionable due to the competition between dolomite and magnesian calcite formation. The mechanisms involved in dolomite crystal growth seems similar to those involved in calcite.

Arvidson and Mackenzie fitted their data on a crystal growth reaction equation:

$$rate = A\exp\left(\frac{-A_e}{RT}\right)\left(\frac{Q}{K}-1\right)^n \qquad \text{Eq. 4.3.8}$$

Then, the dolomite precipitation will be (Figure 4.3.4):

$$v = 1.122\cdot10^5 s\exp\left(\frac{-16060}{T}\right)\left(\frac{Q}{K}-1\right)^{2.26} \qquad \text{Eq. 4.3.9}$$

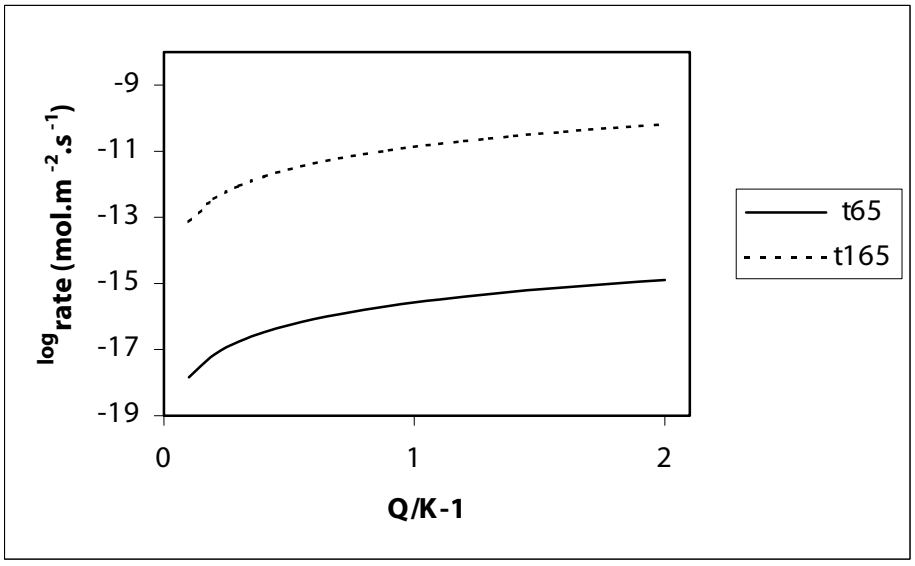

Figure 4.3.4 Dolomite precipitation in function of saturation at 65 and 165°C.

These rate are several order of magnitudes less than calcite precipitation rate. This should cause the calcite precipitation to consume all the Ca^{++} and the CO_2 available first. The precipitation of dolomite in the Soultz system is not likely to happen before a significant increase of the Mg^{++} in the fluid due to dolomite dissolution.

4.4 Quartz

4.4.1 Quartz dissolution

The quartz dissolution equation comes from the work of Dove (1994). This study quantifies the reaction kinetics from 25 to 300°C for solution with pH of 2 to 12 and 0 to 0.3 molal sodium. It is based on the respective participation of three reactions involving the three different surface complexes: >SiOH, >SiO$^-$ and >SiO-Na$^+$.

$$v_c = k_{c0} f(a_i) g(T) = \exp^{-10.7} T \exp\left(\frac{-66}{10^{-3} RT}\right)\theta_{>SiOH} + \exp^{4.7} T \exp\left(\frac{-82.7}{10^{-3} RT}\right)\left(\theta_{>SiO^-_{tot}}\right)^{1.1} \quad \text{Eq 4.4.1}$$

where:

v_c is the constant dissolution rate far from equilibrium in mol.m^{-2}.s^{-1}

$\theta_{>SiOH}$ is the fraction of the total surface sites occupied by hydrogen ion as >SiOH

$\theta_{>SiO^-_{tot}}$ is the sum of the fractions of the total sites existing as deprotonated >SiO$^-$ site and as a complex with sodium ion as >SiO-Na$^+$

The data published by Dove does not go beyond at 0.5 sodium molal but show that the influence of the salinity variation on the dissolution rate is low over 0.1 molal, especially in acidic solution. The data have been extrapolated to 1.0 molal NaCl solution for pH from 3.6 to 6.0.

$$\theta_{>SiOH} = 1.055768 - 4.464707 \cdot 10^{-2}\, pH + 1.224392 \cdot 10^{-2}\, pH^2 - 1.168033 \cdot 10^{-3}\, pH^3 \quad \text{Eq 4.4.2}$$

$$\theta_{>SiO^-_{tot}} = -5.639672 \cdot 10^{-2} + 4.505011 \cdot 10^{-2}\, pH - 1.232825 \cdot 10^{-2}\, pH^2 + 1.173820 \cdot 10^{-3}\, pH^3 \quad \text{Eq 4.4.3}$$

The Figures 4.4.1 and 4.4.2 show the dependency of the quartz dissolution rate in function of pH and temperature when the solution is far from equilibrium.

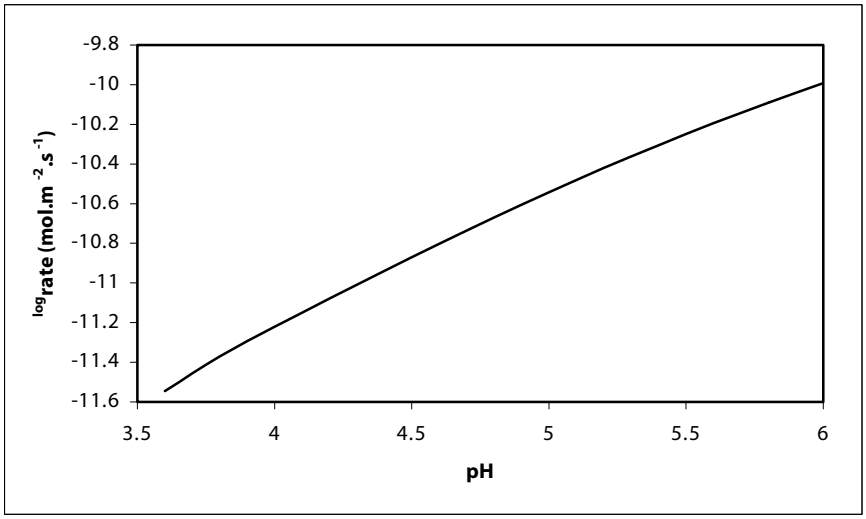

Figure 4.4.1 Evolution of quartz dissolution rate in function of pH at 65°C, far from equilibrium.

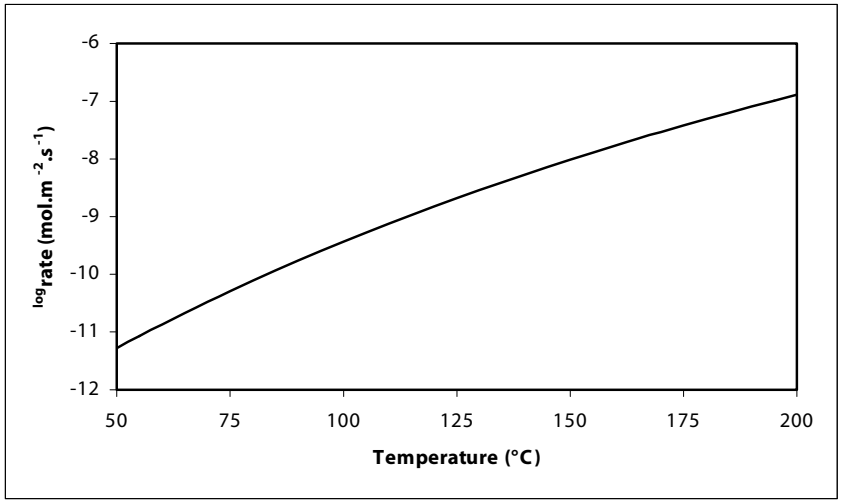

Figure 4.4.2 Evolution of quartz dissolution rate in function of temperature at pH=4.8, far from equilibrium.

The complete equation for quartz dissolution rate will then be:

$$v = \left[\exp^{-10.7} T \exp\left(\frac{-66}{10^{-3} RT} \right) \theta_{>SiOH} + \exp^{4.7} T \exp\left(\frac{-82.7}{10^{-3} RT} \right) \left(\theta_{>SiO^-_{tot}} \right)^{1.1} \right] s \left(1 - \left(\frac{Q}{K} \right) \right) \quad \text{Eq. 4.4.4}$$

Given that the fluid is initially in equilibrium in regard to quartz in the reservoir and that its cooling will lead to oversaturation, the dissolution can only happen if the silica concentration decreases enough due to quartz precipitation. This process can therefore not be estimated without numerical simulation but is not likely to cause significant variations in the reservoir in regard to the low rate values.

4.4.2 Quartz precipitation

The quartz precipitation equation comes from Rimstidt and Barnes (1980). There is no publication on the inhibition of quartz precipitation available at this time, and the influence of the salinity only appear through the H_2O activity.

$$v = \left[a^2_{H_2O} \exp\left(\left(1.174 - 2.02810^{-3} T - \frac{4158}{T} \right) \ln 10 \right) \right] s \left(\left(\frac{Q}{K} \right) - 1 \right) \quad \text{Eq. 4.4.5}$$

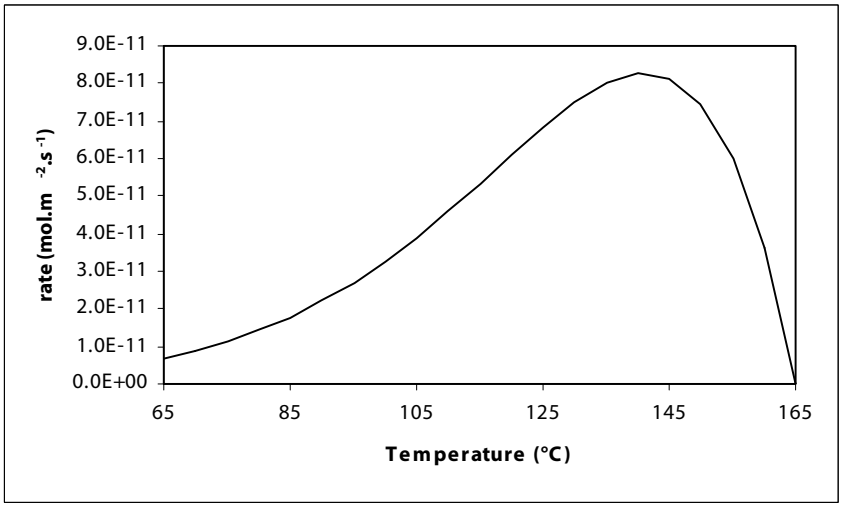

Figure 4.4.3 Quartz precipitation rate in Soultz fluid from 65 to 165°C.

4.5 Pyrite

4.5.1 Pyrite dissolution

The dissolution mechanism of pyrite depends on two reactions:

$FeS_2 + 14Fe^{3+} + 8H_2O \rightarrow 15Fe^{2+} + 2SO_4^{2-} + 16H^+$

in anoxic conditions and

$2FeS_2 + 7O_2 + 2H_2O \rightarrow 2Fe^{2+} + 4SO_4^{2-} + 4H^+$

in presence of dissolved oxygen (Williamson and Rimstidt, 1994). These two reactions lead to two rate equations at ambient temperature and pH range from 0.5 to 3.0:

$$rate = 10^{-8.58} \frac{m_{Fe^{3+}}^{0.30}}{m_{Fe^{2+}}^{0.47} + m_{H^+}^{0.32}} \qquad \text{Eq. 4.5.1}$$

in anoxic conditions and

$$rate = 10^{-6.07} \frac{m_{Fe^{3+}}^{0.93}}{m_{Fe^{2+}}^{0.40}} \qquad \text{Eq. 4.5.2}$$

when dissolved O_2 (DO) is present. They also compiled data available in the literature over a pH range from 2 to 10 which give:

$$rate = 10^{-8.19} \frac{m_{DO}^{0.5}}{m_{H^+}^{0.11}} \qquad \text{Eq. 4.5.3}$$

The activation energy is not well known but is accepted to be between 50 and 80 kJ.mol^{-1} for the two reactions. All these equations show that the rate depends mostly on Fe^{3+}/Fe^{2+} ratio that can only be assumed in the Soultz system. Multiple simulation were performed with PHREEQC. These simulations started with the Soultz fluid at 165°C, which was equilibrated in respect to pyrite and hematite and cooled down to 65°C. The introduction of the results of these runs in Eq. 4.5.1 gives $\log_{rate}$ ranging from –9.5 to –8.5. The equation for pyrite dissolution is assumed to be:

$$v = 250 s \exp\left(\frac{-65000}{RT}\right)\left(1 - \frac{Q}{K}\right) \qquad \text{Eq. 4.5.4}$$

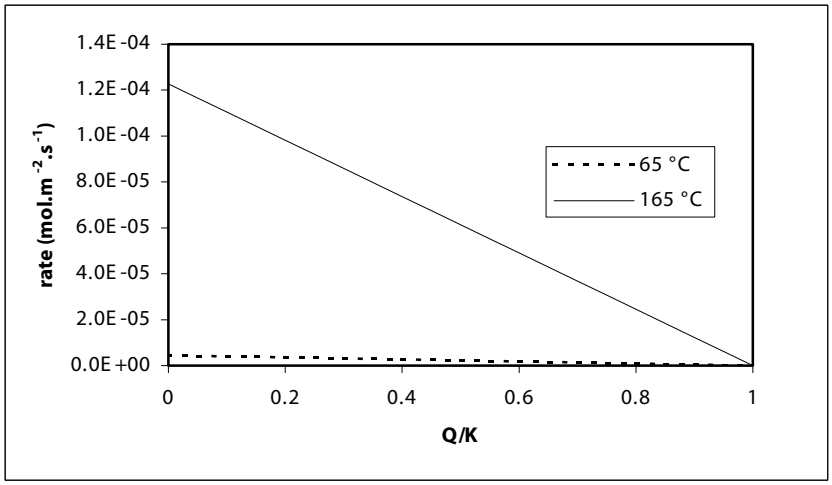

Figure 4.5.1 Pyrite dissolution rate at 65 and 165°C.

Like the quartz dissolution, the pyrite dissolution is subordinated to the decrease of sulphates and sulphides due to pyrite precipitation. Unlike the quartz, the higher rate values (Figure 4.5.1) can eventually make pyrite dissolution a relevant process.

4.5.2 Pyrite precipitation

Schoonen and Barnes (1991a, b and c) showed that below 300°C, pyrite forms via FeS precursor. Their titrations of the solubility of this precursor give:

$$\log K_{FeS,T°C} = 7.394\cdot10^{-10}T^4 - 5.374\cdot10^{-7}T^3 + 1.108\cdot10^{-4}T^2 - 8.847\cdot10^{-3}T - 3.3271 \qquad \text{Eq. 4.5.5}$$

for the reaction

$FeS + H^+ \rightarrow HS^- + Fe^{2+}$

Rickard (1997) and Rickard and Luther (1997) studied the kinetics of the reaction

$FeS_{(s)} + H_2S_{(aq)} \rightarrow FeS_2 + H_{2(g)}$

between 25 and 125 °C. The formation of pyrite occurs mostly by nucleation, so the surface area does not influence the quantity of mineral formed. The formation is:

$$rate = k(FeS)(cH_2S_{(aq)}) \qquad \text{Eq. 4.5.6}$$

where the rate is in $mol.l^{-3}.s^{-1}$ and (FeS) and (cH_2S) are in $mol.l^{-1}$. The thermodynamic model does not include H_2S because the speciation between HS^- and H_2S is included in the γ_{HS^-}. However the use of a Debye-Huckel calculation for the activity coefficients of H_2S and HS^- should give an error below the incertitude of the experimental determination of the rate. Consequently, this assumption gives:

$$a_{H_2S} = \frac{a_{HS^-}a_{H^+}}{K_{H_2S}} \qquad \text{Eq. 4.5.7}$$

therefore, with $\gamma H_2S/\gamma HS^- \approx 3$ Eq. 4.5.7 can be written:

$$cH_2S = \frac{\sum S^{2-}a_{H^+}}{3K_{H_2S} + a_{H^+}} \qquad \text{Eq.4.5.8}$$

with

$$\log K_{H_2S,T°C} = -4.406\cdot10^{-10}T^4 + 3.344\cdot10^{-7}T^3 - 1.243\cdot10^{-4}T^2 + 1.848\cdot10^{-2}T - 7.377 \qquad \text{Eq. 4.5.9}$$

and

$$\sum S^{2-} = cH_2S + cHS^-$$

The activation energy of the reaction is 35 $kJ.mol^{-1}$ and $k=3.2\cdot10^{-3}$ $mol.l^{-1}.s^{-1}$ at 125°C, this gives:

$$k = 125\exp\left(\frac{-35000}{RT}\right) \qquad \text{Eq. 4.5.10}$$

The formation of FeS in FeS oversaturated solution is fast enough for assuming a thermodynamic equilibrium. The combination of the equations 4.5.6, 4.5.8 and 4.5.10 gives:

$$v = 0.125\frac{a_{HS^-}a_{Fe^{2+}}\sum S^{2-}}{K_{FeS}\left(3K_{H_2S} + a_{H^+}\right)}V\exp\left(\frac{-35000}{RT}\right) \qquad \text{Eq. 4.5.11}$$

where V is the fluid volume in m^3.

The pyrite precipitation rate can then be calculated for the initial Soultz fluid in function of temperature (Figure 4.5.2).

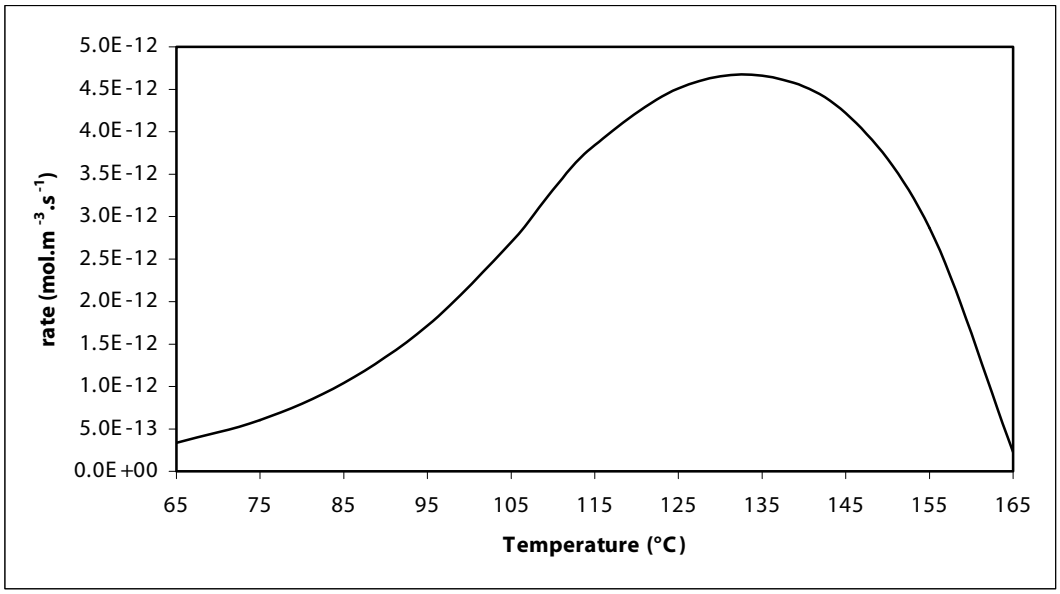

Figure 4.5.2 Pyrite precipitation rate in initial Soultz fluid in function of temperature.

A maximum precipitation rate is expected around 135°C (Figure 4.4.3). This is due to the competition between the augmentation of precipitation rate and the diminution of oversaturation with temperature increase, like for the quartz precipitation rate. Nevertheless, in regard of the really low rate values, this process is not likely to cause any significant change in the reservoir.

4.6 Effect of dissolution/precipitation processes on the permeability

The main goal of the geochemical modelling of the Soultz system is to estimate the effect of the mineral precipitation or dissolution on the fluid flow characteristics in the reservoir. The geochemical model gives the evolution of the volume of the different minerals and thus the porosity variation induced by each mineral reaction. The calculation of the permeability changes requires some type of porous space modelling. The models of the porous space evolution will also provide the area of the contact surface between the fluid and the different minerals.

At the simplest level, two type of porosity/permeability can be distinguished. In the first one, the circulation occurs in fractures filled with a constant thickness layer of reactive mineral (Figure 4.6.1.a). In the second case, the circulation occurs in the interstitial space between spherical grains of the reactive mineral (Figure 4.6.1.b). Knowing that the circulation in the Soultz system occurs in clusters of fractures and highly altered granite. The two type of model should then be considered.

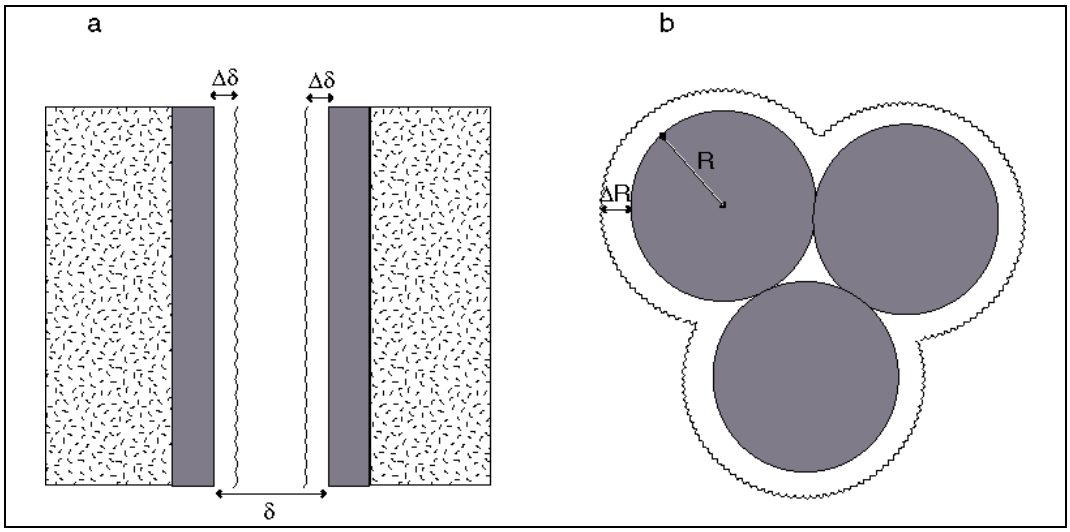

Figure 4.6.1 Schema of two basic porosity/permeability models: (a) the fracture model and (b) the grain model.

4.6.1 Fracture model

Norton and Knapp (1977) showed that for a single set of parallel fractures, the permeability can be expressed by:

$$k_F = \frac{\Phi_F \delta^2}{12} \qquad \text{Eq. 4.6.1}$$

where: k_F is the permeability in m^2

Φ_F is the fracture porosity (dimensionless)

δ is the fracture aperture in m.

Accounting for the effect of the intersection between the three orthogonal fracture sets defining an isotropic permeability, Steefel and Lasaga (1994) used $\Phi_F = 3\delta\, n_f$ that gives:

$$k_F = \frac{\Phi_F \delta^2}{36} = \frac{{\Phi_F}^3}{324 {n_f}^2} \qquad \text{Eq. 4.6.2}$$

that gives, for the variation of fracture porosity associated to the mineral i:

$$\frac{dk_{Fi}}{d\Phi_{Fi}} = \frac{{\Phi_F}^2}{108 {n_f}^2} \qquad \text{Eq. 4.6.3}$$

where n_f is the fracture frequency in m^{-1}.

The total surface area of mineral per rock volume will then be:

$$A_{F0} = \Phi_F \frac{2}{\delta_o} = 6 n_f \qquad \text{Eq. 4.6.4}$$

This equation can give the initial surface area A_{F0} in $m^2.m^{-3}$. However, the evolution of this surface with mineral quantity requires more attention. If the mineral layers are considered regular and the fracture apertures are all identical, the surface area will remain constant until all the mineral is dissolved or until all the fractures are clogged. If the aperture of the fracture and the thickness of the mineral layer are considered to follow a Gaussian distribution, the surface area of a mineral i can be expressed as:

$$A_{F,i} = A_{F0,i} \frac{V_i}{V_{tot}(1-\Phi_F)} \exp\left(-\left((\Phi_F - \Phi_{F_0})\sigma\right)^2\right) \quad \text{Eq. 4.6.5}$$

where: V_i is the volume of the mineral i

V_{tot} is the total volume of rock

that give, for the variation of fracture porosity associated to the mineral i:

$$\frac{dA_{F,i}}{d\Phi_{F_i}} = -A_{F0,i} \exp\left(-\left((\Phi_F - \Phi_{F_0})\sigma\right)^2\right)\left[2\frac{V_i}{V_{tot}(1-\Phi_F)}(\Phi_F - \Phi_{F_0})\sigma^2 + 1\right] \quad \text{Eq. 4.6.6}$$

where: σ is an empirical parameter defining the shape of the Gaussian distribution

Φ_{Fo} is the initial fracture porosity.

4.6.2 Grain model

The grain model is based on the work of Bolton et al. (1996). The permeability can be expressed as:

$$k_G = \frac{R_0^{I\,2}}{45}\frac{\Phi_G{}^3}{(1-\Phi_G)^2} \quad \text{Eq. 4.6.7}$$

where: Φ_G is the grain porosity (dimensionless)

R_o^I is the initial radius of closed pack spherical grains.

that give, for the variation of fracture porosity associated to the mineral i:

$$\frac{dk_{Gi}}{d\Phi_{Gi}} = \frac{R_0^{I\,2}}{45}\frac{\Phi_G{}^2(3-\Phi_G)}{(1-\Phi_G)^3} \quad \text{Eq. 4.6.8}$$

The total surface area of mineral i per rock volume will then be:

$$A_{Gi} = \frac{V_i}{V_{tot}(1-\Phi_F)}\frac{\pi\varepsilon(6-\varepsilon)}{\sqrt{2}R_0^I} \quad \text{Eq. 4.6.9}$$

where ε is the ratio between the actual grain radius and R_o^I. ε can be linked to the porosity, for a porosity between 0.036 and 0.26, with the equation:

$$\varepsilon^3 - \frac{9}{5}\varepsilon^2 + \frac{3}{5}\left(1 + \frac{\sqrt{2}}{\pi} - \frac{\sqrt{2}}{\pi}\Phi_G\right) = 0 \quad \text{Eq. 4.6.10}$$

The solution of this equation can be approximated by:

$$\varepsilon = -1.432\cdot 10^1 \Phi_G^3 + 7.215\Phi_G^2 - 1.769\Phi_G + 1.207 \quad \text{Eq. 4.6.11}$$

4.6.3 Model construction

There are a lot of more complex models for the description of the porosity/permeability relation. Those modelling the geometry of the porous space at a small scale are useless for a global reservoir modelling. Some models using fractal approach like the one developed by Pape et al. (1999) can be envisaged. This model leads to the equation:

$$k = A\Phi + B\Phi^{n1} + C(10\Phi)^{n2} \quad \text{Eq. 4.6.12}$$

However the determination of the coefficient A, B, C, n1 and n2 will require laboratory experiments on core samples from the Soultz reservoir. These data will not be available during this study. For the two models presented in the preceding paragraph, the parameters can be calculated knowing the initial

permeability and porosity. As an example, for a rock formed by 10 % of a given mineral, with an initial porosity of 0.1 and an initial permeability of 10^{-10} m^2, the parameters for the fracture model will be $\delta_0 = 1.898.10^{-4}$ m and $n_f = 176$ m^{-1} and for the grain model, $R_0^I = 1.910.10^{-3}$ m. The figure 4.6.2 shows the evolution of the permeability and surface area along with the porosity variation for this case. The evolution of the permeability is nearly identical for the two models but the surface area evolution is different. The surface area of the grain model reflects the variation of the grain radius as well as the clogging of the porous space, while the surface area of the fracture model reflects the Gaussian distribution of the fracture aperture and the mineral layer thickness.

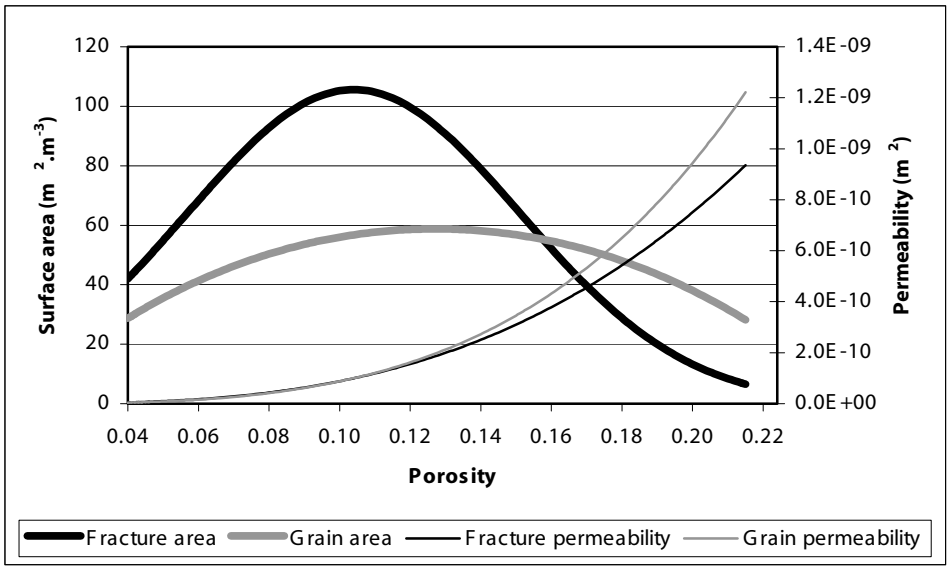

Figure 4.6.2 Evolution of permeability and surface area in function of porosity for the two basic models.

For the modelling of the Soultz reservoir, two parameters are attributed to each mineral for simulating the complexity of the porous space. First, the proportion of the mineral i in grain type porous space α_{Gi}: this parameter reflects the difference in proportion of the amount of mineral found in the altered granite facies and in the vein facies. Second, the ratio between the fracture permeability and the grain permeability κ_i. The initial porosity is supposed to be the same in the two porous space types. κ_i should be the same for all minerals. This method will give:

$$n_f = \sqrt{\frac{\Phi_0^3}{324 k_0}} \qquad \text{Eq. 4.6.13}$$

$$R_{0,i}^I = \sqrt{45 \kappa_i k_0 \frac{(1-\Phi)^2}{\Phi^3}} \qquad \text{Eq. 4.6.14}$$

$$\frac{dk}{d\Phi_i} = (1-\alpha_{G,i}) \frac{dk_F}{d\Phi_i} + \alpha_{G,i} \frac{dk_G}{d\Phi_i} \qquad \text{Eq. 4.6.15}$$

$$\frac{dA_i}{d\Phi_i} = (1-\alpha_{G,i}) \frac{dA_{F,i}}{d\Phi_i} + \alpha_{G,i} \frac{dA_{G,i}}{d\Phi_i} \qquad \text{Eq. 4.6.16}$$

The geochemical model is able to calculate for a time step the variation of quantity of each mineral and thus the variation of porosity associated to this mineral $\Delta\Phi_i$. The equations 4.6.15 and 4.6.16 can then be used to calculate the total porosity and permeability variation, as well as the variation of reaction surface area for each mineral using the following equations:

$$\Delta\Phi = \sum_i \Delta\Phi_i \qquad \text{Eq. 4.6.17}$$

$$\Delta k = \sum_i \frac{dk}{d\Phi_i}\Delta\Phi_i \qquad \text{Eq. 4.6.18}$$

$$\Delta A_i = \frac{dA_i}{d\Phi_i}\Delta\Phi_i \qquad \text{Eq. 4.6.19}$$

These equations will be used to control the feedback of the chemical reactions on the fluid flow (Eq. 4.6.17 and 4.6.18) and on the reaction rates (Eq 4.6.19) in the coupled numerical codes (see 5.2 and 5.3).

4.7 Synthesis

The thermodynamic disequilibria are the drive of the chemical reactions and the kinetic model has to verify the mechanisms involved in each reaction in order to predict its occurrence and its rate. The complete modelling of the reaction rates requires the knowledge of many parameters which do not always exist, especially for hot brines. Consequently, the method chosen has been simplified and is built on one kinetic law for each dissolution or precipitation reaction of the four main minerals considered, namely calcite, dolomite, quartz and pyrite.

Table 4.7.1 Dissolution – precipitation reactions during the cooling – re-heating processes of the fluid circulation in the deep Soultz reservoir.

Mineral	**Dissolution rate**	**Precipitation rate**
Calcite	Strong: mainly in the vicinity of injection point.	Low: in the wide zone of reinjection.
Dolomite	Much lower than the calcite rate, but in a wider zone.	Much lower than the calcite rate; most probably no precipitation in the system before dolomite dissolution.
Quartz	Due to oversaturation after cooling, no dissolution before significant precipitation of silica.	Low precipitation rate should occur with a maximum at 140°C.
Pyrite	Due to oversaturation after cooling, no dissolution before significant precipitation of sulphide. However, high rate values may induce pyrite dissolution.	Maximum precipitation rate should occur at 135°C. However, low rate values may not induce significant pyrite precipitation.

In order to estimate the influence of the dissolution/precipitation processes on the permeability, two parameters are attributed to each mineral in order to simulate the complexity of the porous space. Equations have been developed for the geochemical model, which can calculate the total porosity and permeability variations.

5. Development of the geochemical module into Chem-TOUGH2

5.1 Presentation of Chem-TOUGH2 code

Instead of creating and building a totally new code, the model used to simulate the geochemical processes between the fluid and the reservoir rock in Soultz was developed by modifying an existing reactive transport code, Chem-TOUGH2. Chem-TOUGH2 has been developed by White (1995) starting from the well-known reservoir simulator TOUGH2.

TOUGH2 is an improved version of the TOUGH simulator ("transport of unsaturated groundwater and heat") developed by Pruess (1991) for geothermal fields. It is a 3-D numerical model for simulating the coupled transport of water, vapour, non-condensable gas, and heat in porous and fractured media. TOUGH2 uses an integral finite difference method for space discretisation, and first-order fully implicit time differencing. A choice of a sparse direct solver or various preconditioned conjugate gradient algorithms are available for linear equations solution. Thermophysical properties of water, steam and CO_2 are represented. The programme can model injection or withdrawal of heat and fluids. Double-porosity, dual-permeability, and multiple interacting continua methods are available for modelling flow in fractured porous media.

Chem-TOUGH2 adds the possibility to transport chemical species and to model the chemical water-rock interactions as well as the chemical reactions driven by pressure and temperature changes. The transport and reaction are coupled using a one-step approach. The basic equations in TOUGH2 are conservation laws in the form of:

$$\frac{\partial Qt_{in}}{\partial t} = -\nabla \cdot F_{in} + qr_{in} \qquad \text{Eq. 5.1.1}$$

in each volume element, where:

- Qt_{in} is the quantity of component i (water, steam, gas or heat) in the volume element n
- $\nabla.F_{in}$ is variation of Qt_{in} due to transport
- qr_{in} is the variation of Qt_{in} due to the reactions in the volume element (heat exchange, condensation, injection...)

In Chem-TOUGH2, one equation of this type is added for each chemical species. The species can be transported via advection and diffusion. The geochemical part of the code calculates the qr_{in} terms for the chemical species.

There is no internal chemical database in this code. All chemical parameters, including the thermodynamic database, should be included in the TOUGH2 input file, following the keyword 'CHEM '. For example:

```
CHEM                                                                    1
1 4 0 .T.                                                               2
H2O         0.00   1.00  L  55.55        18.015301     0.000000         3
H+          1.00   3.08  L  1.0d-7       1.007970      0.000000         4
HCO3-      -1.00   2.10  L  1.0d-10      61.017200     0.000000         5
CO3--      -2.00   3.00  L  0.000000    60.009232      0.000000         6
CO3--                                                                   7
 0 -1  1     1       CO3--= 0*H2O  - 1*H+ + 1*HCO3-                     8
  0.106030E+02 -0.138090E-01  0.119260E-03 -0.292150E-06  0.319220E-09    9
```

Line 1: indicates the beginning of the chemical data.

Line 2: 1 is the number of reaction, 4 the number of species, 0 the number of gas/liquid reactions and .T. the indication that the standard calculation way should be used.

Lines 3 to 6: species name, species charge, a_0 parameter, species phase, initial concentration in $kg.m^{-3}$ molecular weight in $g.mol^{-1}$ and diffusion coefficient.

Line 7: reaction name:

Line 8: contains the stoechiometry of the reaction, here $CO_3^{--} = 0*H_2O - 1*H^+ + 1*HCO_3^-$ and the type of the reaction: 1 for equilibrium reaction in aqueous phase, 2 for gas equilibrium, 3 for gas-liquid equilibrium reaction, 4 for liquid-solid reaction and 5 for non-equilibrium reaction.

Line 9: contains the polynomial coefficients for the calculation of the equilibrium constant of the reaction in function of temperature.

For non equilibrium reactions, an additional line is provided with five parameters. The first is the reaction surface area, which will be recalculated by the code. The 2nd and 3rd are specific to the kinetic routine called, the 4th indicates which subroutine should be used and the 5th provides the volumic mass of the mineral.

All chemical reactions can be thermodynamically or kinetically controlled. The thermodynamic equilibrium is performed using an extended Debye-Huckel equation for the calculation of aqueous species activity coefficient and Henry law for gaseous CO_2. The reaction rates for the kinetic reactions are calculated in subroutines written for each reaction. The reaction surface area for the kinetic reaction is calculated using an equation from Darot et al. (1992)

$$s = \left(2.18 \cdot 10^{-6} + 1.32 \cdot 10^{6} \cdot \log(\Phi) + 2.14 \cdot 10^{5} \cdot \log(\Phi)^2\right) / \Phi \qquad \text{Eq. 5.1.2}$$

The program can also model the effect of the porosity changes on permeability using a simple empirical equation for porous rock, which has not being used in the present study.

5.2 Implementation of the geochemical model in Chem-TOUGH2

The geochemical modelling of the Soultz system has required some modifications of the original Chem-TOUGH2 code: implementation of the new method to calculate activity coefficients, the reaction kinetics subroutines for the minerals taken into account, modification of the calculation of the reaction surface areas and the permeability changes, as well as introduction of the possibility to simulate re-injection processes.

The activity coefficient (γ) calculation method described in chapter 3.2 was introduced in replacement of the existing one in the subroutine 'activity'. Due to the method the variable 'DgammaDm' which represents $\partial\gamma / \partial m$ is equal to zero and has been removed from the subroutines calculating the chemical equilibrium: 'solveequilibrium', 'phase1solveequilibrium' and 'phase1fun'. The polynomial coefficients for the γ calculation are read in the 'CHEM ' part of the input file, following each species information line. They are stored in the array 'gammacoeff (0:4,NumberOfSpecies)' declared in the 'chemistry' module. The gammacoeff (0:4,1) should contain the coefficient for the calculation of H_2O activity instead of γ_{H2O}.

The kinetic laws for the minerals currently taken into account in the model, described in chapter 4, have been introduced in subroutines: 'quartzsoultz', 'calcitesoultz', 'dolomitesoultz' and 'pyritesoultz'. The corresponding modifications have been made in the subroutine 'rate' which is in charge of calling the relevant kinetic subroutine. The 4th kinetic parameter should be 1 for quartz, 2 for calcite, 3 for dolomite and 4 for pyrite.

The calculation of the reaction surface area has been modified by rewriting the function 'areaphi' into a subroutine 'areaphi'. The method described in paragraph 4.6 requires the introduction of new arrays in the 'chemistry' module: 'nf (NumberOfElements)' for the fracture frequency, 'ri (NumberOfElements)' for the initial radius of closed pack spherical grains and 'area0 (NumberOfElements)' for the initial

fracture area. The surface area for each mineral is stored in 'area (NumberOfElements, NumberOfReactions)'. The ratios α_G and κ are provided in the input file.

The permeability changes 'kred(NumberOfElements)' are now calculated in a new subroutine 'permeability_changes' following the method described in paragraph 4.6.

A new source type has been introduced in Chem-TOUGH2 for the modelling of the reinjection process. Called 'MAST', this source is the injection point, It is similar to the 'MASS' source type except that the volume element name is followed by the name of the volume element where the production takes place. The subroutine 'QCHEM' has been modified in order to calculate the source of each chemical element in the volume element where the fluid injection takes place, in function of the mass of fluid injected and of the concentration in the production volume element. As some concentration drift has been observed in long time simulation due to the accumulation of precision errors, it is possible to specify in the 'MOP(25)' parameter a species that should remain constant. The quantity of the different elements injected is then corrected to maintain the concentration of the conservative element specified. Typically in the Soultz reservoir, this element will be the chloride.

A new output file is generated in the 'OUT' subroutine, containing the geometry of the simulated system, the temperatures, pressures, permeability, porosity, species concentrations and reaction rates in the PLOT3D format, readable by Tecplot.

The modified 'GENER' and 'CHEM ' part of the input file has the following format, given below for the example with only quartz in the mineral phase.

```
GENER                                                                    1
A1  1A1 20                          MAST 10.0       0.335e6              2
                                                                         3
CHEM                                                                     4
  2  5  0.T.                                                             5
H2O          0.00L  5.55000E+01  1.80000E+01  0.00000E+00                6
  0.955608E+00 -0.268621E-04  0.389146E-06 -0.125171E-08  0.257202E-11    7
H+           1.00L  2.20E-05     1.00000E+00  0.00000E+00                8
  0.294133E+01 -0.744534E-01  0.949630E-03 -0.508025E-05  0.956790E-08    9
H4SiO4       0.00L  2.23E-01     96.0000E+00  0.00000E+00                10
  0.193092E+01 -0.268539E-01  0.337269E-03 -0.178498E-05  0.334362E-08    11
OH-         -1.00L  0.00000E-05  17.0000E+00  0.00000E+00                12
  0.163025E+01 -0.481896E-01  0.619779E-03 -0.333916E-05  0.632716E-08    13
QUARTZ       0.00S  10.0000E+03  60.0000E+00  0.00000E+00                14
  0.100000E+01  0.000000E+00  0.000000E+00  0.000000E+00  0.000000E+00    15
OH-                                                                      16
 1.00  -1.00   0.00   1                                                  17
  0.149397E+02 -0.427928E-01  0.221928E-03 -0.752711E-06  0.129450E-08    18
QUARTZ                                                                   19
-2.00   0.00   1.00   5                                                  20
 -0.450127E+01  0.230740E-01 -0.136254E-03  0.554763E-06 -0.955384E-09    21
  0             0.2           0.1           1             2.65E+3         22
```

Line 2: the source declared indicates that a reinjection of 10 $kg.s^{-1}$ of fluid occurs in element A1 1 and that this fluid is produced in element A1 20. The enthalpy of $0.335.10^6$ J is that of the reinjected fluid.

Lines 8, 10, 12 and 14: in the species parameters, the a_0 parameter used in Debye-Huckel equation has been removed.

Line 7: contains the coefficients $B_{1,0\text{-}4}$ for the calculation of H_2O activity

Lines 9, 11, 13 and 15: coefficients $B_{i,0\text{-}4}$ for the calculation of the activity coefficient of the species, as described in equation 3.2.14:

$$\gamma_i = B_{i0} + B_{i1}.T + B_{i2}.T^2 + B_{i3}.T^3 + B_{i4}.T^4$$

Line 22: the 2nd parameter contains the α_G ratio, indicating that 20% of the quartz is assumed to be in the porous matrix. The 3rd parameter contains the κ ratio, indicating that the initial grain permeability is 10 time less than the fracture permeability. The 4th parameter indicates which kinetic subroutine should be used for the quartz reaction rate, here 'quartzsoultz'. The last parameter contains the volumic mass of the quartz in $kg.m^{-3}$.

The flow chart of Chem-TOUGH2 including the different modifications realised within this study is schematised in Figure 5.2.1.

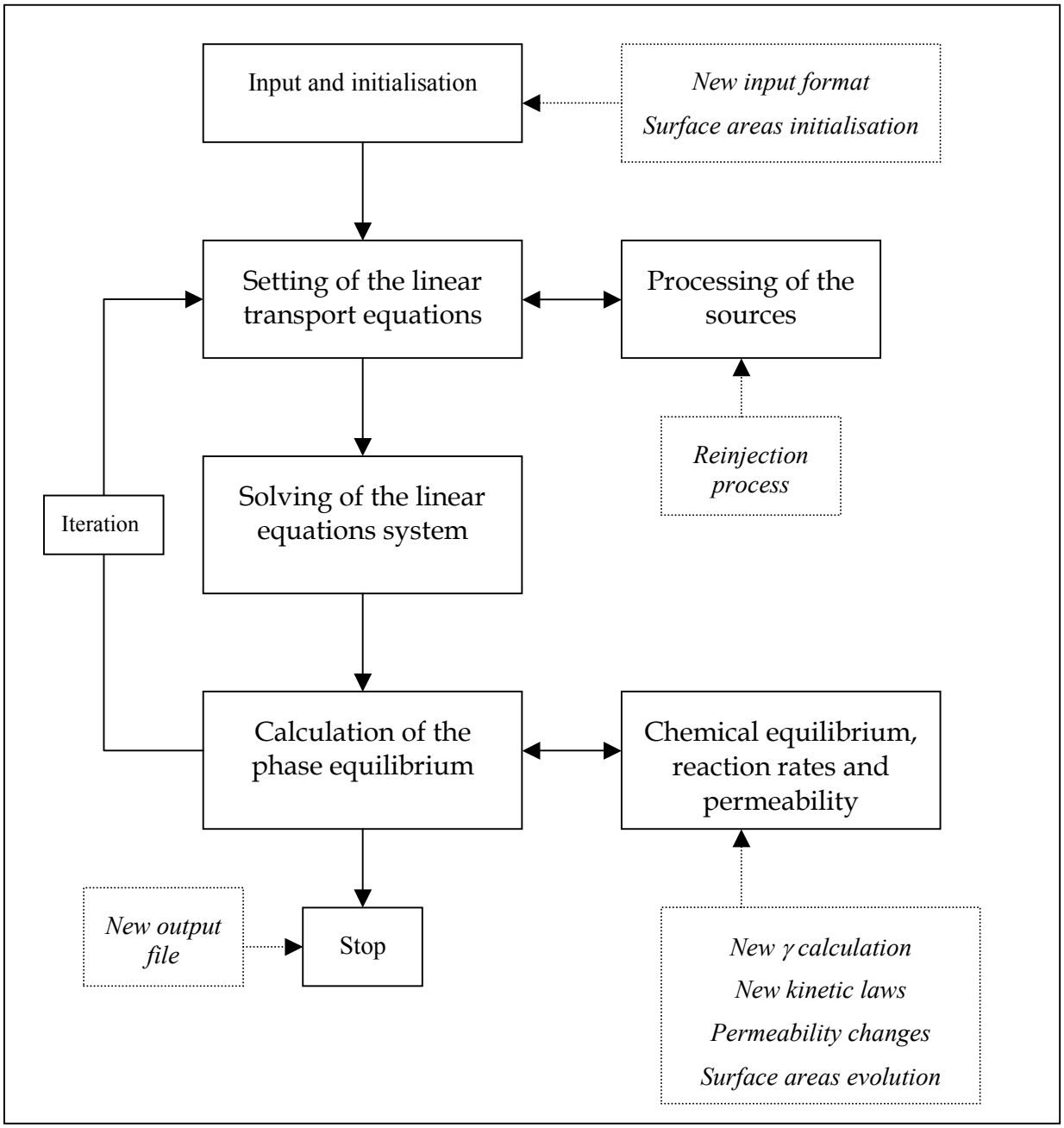

Figure 5.2.1 Flow chart of Chem-TOUGH2 with the modifications introduced in this study in italic.

5.3 Application of the model to a 1-D fracture

5.3.1 Model description

The new version of Chem-TOUGH2 has been used to simulate the chemical reaction along a 1-D fracture with water injected at 65°C and progressively heated to 165°C, similarly to the 1997 circulation test.

The circulation in the Soultz reservoir takes place in clusters of fractures filled with quartz, calcite, hematite, illite or chlorite, surrounded by porous altered granite. A fine simulation will require a complex geometry at such a small scale that it will not allow the modelling of the circulation within the entire system. For this study the circulation zone is reduced to an homogeneous medium in which the circulation takes place for 90% in fractured medium and 10% in porous medium, the permeability of the porous space is assumed to be ten time less than that in the fractures.

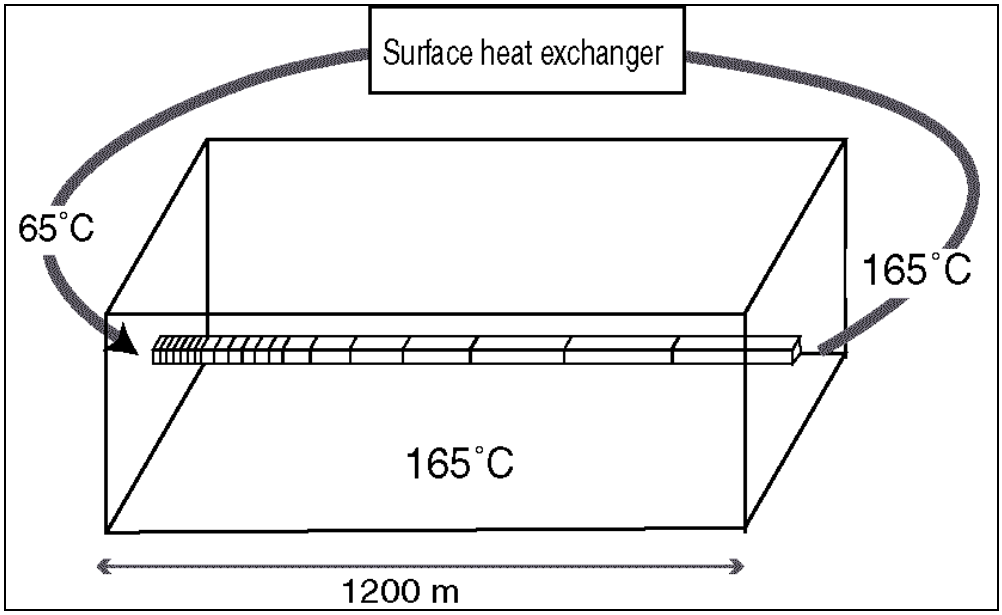

Figure 5.3.1 Simulation geometry.

The model is constituted of twenty volumes as shown in Figure 5.3.1. The grid has a higher density near the injection point, where the system is more reactive. A total length of 1200 m is chosen to allow a temperature increase up to 165°C along this 1-D geometry. The rock mass is formed by 40% of quartz, 4% of calcite, 1% of dolomite and 1% of pyrite. The remaining 54 % of the mass contains minerals not included in this simulation, principally clays. The values of the main parameters for the simulation are listed in Table 5.3.1.

Table 5.3.1 Values of the physical parameters considered for the simulation.

Porosity	10 %
Permeability	10^{-11} m^2
Rock density	2650 $kg.m^{-3}$
Rock matrix temperature	165°C
Reservoir pressure	40 MPa
Conduit injection rate	10 $kg.s^{-1}$
Injection temperature	65°C

The thermal-hydraulic and geometrical part of this simulation are not fully realistic and have been designed to allow the test of the modified geochemical part, the re-injection process and the permeability variation process. For this reason the system has been set in a thermal-hydraulic equilibrium from the beginning of the simulation. The evolution of the equilibrium temperatures along the 1-D fracture can be seen in Figure 5.3.2. The fluid velocity is 2.62 $m.day^{-1}$ all along the fracture.

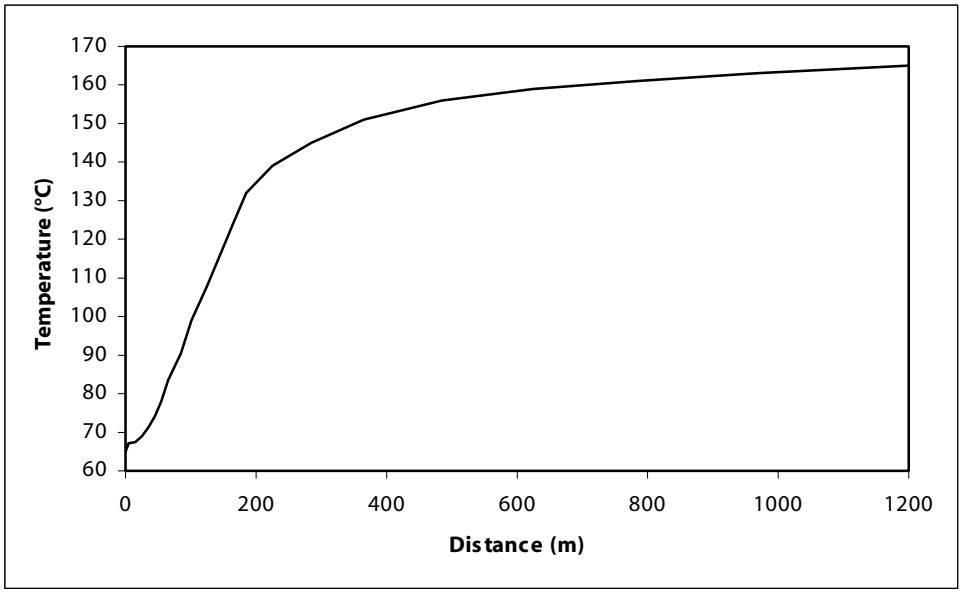

Figure 5.3.2 Fluid temperature in function of distance from injection point.

Starting at thermal equilibrium, the only potentials leading to a modification of the system are the saturation indexes of the fluid with regard to quartz, calcite, dolomite and pyrite shown in Figure 5.3.3. The chemical disequilibrium observed near the injection point induces the reaction of the system, namely dissolution of carbonates and precipitation of quartz and pyrite.

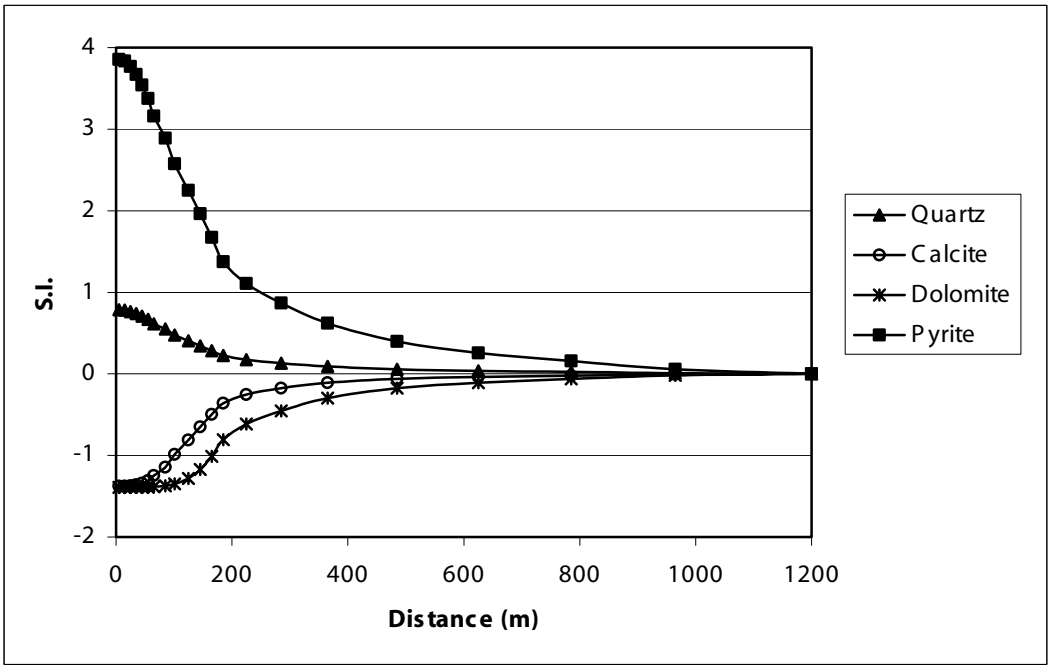

Figure 5.3.3 Saturation indexes of the fluid at the beginning of the simulation.

5.3.2 Evolution of the pH and the carbonates

The more reactive minerals are the carbonates and their dissolution and precipitation are linked to the fluid pH variations. These three parameters should be studied together.

The initial pH of the fluid reflects the non-reactive cooling of the fluid in equilibrium with the reservoir minerals at 165 °C, ranging from 4.3 at 65°C to 4.8 at 165°C (Figure 5.3.4). One day after the beginning of the reaction, the pH rises in all the fracture. It reaches 4.85 at the injection point, goes up to 5.1 in the first ten meters and decrease to regain 4.8 at the end of the fracture. After ten years, the pH at the injection point decreases to 4.55 and reaches 5.2 in the first tens of meter before decreasing to 4.8.

The first day after the start of the simulation, the calcite dissolves at $4.4.10^{-5}$ mol.m^{-3}.s^{-1} at the injection point and at $2.5.10^{-5}$ mol.m^{-3}.s^{-1} in the first 60 m (Figure 5.3.5). It then starts to precipitate, reaching a maximum rate of $3.3.10^{-6}$ mol.m^{-3}.s^{-1} at 185 m. The precipitation rate decreases up to 0 at the production point. In the following of the simulation, the calcite only dissolves in the volume element where the injection take place at a rate decreasing slowly form $8.2.10^{-6}$ mol.m^{-3}.s^{-1} after one week to $6.8.10^{-6}$ mol.m^{-3}.s^{-1} after 10 years. The maximum precipitation rate decreases to $7.5.10^{-7}$ mol.m^{-3}.s^{-1} during the first month and the precipitation concentrates more and more in the beginning of the fracture. After ten year, the precipitation only occurs between 10 and 20 m at a rate of $4.22.10^{-7}$ mol.m^{-3}.s^{-1}.

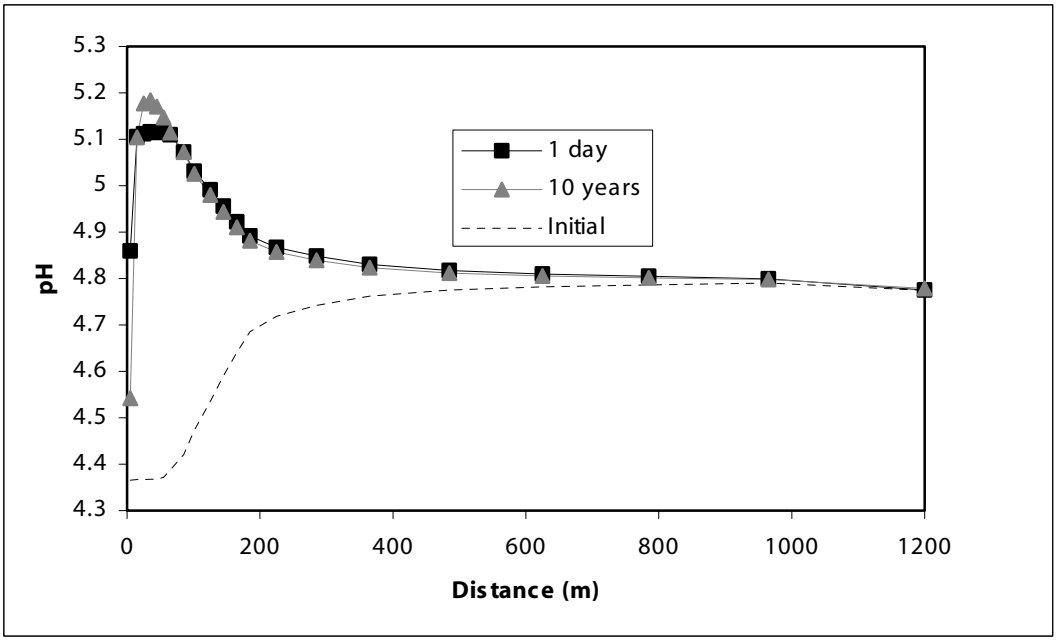

Figure 5.3.4 pH evolution with the time in function of the distance from injection point.

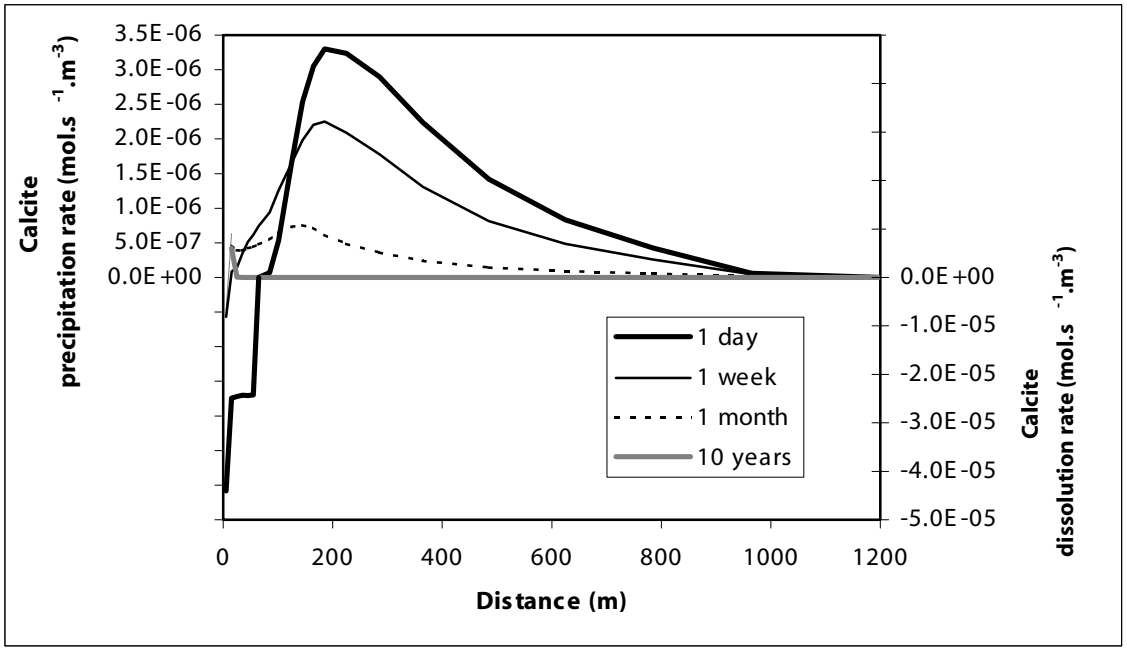

Figure 5.3.5 Calcite reaction rate in function of the distance from injection point. Warning: the dissolution rate scale is different from the precipitation rate scale.

The dolomite dissolves all along the fracture during the entire simulation (Figure 5.3.6). After one day the dissolution rate is $4.1.10^{-6}$ mol.m^{-3}.s^{-1} at the injection point, decreases to $7.9.10^{-7}$ mol.m^{-3}.s^{-1}at 65 m, reincreases to $1.6.10^{-6}$ mol.m^{-3}.s^{-1} at 185 m and decreases to 0 at the production point. With the evolution of the simulation, the dissolution rate decrease, quickly during the first month and more slowly during the next ten years. At the end of the simulation, the dolomite only dissolves in the first 20 m with a maximum rate of $7.2.10^{-7}$ mol.m^{-3}.s^{-1}.

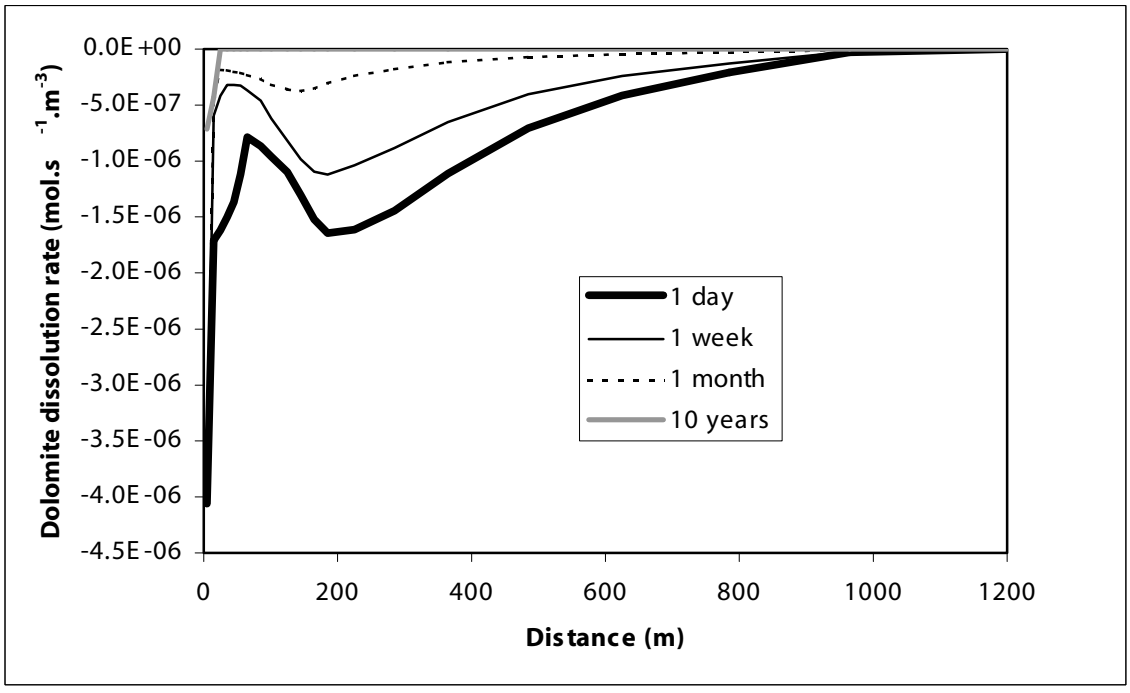

Figure 5.3.6 Dolomite reaction rate in function of the distance from injection point.

It seems from these results that the leading process is the fluid-calcite reaction. The high reaction rates observed during the first month are due principally to the initial thermal equilibrium assumption that causes a great disequilibrium in the fluid. Once this initial disequilibrium reduced, the injection of fresh fluid maintains a lower pH (4.5-4.9) in the first 10 m and causes the dissolution of calcite and dolomite in this area. In the next 10 m, the pH remains higher (5.1-5.2) and the calcite precipitates causing dolomite to still dissolves. As the composition of the produced fluid, and thus of the reinjected fluid, does not evolve significantly during the first 10 years, the slow decrease observed in the reaction rates from one year to 10 years is mainly due to the diminution in calcite and dolomite surface area in the first element.

5.3.3 Quartz and pyrite evolution

The quartz precipitates in the whole fracture (Figure 5.3.7). At the beginning of the simulation, the precipitation rate starts at $1.2.10^{-9}$ mol.m^{-3}.s^{-1} at the injection point, rises up to $1.3.10^{-8}$ mol.m^{-3}.s^{-1} at 250 m and then decreases to 0 at the end of the fracture. During the next 10 years, the rate decreases slowly, with a maximum going to $1.9.10^{-9}$ mol.m^{-3}.s^{-1} at 100 m, except in the first element where the rate slowly rises to $1.7.10^{-9}$ mol.m^{-3}.s^{-1}. The global diminution seems to come from the reequilibrium from initial conditions. The first element precipitation rate is more controlled by the composition of the injected fluid, and the augmentation comes from the increasing of the reaction surface area.

The pyrite precipitates in the whole fracture with a maximum rate of $3.9.10^{-12}$ mol.m^{-3}.s^{-1} at 285 m (Figure 5.3.8). This rate does not significantly evolve during the simulation.

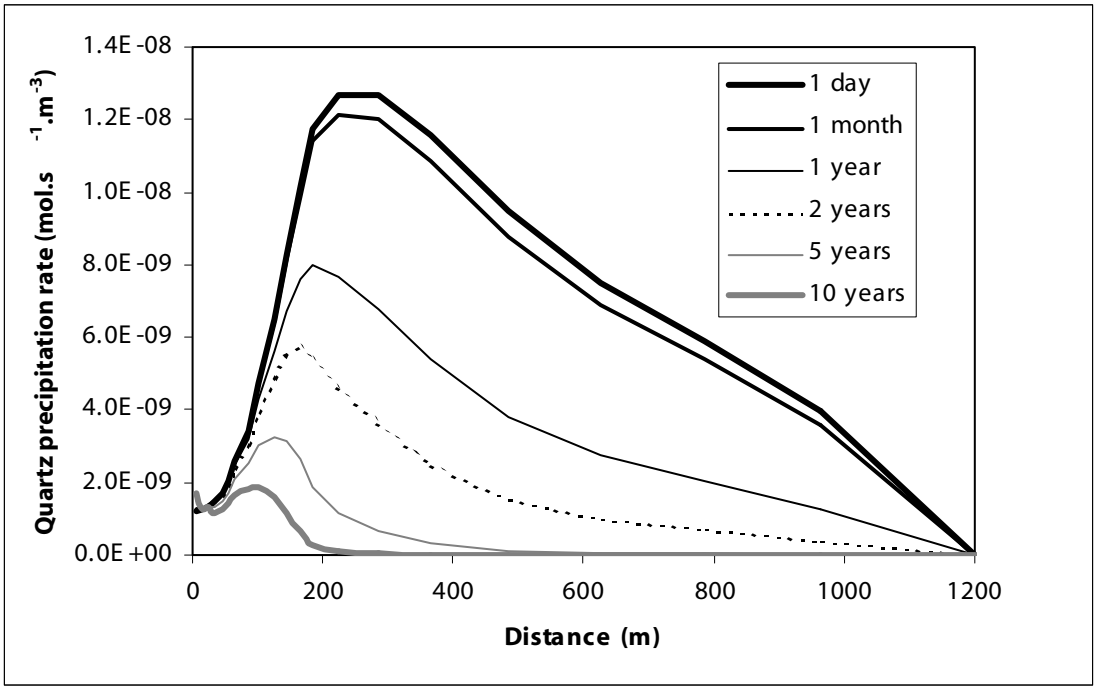

Figure 5.3.7 Quartz reaction rate in function of the distance from injection point.

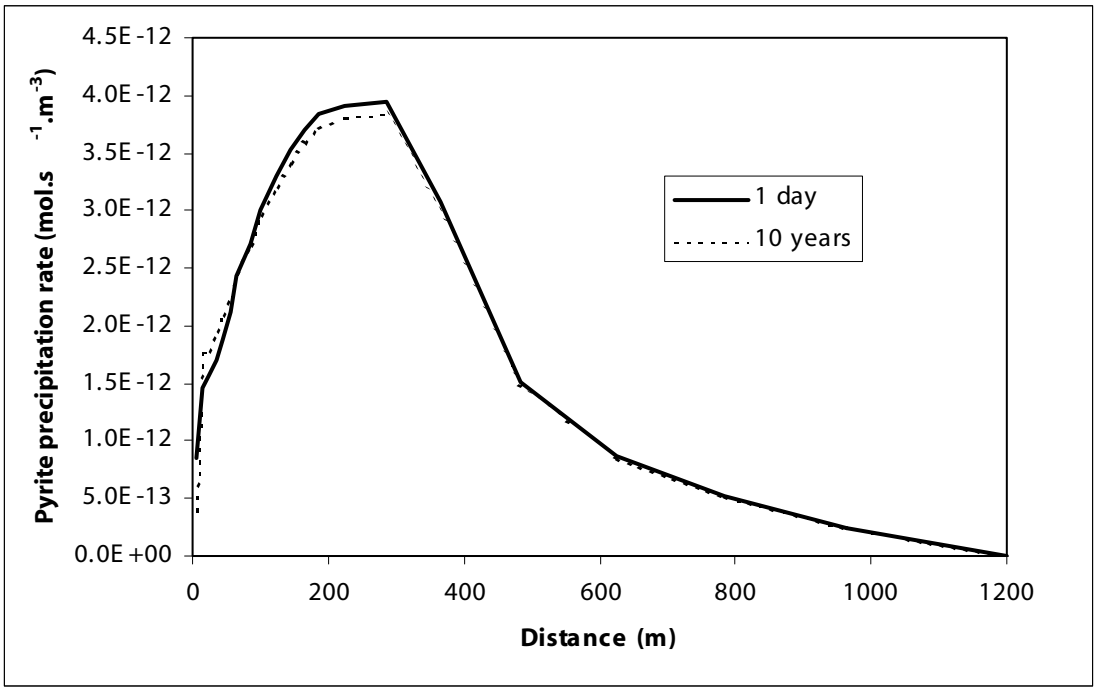

Figure 5.3.8 Pyrite reaction rate in function of the distance from injection point.

5.3.4 Evolution of the porosity and the permeability

At the end of the simulation, the porosity in the first 10 m reaches 13.4 % (Figure 5.3.9). It only increases to 10.1 % in the next 10 m and stays constant in the rest of the fracture. In the first 10 m, it increases more or less linearly with time as shown in Figure 5.3.10.

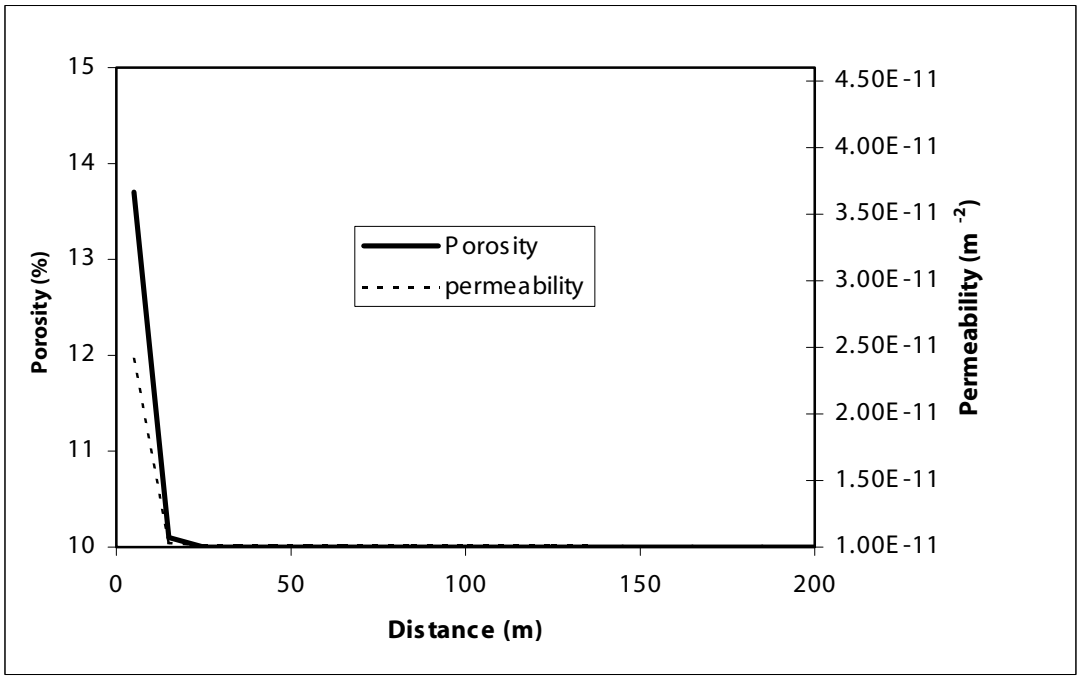

Figure 5.3.9 Porosity and permeability as a function of the distance from injection point in the first 200 m.

The permeability acts similarly. At the end of the 10 years, it reaches $2.4.10^{-11}$ m^2 in the first 10 m and stays constant in the rest of the fracture (Figure 5.3.9). In the first 10 m, it increases more or less linearly with the time as shown in Figure 5.3.10.

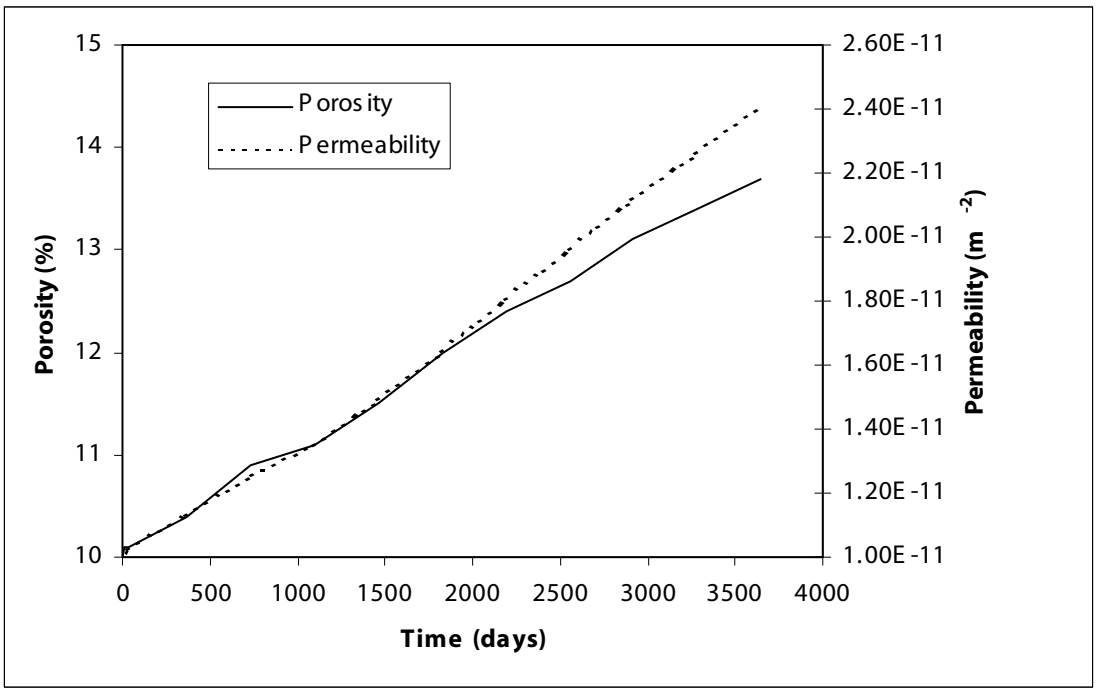

Figure 5.3.10 Porosity and permeability in the first 10 m function of the elapsed time.

These variations are caused by carbonates dissolution. It should be noted that the volume of calcite re-precipitated always stays below the volume of dissolved dolomite.

5.4 Synthesis

To simulate the geochemical processes between the Soultz brine and the fractured granite, a reactive transport code Chem-TOUGH2, based on TOUGH2 simulator, has been used and modified. The chemical species are transported by advection and diffusion. All reactions can be thermodynamically or kinetically controlled. It required some modifications of the original code, in order to consider the Soultz system: the new method to calculate the activity coefficient, the reaction kinetics subroutines for selected minerals and the calculation of the reaction surface areas and the permeability changes.

In order to test the revised version of Chem-TOUGH2, a very simple geometry has been used, to simulate the chemical reaction along a 1-D fracture with water injected at 65°C and progressively heated to 165°C. Most of the circulation takes place in the fracture itself and only 10% in a porous altered granite. The chemical disequilibrium observed near the injection point induces the reaction of the system, namely the dissolution of calcite and dolomite, as well as the precipitation of quartz and pyrite. It should be mentioned that the system starts at thermal equilibrium. The simulation considered a fracture length of 1200 m over a period of 10 years.

The results show that the leading process is the fluid-calcite reaction, including dissolution during the first month and near the injection zone. Then, due to temperature increase, precipitation occurs further in the fracture, with a maximum around 200 m, and equilibrium is reached near 900 m. During the whole simulation, dolomite dissolves all along the fracture. Quartz precipitates at various rates in the whole fracture and pyrite also precipitates all along the fracture, but at the same rate.

Due to carbonates dissolution, both porosity and permeability increase linearly with time, but only in the first 10 m of the fracture.

6. Building of the coupled code: FRACHEM

6.1 Presentation of FRACTure and coupling strategy

One of the main goals of the present study is to couple the geochemical model developed into Chem-TOUGH2 with the thermal-hydraulic-mechanical code FRACTURE.

FRACTure is a 3-D finite element code for modelling hydraulic, transport and elastic processes that was developed originally for the study of flow driven interactions in fractured rock (Kohl & Hopkirk, 1995). Its name is an acronym for its functional capabilities (Flow, Rock And Coupled Temperature effects). The code was originally developed for studying and simulating the long-term behaviour of HDR reservoirs. Since 1992, further developments have been made in the framework of two Swiss projects simulating hydraulic data sets of Hot Dry Rock systems and hydrothermal fields around the German KTB (Continental Deep Drilling project) site. A description of the elastic processes can be found in Kohl (1992).

For the modelling of the Soultz system, FRACTURE has the advantage of being able to model turbulent flows, thermal-elastic variations of the fractures aperture and a finite element approach more suited to model the geometry of the fractured reservoir.

Different approaches for the coupling of transport and reaction processes can be envisaged (Steefeld and MacQuarrie, 1996). One-step or global implicit approach, sequential non-iterative approach and sequential iterative approach.

The one-step method consists in solving simultaneously the transport and reaction equations. This approach should provide the more "exact" results from a mathematical point of view but the size of the equation system to be resolved restricts its use to the system containing only one or few aqueous species.

The sequential non-iterative method is simpler numerically speaking. It consists in resolving the reaction equations in all elements, then calculating the fluid flow between the elements and finally transporting the chemical species from element to element. Despite its simplicity, this method can lead to numerical oscillations or imprecisions as the reaction rates calculated at time t are supposed constant until time $t+\Delta t$ without considering the changes in fluid composition and temperature during the interval Δt. The time step can be set small enough to reduce these imprecisions but this increases the calculation time.

The sequential iterative method moves to fully coupled solution by iterating between the transport and reaction equation. This can be done by considering alternatively reaction and transport as a constant source term and to iterate until the concentrations given by the two sets of equations converge. This method is mathematically more elegant than the non-iterative approach and can be used for systems containing multiple aqueous species, however it is numerically more complex and can fail to converge in some cases.

Although FRACTure provides the possibility for diffusive and advective solute transport modelling, the number of chemical elements that have to be taken into account prevented the use of this feature for the coupled code. The building of more implicit coupling is still in study but the method chosen as a first step was a sequential non-iterative coupling. Each hydraulic and thermal step is followed by a chemical step. This new code, developed with the ETH-Zurich team, has been called FRACHEM.

6.2 Extraction of geochemical module for coupling with FRACTURE

6.2.1 Description of the geochemical module

The flowchart of the integration of the geochemical module is schematised in Figure 6.2.1. This module articulates in two main subroutines, 'Chem_init' and 'Main_chem'.

'Chem_init' performs all the input and initialisation. It calls 'Chem_input', which reads a file 'chem.dat' containing the chemical parameters as described in the 'CHEM ' part of the input file (see paragraph 5.2). The 'chem.dat' file can also contain the initial chemical concentrations for volumes elements if these concentrations are not initially homogenous and the informations about injection and production elements as well as "surface installation".

The second main chemical subroutine is 'Main_chem'. The first task of 'Main_chem' is to test if more than 10% of the fluid of a volume element is displaced during a time step. If this is the case, the chemical reactions and transport of chemical species calculation will be split into lower time step: 'max_transtime'. The critical value of 10% has been chosen to avoid the boundary effects that can happen with sequential non-iterative coupling method. The main calculations are performed in five subroutines called by 'Main_chem': 'Chemical_state', 'Steady_reaction', 'Chemical_transport' and 'Permeability_change'.

'Chemical_state' performs the calculation of the chemical thermodynamic equilibrium and of the kinetic reaction rate as well as the porosity variation caused by each fluid-mineral reaction. This subroutine content comes principally from the modified version of Chem-TOUGH2. All parts of the original code designed to deal with more than one liquid phase as well as the parts designed to allow the use of a full coupling method have been removed. If a brutal variation in any aqueous species concentration is detected, the time step is reduced in order to avoid numerical aberrations in case of reaction front.

'Steady_reaction' calculates the variation of chemical concentration due to the water-rock interactions

'Chemical_transport' calculates the variation of chemical concentration due to advective transport. This subroutine has been created for the coupling with FRACTURE. The method of calculation is the following:

- A temporary concentration C^1 is set equal to the present concentration C:

  $$C^1_{n,i} = C_{n,i} \qquad \text{Eq. 6.2.1}$$

  where n is the volume element number

  i is the chemical species.

- A loop is performed over all the advective flows:

  $$C^1_{to,i} = \left(C_{to,i} \cdot \left(V^{el}_{to} - V^{adv}_{j}\right) + C_{from,i} \cdot V^{adv}_{j}\right) / V^{el}_{to} \qquad \text{Eq. 6.2.2}$$

  where to is the number of the destination volume element

  from is the number of the origin volume element

  V_j^{adv} is the fluid volume coming from the j^{th} advective flow, from element 'from' to element 'to'

  V_{to}^{el} is the fluid volume of the destination element.

- The concentrations are updated:

  $$C_{n,i} = C^1_{n,i} \qquad \text{Eq. 6.2.3}$$

For each time step, a first calculation of the reaction rates (v_1) is performed into 'Chemical_state', then 'Steady_reaction' and 'Chemical_transport' compute the variations in concentrations in iterations over the reduced time step 'max_transtime'. The reaction rates (v_2) corresponding to the final concentrations are calculated in 'Chemical_state' and the concentration are reset to their values at the beginning of the time step. A new set of reactive transport iterations is finally computed in 'Steady_reaction' and 'Chemical_transport' with averages reaction rates $(v_1+v_2)/2$.

'Permeability_change' computes the variations of porosity, permeability and reaction surface areas according to the equations defined in paragraph 4.6.

Last the subroutine 'Chem_output' is designed to write the chemical parameters like pH, chemical concentrations and reaction rates in the file 'Chem_ouput.dat'.

6.2.2 Integration into FRACHEM

The new-coupled code FRACHEM has been build by introducing the geochemical subroutines into the body of the code FRACTURE, which has been modified in this perspective (Baechler and Kohl, 2001). The flowchart can be seen in Figure 6.2.1.

The programme starts by the input initialisation of the former FRACTURE parameters. It is followed by the input and initialisation of the part designed to play the interface between the finite element approach from FRACTURE and the finite volume approach of the geochemical modules. The aim of this new module is to convert the vectorial fluid velocities known at the elements nodes into the total fluid flow between two elements. The initialisation phase ends by the call to the subroutine 'Chem_init' described above.

The programme then enters its main loop over each FRACHEM time step. This loop begins with the thermal and hydraulic calculation from FRACTURE. Next, the interface module is called for calculating the advective flow used in the geochemical modules. The temperatures, pressures and advective flow values are stored in arrays common to FRACHEM body and to the geochemical modules. At this point the programme calls the subroutine 'Main_chem', which calculate the chemical reactions, the advective transport of chemical species and the variation of porosity and permeability, as described in the preceding paragraph. Once this calculation performed, the porosity and permeability into the FRACTURE part are updated and different output files are written or updated, including 'Chem_ouput.dat'. The programme then returns to the start of the loop until the end of the simulation time.

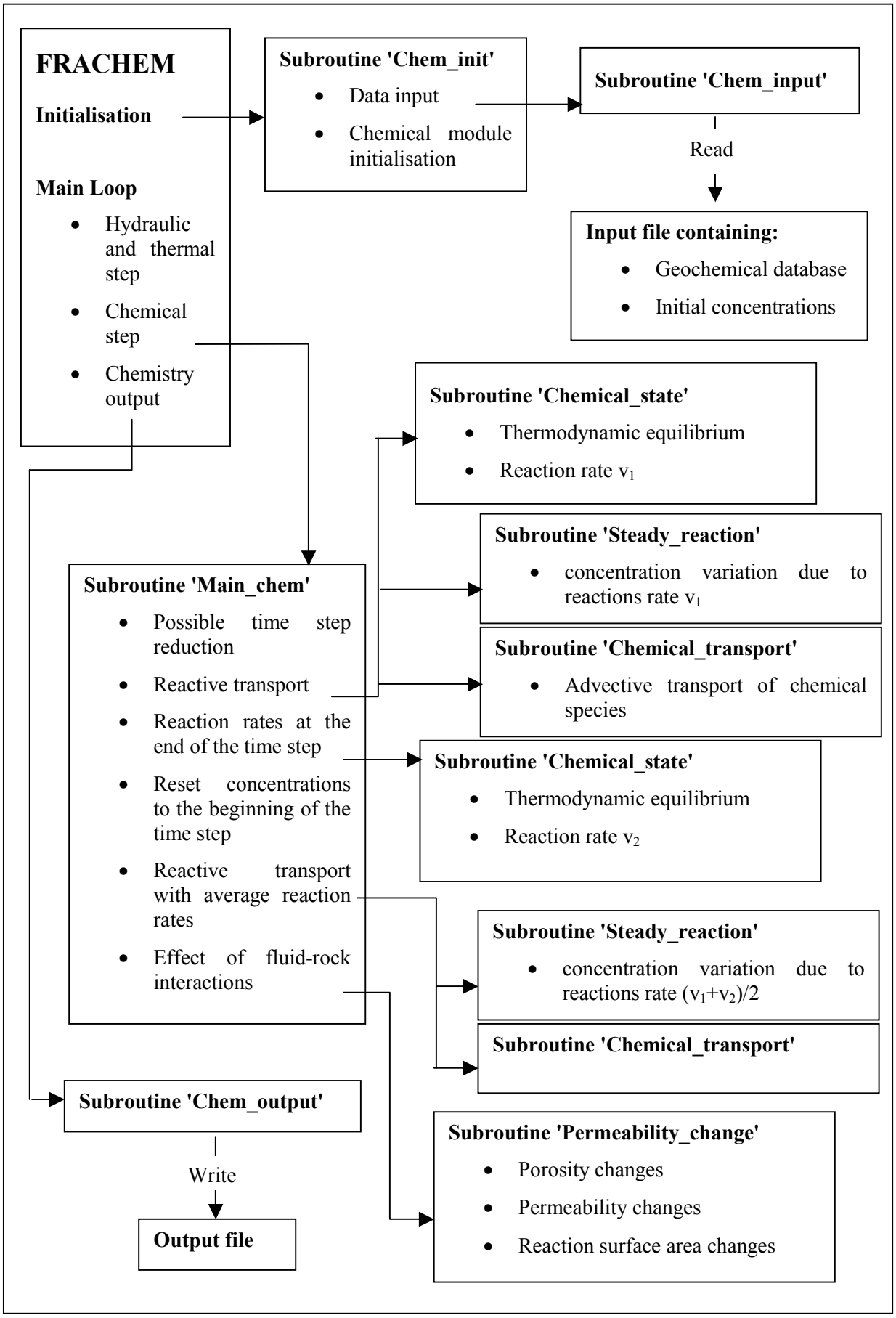

Figure 6.2.1 Flowchart of the coupling between FRACTURE and the geochemical module.

6.3 Synthesis

Geochemical modules developed into Chem-TOUGH2 have been extracted for coupling with FRACTURE, according to a two-step sequential non-iterative coupling method. Each hydraulic and thermal step is followed by a chemical step. This new code is called FRACHEM. An interface was created between the finite element approach of FRACTURE and the finite volume approach of the geochemical modules. Several geochemical routines are introduced in the body of the code FRACTURE, which finally calculate the chemical reactions, the advective transport of chemical species, and the variation of porosity and permeability.

7. Coupled simulation with FRACHEM

7.1 Single fracture model

7.1.1 Model description

The first application of the new code FRACHEM was the modelling of a simple case, which reproduces at a smaller scale what can happen if a cooled Soultz fluid is reinjected in a hot reservoir. The model schematised on Figure 7.1.1 consists of a 50-m long, 1-m wide fracture cluster composed of 13 volume elements, surrounded by 52 matrix volume elements. It is a 2-D thermal-hydraulic model, and a thickness of 1 m has been considered for the geochemical section. The thermal-hydraulic section has been set by D. Baechler at ETH-Zurich in order to have a model simple enough to test FRACHEM, but still relevant for the study of the Soultz reservoir.

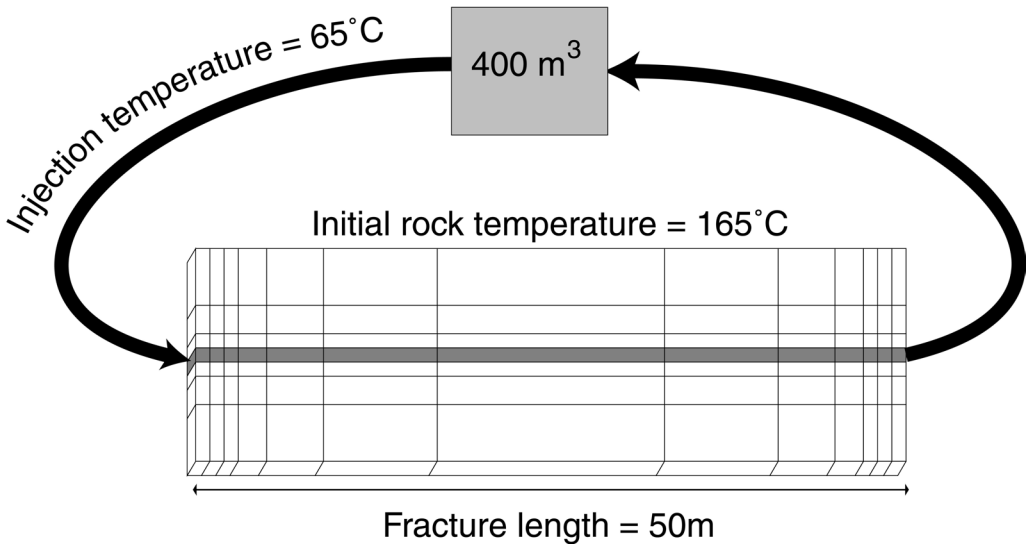

Figure 7.1.1 Simulation geometry.

Table 7.1.1 Values of the thermal-hydraulic parameters selected for the simulation.

Parameters	**Fracture cluster**	**Matrix**
Hydraulic conductivity	10^{-7} m.s^{-1}	10^{-12} m.s^{-1}
Storage coefficient	0	0
Porosity	10 %	0 %
Thermal conductivity	2.2 W.m^{-1}.K^{-1}	3 W.m^{-1}.K^{-1}
Density of fluid for hydraulic calculation	1000 kg.m^{-3}	1000 kg.m^{-3}
Density of rock	2650 kg.m^{-3}	2650 kg.m^{-3}
Heat capacity of rock	1000 J.kg^{-1}.K^{-1}	1000 J.kg^{-1}.K^{-1}
Heat capacity of fluid	4200 J.kg^{-1}.K^{-1}	4200 J.kg^{-1}.K^{-1}
Heat production	0 W.m^{-3}	0 W.m^{-3}
Injection pressure (bottom of well GPK-1)	44 MPa	-
Production pressure (bottom of well GPK-2)	25 MPa	-

The thermal-hydraulic parameters are listed in Table 7.1.1. With a porosity of 0%, the matrix is not concerned by fluid/rock chemical reactions. The initial temperature is 165°C for all volume elements, fracture and matrix. Then the fluid is injected at 65°C, at a rate of 4.10^{-6} $m^3.s^{-1}.m^{-1}$ in the first volume element of the fracture cluster. The fluid flowing out of the last volume element is reinjected in the first one through a buffer of 400 m^3 representing the fluid volume contained in wells and surface installation. The simulation lasted a total of $2.01.10^8$ seconds, which represents roughly 6.4 years. It required 14.5 hours of computer time on a Dell Precision 610 workstation, nevertheless the code was not optimised for speed.

The most significant change in the case modelled, in regard to the 1-D fracture modelled with Chem-TOUGH2 only (see 6) is the absence of initial thermal equilibrium. However as there is still a single flow path, the permeability variation does not affect the fluid circulation. Further simulation will involve a more complex circulation geometry.

7.1.2 Temperature evolution

In this very simple model, the initial temperature of the system reaches 165°C, whereas at the injection point the water has been cooled to 65°C (Figure 7.1.2). After a simulation of 10 months of circulation, the production point located at the end of the 50-m fracture goes below 160°C. At the end of the simulation (6.4 years), the entire fracture has cooled down to 65C. It reflects that this simulation only take into account what happens in the vicinity of the injection well, where most of the chemical reactions are assumed to occur and it does not look at what happens farther in the reservoir, where the temperature remains high.

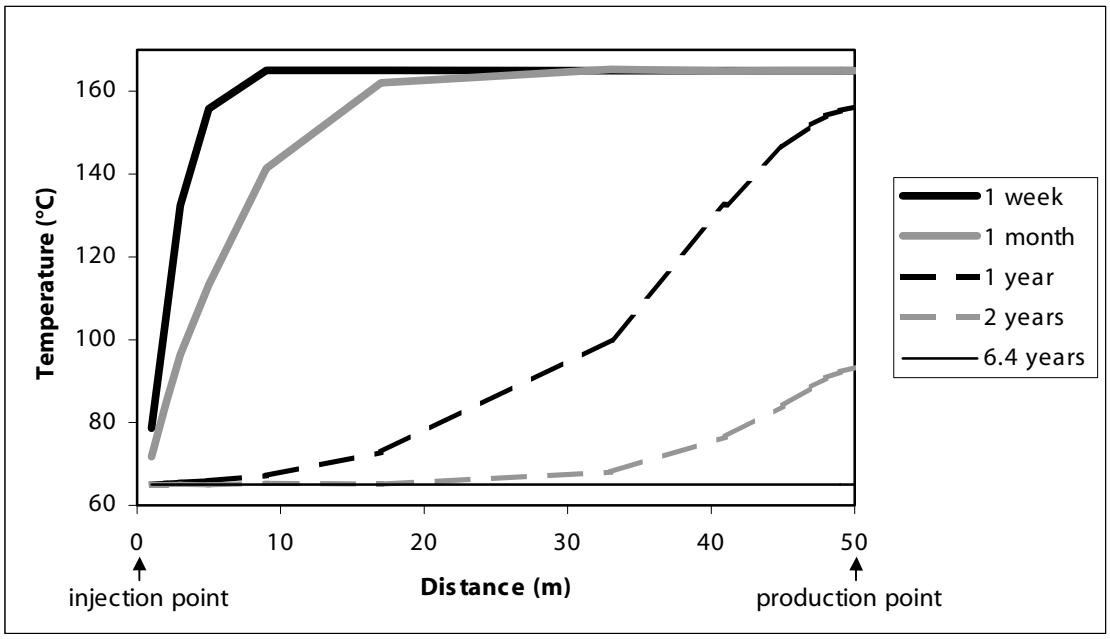

Figure 7.1.2 Temperature evolution in function of the distance from injection point

7.1.3. Evolution of the pH and the carbonates

As in the simulation at thermal equilibrium (see 5.3), the pH and the carbonates behaviour are directly linked. During the first month the pH starts at 4.6 at the injection point, reaches 5.0 at 5 m from the injection point and decreases to 4.8 in the next 10 m (Figure 7.1.3). After one year, the pH start at 4.4, reaches 5.0 between 15 and 35 m and goes down to 4.8. After 6 years, it starts at 4.7 in the first 10 m, then reaches 5.2 at 15 m and stay at this value in the whole 50 m.

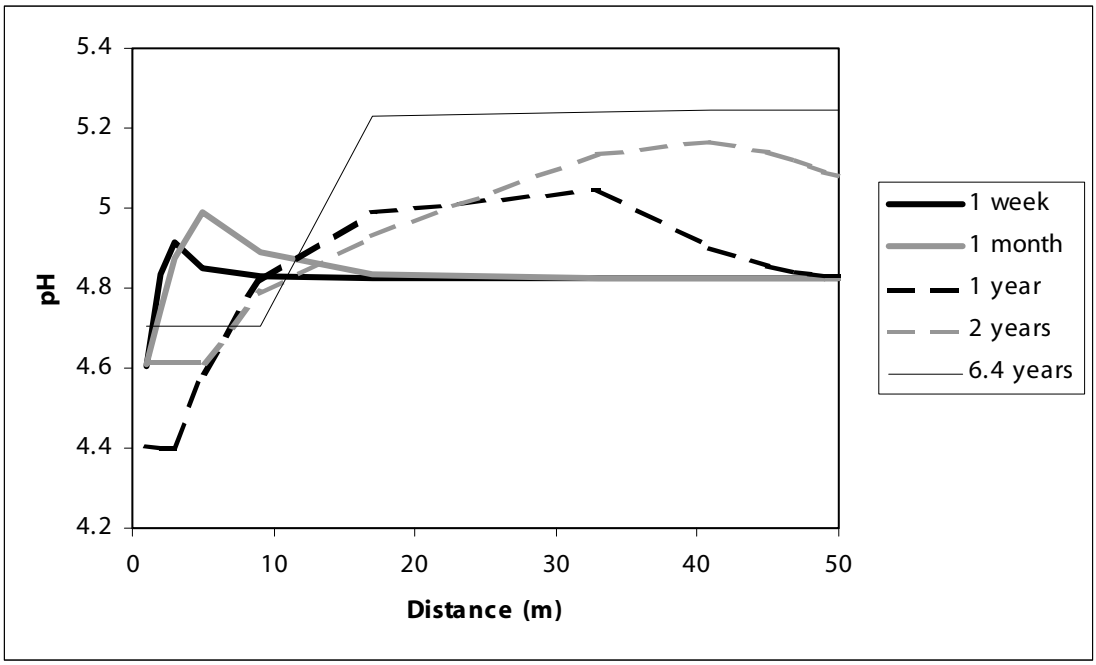

Figure 7.1.3 pH evolution in function of the distance from injection point

During the first month, calcite dissolves more than 10^{-4} mol.s^{-1}.m^{-3} in the first volume element and starts to precipitate in the second, third or fourth element at respectively 1day, one week and one month up to $2.5.10^{-4}$ mol.s^{-1}.m^{-3} (Figure 7.1.4). After one year, nothing happens in the first 3 m, then calcite dissolves in the next 20 m and starts to precipitate with a maximum rate at 40 m. After 3 years, calcite does not dissolve significantly anymore and starts to slowly precipitate at 20 m.

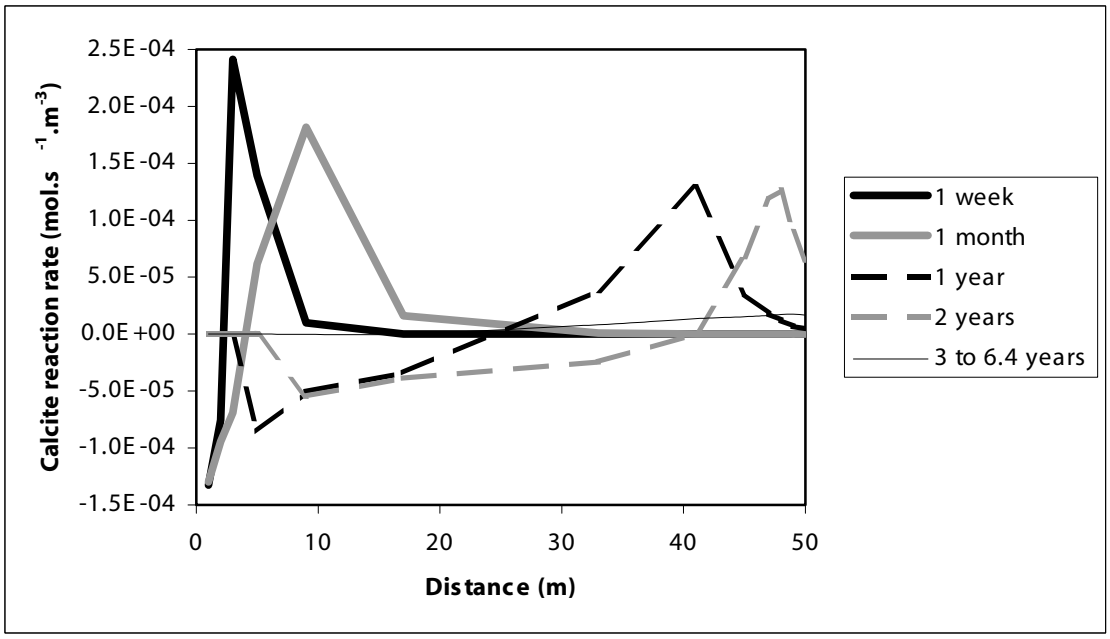

Figure 7.1.4 Calcite reaction rate in function of the distance from injection point

The evolution of the total Ca^{++} concentration in the fracture reflects the calcite behaviour, shifted by the fluid displacement (Figure 7.1.5). After one month it goes up to 10^{-3} mol.kg^{-1} higher than the initial

concentration in the first 7 m and goes down to 10^{-3} mol.kg^{-1} below the initial concentration in the rest of the fracture. After one year, it starts at 10^{-3} mol.kg^{-1} below the initial value then rises to $1.5.10^{-3}$ mol.kg^{-1} above the initial value at 17 m, before decreasing to 2.10^{-3} mol.kg^{-1} below the initial value at 40 m. At the end of the 6.4 years, the Ca^{++} concentration starts at 10^{-3} mol.kg^{-1} below the initial content then rises to 4.10^{-3} mol.kg^{-1} above the initial content after 10 m and remains at this value in the rest of the 50 m.

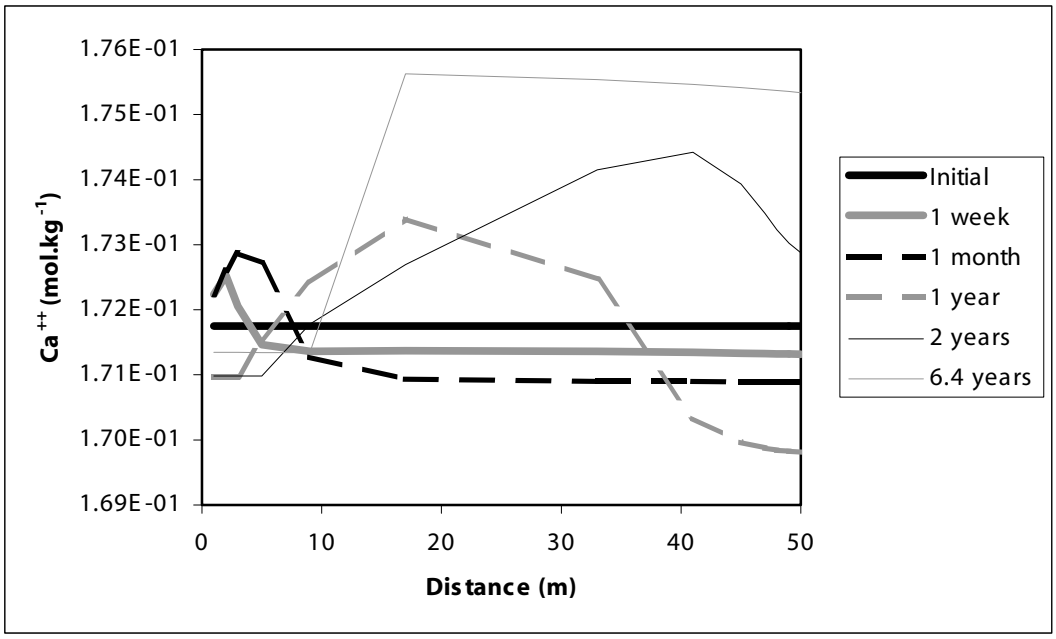

Figure 7.1.5 Calcium concentration in function of the distance from injection point

The dolomite never precipitates at any significant rate (Figure 7.1.6). During the first week it dissolves only in the first 5 m up to $6.5.10^{-5}$ mol.s^{-1}.m^{-3}. After one month the dissolution zone spreads to 17 m, with a rate decreasing from $6.5.10^{-5}$ mol.s^{-1}.m^{-3} at the injection point with a small peak at 10 m. After one year, the dissolution occurs between 5 and 41 m with a rate up to $2.5.10^{-5}$ mol.s^{-1}.m^{-3}. From 3 years to the end of the simulation, the dissolution occurs between 17 m to the end of the fracture with a rate up to $0.8.10^{-5}$ mol.s^{-1}.m^{-3}.

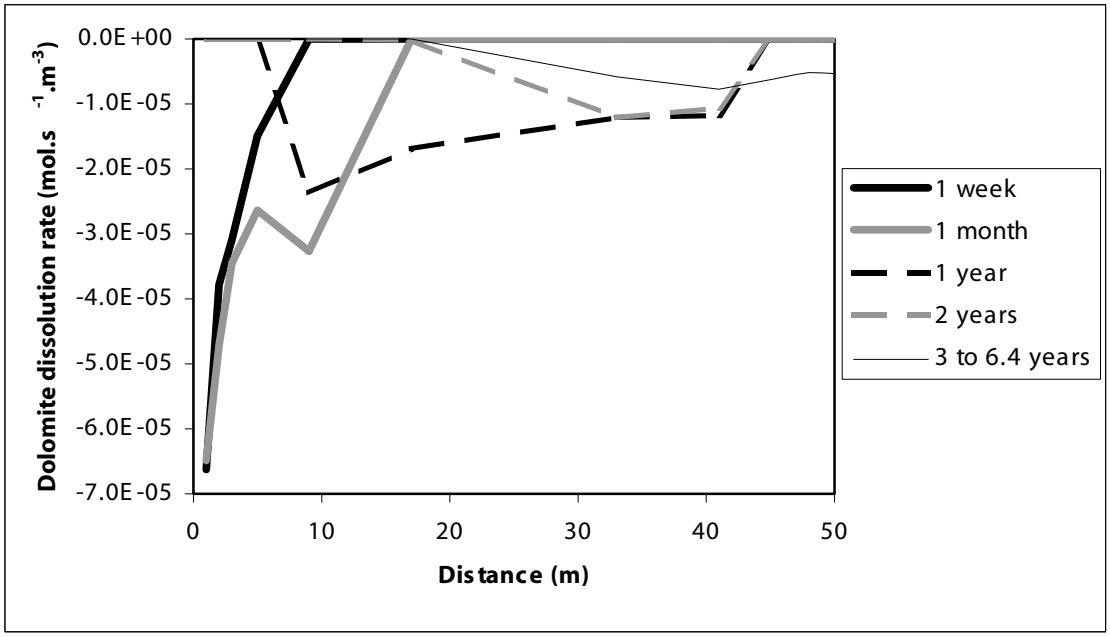

Figure 7.1.6 Dolomite reaction rate in function of the distance from injection point

Coming with dolomite dissolution, the Mg^{++} concentration increases during the simulation (Figure 7.1.7). After one month, it starts at $2.5.10^{-4}$ $mol.s^{-1}.m^{-3}$ above the initial concentration, reaches10^{-3} $mol.s^{-1}.m^{-3}$above the initial value after 10 m and stays at this value in the whole fracture. After 6.4 years, the concentration in the first 17 m is $1.5.10^{-3}$ $mol.s^{-1}.m^{-3}$ above the initial content and increases to 2.10^{-3} $mol.s^{-1}.m^{-3}$ above the initial content at the end of the 50 m.

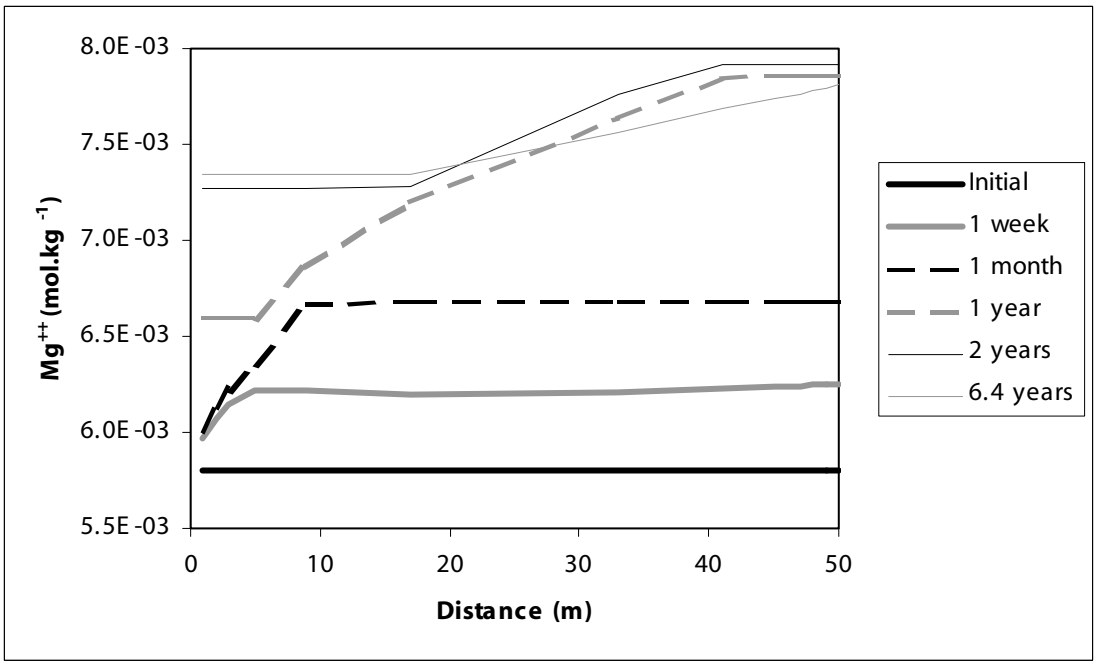

Figure 7.1.7 Magnesium concentration in function of the distance from injection point

These results show that at the beginning the low pH cooled fluid dissolves calcite and dolomite at a high rate next to the injection point. This causes an augmentation of Ca^{++}, Mg^{++} and CO_3^{--}

concentrations and with rapid reheating the fluid quickly precipitates calcite with a rise of the pH. The kinetics of calcite precipitation being faster than the dolomite one prevents dolomite precipitation. With the evolution of the temperature field, this process occurs on a wider zone with lower reaction rates. With time the reactions near to injection point vanish due to the decrease of available carbonates. Dolomite dissolution at the beginning of the simulation is controlled by the temperature field but slowly changes to be controlled by calcite precipitation.

7.1.4 Quartz and pyrite evolution

The quartz precipitates in the fracture during the simulation with a maximum rate of 6.10^{-7} mol.s^{-1}.m^{-3} during the first year (Figure 7.1.8). This maximum rate decreases during the following of the simulation and becomes lower than 10^{-7} mol.s^{-1}.m^{-3} after 2 years. No quartz dissolution occurs during the simulation.

The quartz precipitation rate is controlled essentially by the temperature field as shown in Figure 4.4.3.

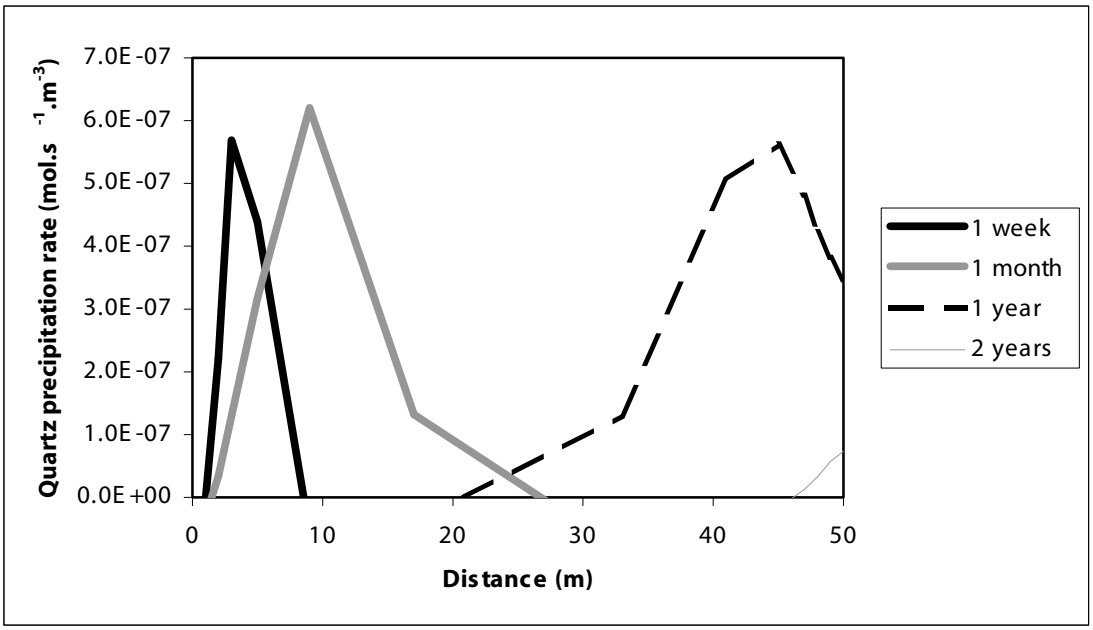

Figure 7.1.8 Quartz reaction rate in function of the distance from injection point

The pyrite precipitates similarly to the quartz with a maximum rate of 4.10^{-12} mol.s^{-1}.m^{-3} during the first year (Figure 7.1.9). However, unlike quartz, there are some punctual dissolution events. The first day, at 3 m from the injection point, it dissolves at $3.6.10^{-6}$ mol.s^{-1}.m^{-3} and at 33 m after one month it dissolves at $2.8.10^{-8}$ mol.s^{-1}.m^{-3} but no dissolution occurs after one week of simulation. Another difference from the quartz kinetics is the $1.9.10^{-12}$ mol.s^{-1}.m^{-3} precipitation rate after 17 m that stays after 3 years.

These differences are due to the fact that even if the pyrite reaction depends principally on the evolution of the temperature field, there is still an influence from the pH variations which may cause some exceptional dissolution events.

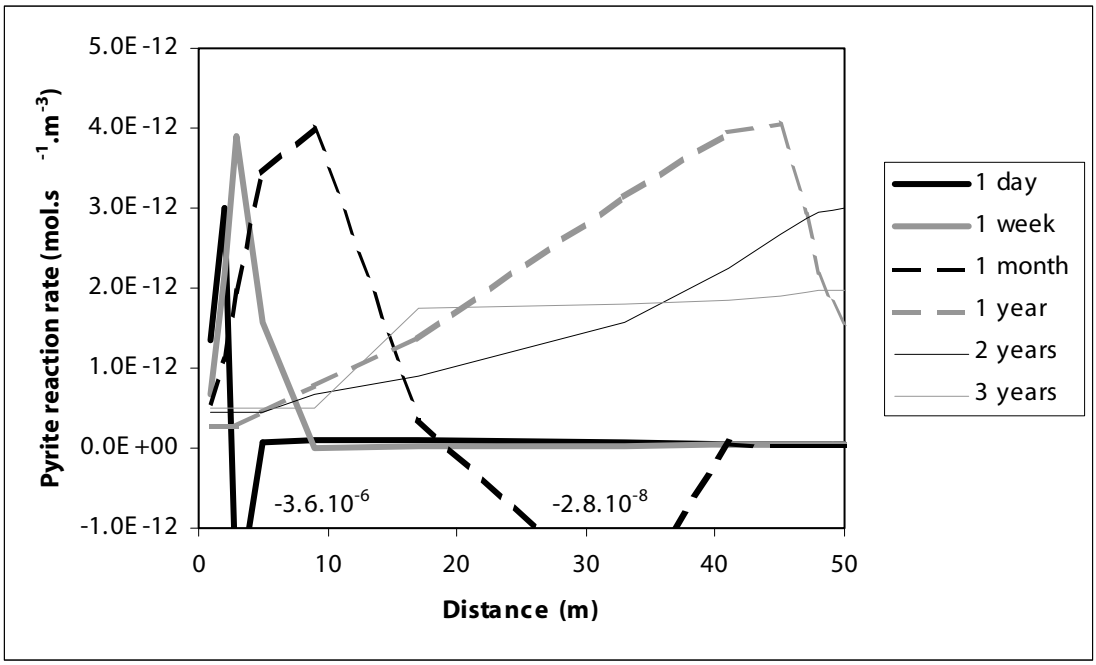

Figure 7.1.9 Pyrite reaction rate in function of the distance from injection point

7.1.5 Evolution of the porosity

After one month, the porosity near the injection point increases by 12% and shows a light decrease between 3 and 10 m (Figure 7.1.10). One year later, the porosity near the injection point reaches 1.6 times its initial value. This augmentation decreases to zero at 15 m and the porosity drops below its initial value (15 to 45 m) with a maximum decrease of 10%. After 6.4 years, the porosity near the injection point stays 1.6 times higher than its initial value. The augmentation decreases to zero at 33 m and the following decrease goes down to 75% of the initial porosity between 40 and 48 m. This correspond to a maximum increase of 350% in permeability followed by a maximum decrease of 50%.

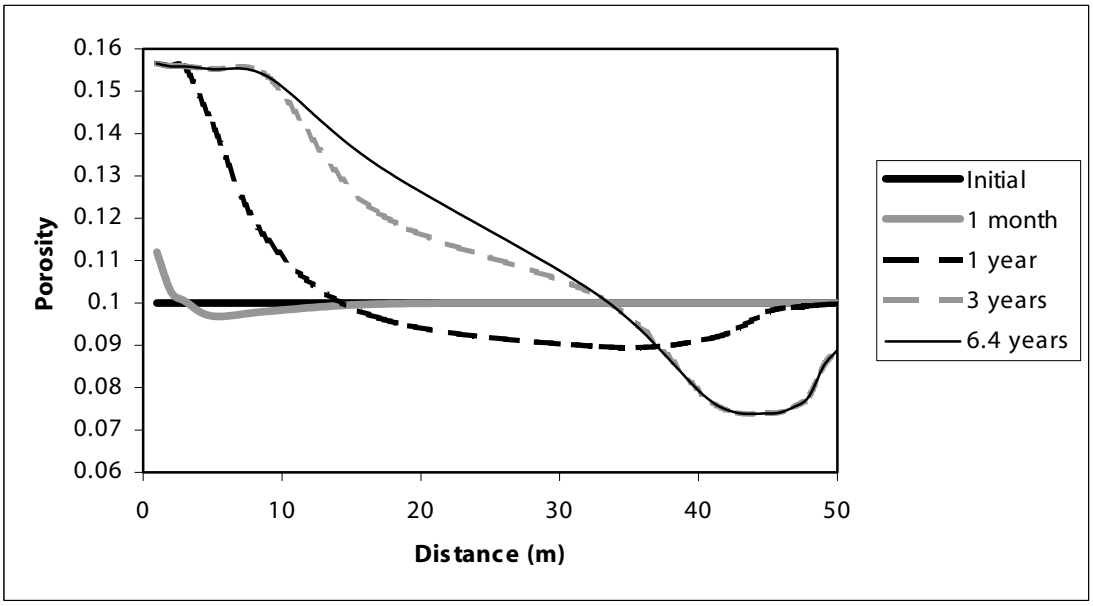

Figure 7.1.10 Porosity in function of the distance from injection point

The high increase of permeability near the injection point is due to the carbonates dissolution and is limited by the initial amount of calcite and dolomite. The following decrease is due to the calcite

reprecipitation and is limited by the parallel dolomite dissolution. The stabilisation after 3 years is caused by the stabilisation of the temperature field at 65°C and the diminution of available carbonates that decreases the reaction rates.

7.2 Two fractures model

7.2.1 Model description

The model consists of a 650*600 m granitic matrix zone. An injection and a production well separated by 450 m have been set. The two wells are linked by two types of fracture cluster: a 0.2 m wide fracture cluster going directly from injection to production and a set of 1 m wide fracture clusters traversing 850 m between the two wells (Figure 7.2.10). The model, which is set up, is only the upper half of the overall model. The lower part of the model, which is not set up, is mirror-inverted along the x-axis. Therefore only half the fracture (0.1 m) along the x-axis is taken into the model.

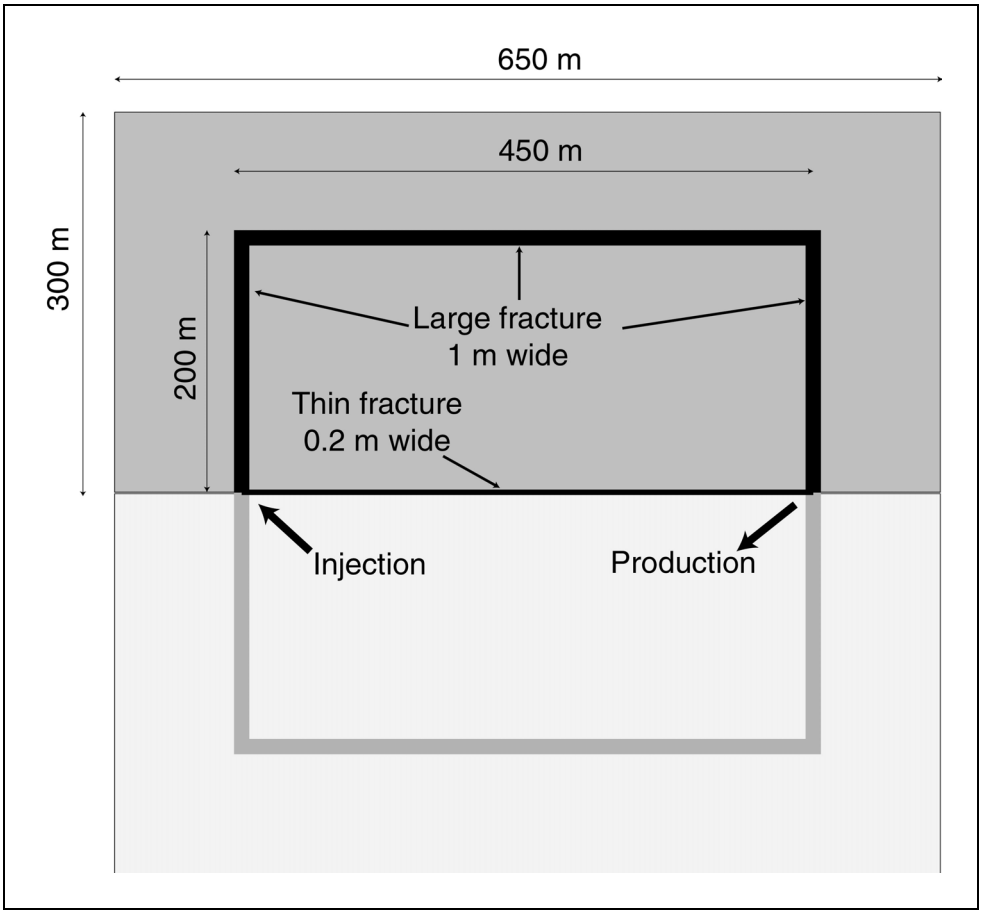

Figure 7.2.10 Model geometry. Due to the symmetry, only the upper part is taken into account.

The model is composed of 3381 2-D elements and is discretized finer along the fractures as shown in Figure 7.2.11. which illustrates the model. The fluid is injected at the beginning of both fracture clusters, and produced at the end of both fracture clusters.

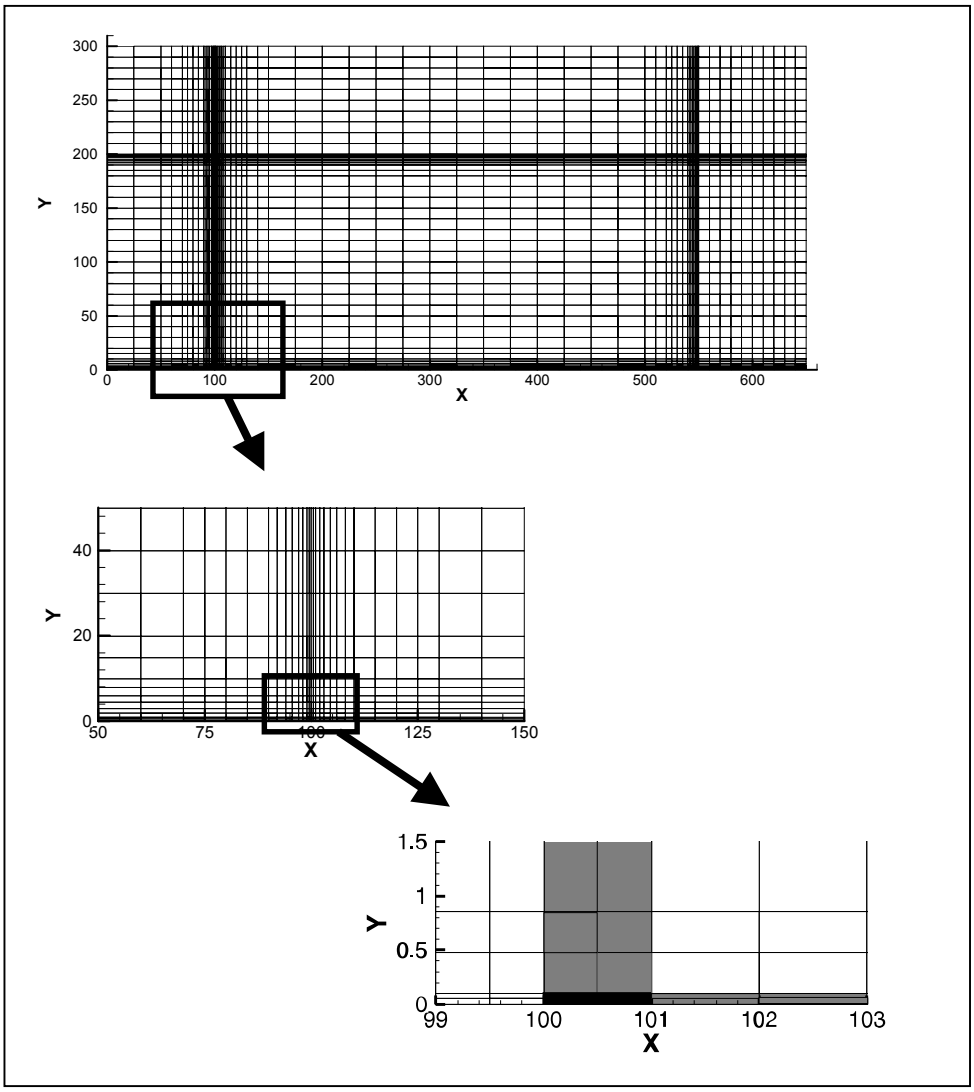

*Figure 7.2.11 Model discretisation. at different scales (all distances are in m). a) Whole model. b) 100*50 m zone around the injection point. c) 4*1.5 m zone around the injection point with the four injection elements in black and the fracture elements in grey.*

The thermal-hydraulic parameters shown in Table 7.2.1 are chosen in order to receive 'realistic' pressure (pressure difference between injection and production ~ 5 MPa) and temperature conditions (65°C at the injection and 165°C at the production) during the model simulation.

Table 7.1.2 Thermal-hydraulic parameters

Parameters	Fracture 0.2 m	Fracture 1 m	Matrix and boundary	Injection and production
Hydraulic conductivity $m.s^{-1}$	$1.4.10^{-9}$	$1.4.10^{-9}$	$1.0.10^{-13}$	$1.4.10^{-9}$
Storage coefficient Pa^{-1}	$1.00.10^{-10}$	$1.00.10^{-10}$	$1.00.10^{-10}$	$1.00.10^{-10}$
Porosity %	0.1	0.1	0	0.1
Thermal conductivity $W.m^{-1}.K^{-1}$	2.2	2.2	3	2.2

The fluid density is 1070 $kg.m^{-3}$, the rock density 2650 $kg.m^{-3}$, the heat capacity of the rock is 1000 $J.kg^{-1}.K^{-1}$ and the heat capacity of the fluid is 4200 $J.kg^{-1}.K^{-1}$. No radiogenic heat production is integrated in the model.

Initially the temperature is 165°C and the pressure 10^5 Pa in the whole model. The left, upper and right boundaries are set to a constant temperature of 165°C. Then, an amount of 10^{-3} $m^3.s^{-1}.m^{-1}$ fluid at 65°C is injected in four adjacent elements, resulting in a pressure of 5 MPa at the injection. Taking into account the symmetry of the model, the injected amount represents 2.10^{-3} $m^3.s^{-1}$. At the four adjacent production elements the pressure is held constant at 0 Pa. The produced fluid flows through a buffer of 2000 m^3, which represents the fluid volume contained in wells and surface installations, before being re-injected. The fluid flow in the matrix is negligible due to low hydraulic conductivity and zero matrix porosity. Thus, all chemical reactions happen in the fracture, whereas in the matrix no reactions take place. The total simulation time is $1.67.10^8$ s (≈ 5 years and 100 days).

7.2.2 Results

The results are concordant to those of the 1-D simulation. Calcite dissolves at the vicinity of the injection zone and reprecipitates when the temperature rises. After 6 months, the calcite dissolution rate in the injection elements decreases due to the diminution of available calcite that is almost totally dissolved after 8 months. Dolomite shows a similar dissolution trend but is removed faster at the injection point and the precipitation rate is significantly lower than the dissolution. The quartz precipitate in the low temperature zone and dissolves when the fluid warms up. Due to the relatively low reaction rates both precipitation and dissolution occur on a wide portion of the fracture. The pyrite does not present significant variations. Concerning the evolution of the fluid concentration in the whole model, two major evolutions appears (Figure 7.2.12). First, the total calcium concentration decreases from 172 $mmol.kg^{-1}$ and stabilizes at 154 $mmol.kg^{-1}$ after 3 years. Second, the total magnesium concentration rises from 5.8 $mmol.kg^{-1}$ and stabilizes at 22.2 $mmol.kg^{-1}$ after 3 years. This illustrates the preferential precipitation of calcite over dolomite.

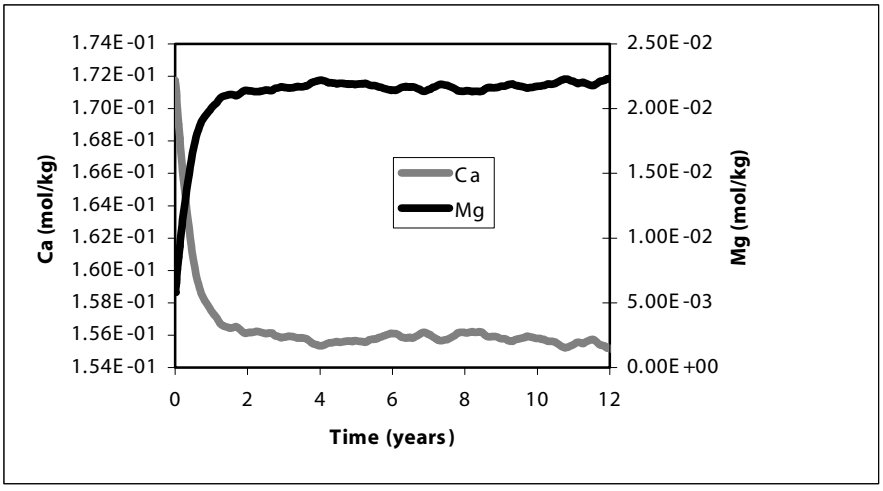

Figure 7.2.12 Calcium and Magnesium evolution in the produced fluid.

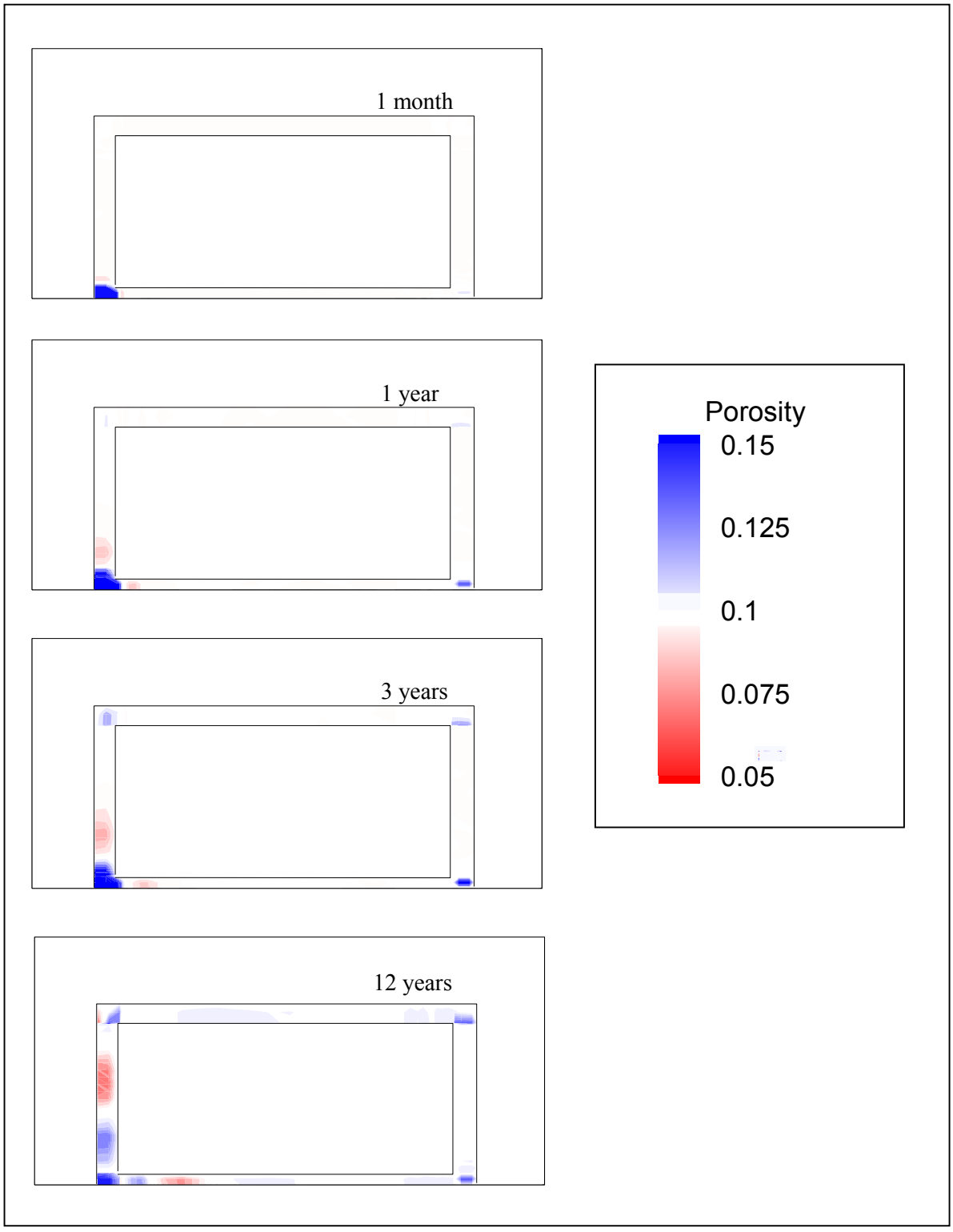

Figure 7.2.13 Evolution of the porosity in the fractures during the first 12 years. The fractures width are exaggerated in the figure.

The Figure 7.2.13 shows the evolution of the porosity along the two types of fractures. The initial porosity of the fracture was 0.1.

- After one month the porosity at the injection point reaches 0.13 and goes down to 0.09 in the fractures.
- After one year the porosity at the injection reaches 0.16 and goes down to 0.08 at 25 m and 0.09 at 17 m respectively in the large and thin fracture. The area affected by the porosity reduction is wider.

- After three years, the porosity at the injection point stays around 0.16 and the more porous zone extends up to 20 m in the large fracture and 10 m in the thin fracture. The low porosity zone has also grown with a minimum of 0.08 at 50m in the large fracture and at 30 m in the thin fracture.
- After 12 years, the high porosity zone extends to 30 m in the large fracture and 15 m in the thin fracture. The low porosity zone has also grown with a minimum at 60m in the large fracture and at 40 m in the thin fracture. The smaller porosity variations appearing at the angle of the large fracture and at the production point are supposed to represent numerical artefacts.

The high porosity zone corresponds to an increase of 350% of the porosity and the subsequent low porosity to a decrease of 60%. Considering that there are only two fluid pathways and that the value of the permeability reduction in these two paths are small and close to each other, the geochemical reactions do not significantly modify the thermal-hydraulic parameter in this model.

7.3 Sensitivity and critical parameters

The solver of chemical equilibrium equations tries to resolve the system based on the total concentrations in basic species. This means the concentration in basic species plus the stoechiometric quantity of each basic species in secondary species. The choice of the basic and secondary species should be done to avoid a negative total concentration. For example, if the $CO_{2(aq)}$ is chosen as the basic species for carbon, then the secondary species HCO_3^- obtained by the reaction $HCO_3^- + H^+ \rightarrow CO_{2(aq)} + H_2O$ will count for 1 $CO_{2(aq)}$ and –1 H^+. In this case, if there is more HCO_3^- than H^+ in solution, therefore the total concentration in H^+ will be negative and the program calculation will fail.

There is no method to fix a target value for a given species, like H^+ for the pH. The initial concentration has to be set in order to obtain the expected value. The best way is to introduce the concentrations of a solution equilibrated at the desired temperature. The pH can be adjusted by variation of the initial H^+ and OH^- concentrations.

Small variations of the initial pH (0.1) will have a significant effect on the reaction rates of carbonates, but this effect should disappear during the first days of simulation, when the system will tend to recover equilibrium and will not have significant effects for long time simulations.

The best maximum concentration variation allowed per chemical step seemed to be around a factor 10 for the simulations realized. A smaller value ensures that the equilibrium solver will converge rapidly but multiplies the number of iterations. A higher value limits the number of chemical iterations but the solver needs more time to converge and happens to fail in some cases.

No true sensitivity analysis has been made concerning the spatial discretization, but the comparison between the results of the two simulations indicates that the permeability variation depends principally on the evolution of the temperature field calculated by FRACTure and not much on the spatial discretization or the fluid flow rate.

7.4 Synthesis

The first application of the new code FRACHEM consisted of the modelling of a simplified system, including a cooled fluid reinjected in a hot reservoir composed of a 50-m long by 1-m wide fracture cluster surrounded by an impermeable matrix. This 2-D model carried out a 6.4 year-simulation and took a computing time of 14.5 hours. The most significant change compared to the 1-D fracture modelled with Chem-TOUGH2 is the absence of initial thermal equilibrium. At the end of the simulation, the entire fracture is cooled down to 65°C, but this 50-m long model only represents the injection influence area of the full scale Soultz reservoir.

The results show that at the beginning of the simulation, calcite and dolomite are rapidly dissolved near the injection point. Then, warming up induces carbonates precipitation on a wider zone. Later, the carbonates being less available in the injection area, reactions rates decrease significantly. Quartz and pyrite precipitate in the fracture only during the first year. Moreover, some exceptional events of

pyrite dissolution are also observed. Permeability evolution mainly shows a high increase near the injection point, due to carbonates dissolution. On the other hand, a small decrease of permeability is observed later, due to calcite re-precipitation.

The second application was a 2-D model with the dimension of the upper Soultz reservoir. This model includes two fractures of different widths following two different paths. The geochemical evolution is similar to the previous simulation with carbonates dissolving near the injection point and re-precipitating further in the fracture. During the five first years this lead to a permeability increase of 350 % following by a decrease of 60 %. The variations are similar in both fractures and affected the first 50 m of the thin fracture and the first 75 m of the large one.

8. General discussion, conclusions and recommendations

8.1 General discussion

8.1.1 Main objectives and justifications

The main goal of the present study was to provide a numerical simulation code for the Soultz fractured reservoir. This code should be able to account for all geochemical processes occurring during the exploitation of the Soultz reservoir and should be coupled to the simulation of the thermal-hydraulic processes. The final modelling code was expected to simulate the evolution of the hydraulic impedance of the reservoir and of the produced fluid temperature, as well as to predict possible scaling in the wells and the surface installations. Beyond the building of the modelling tool, the study should provide a better understanding of the type of chemical reactions susceptible to occur in Hot Fractured Rock reservoirs.

The previous works on the geochemical modelling of the Soultz system were helpful for the understanding of the problem but are not directly applicable to the expected modelling. Genter (1990) performed simulation based on thermodynamic equilibrium using Debye-Huckel formalism and Azaroual (1994) simulated the interactions between fresh granite and distilled water. Later, Jacquot (2000) carried out kinetic simulation of the interaction between altered granite and formation fluid, including clay minerals, but his model was based on Debye-Huckel formalism and did not integrate sulphides and sulphates. No coupling with a hydraulic code was ever attempted.

8.1.2 Geochemical characterisation of the Soultz system

The characterisation of the fluid from the 3.5 km deep reservoir was elaborated from three sources. The on-site measurements during the 1997 circulation test and two sets of analyses performed at the BRGM (Orléans) and at the CGS (Strasbourg) on the samples taken during this test. These data allowed a good definition of the concentrations in Na, Cl, Ca, K, Mg, Si, Fe and total sulphur. The dissolved carbon content as well as the repartition between sulphates and sulphides had to be calculated. The first concentration was obtained by the assumption that the fluid was in equilibrium in regard to calcite at reservoir temperature. The assumption is realistic but the result depends on the pH chosen, which can only be estimated from on-site measurements. The HS/SO_4 ratio was obtained assuming the equilibrium in regard to anhydrite at 165°C. This equilibrium concentration can be calculated with good confidence but there is no evidence that the reservoir fluid is not undersaturated in regard to anhydrite. There was unfortunately no possibility to obtain a good estimation of the aluminium concentration in the fluid, due to the lack of both reliable analyses and theoretical model. Some data about solubility of aluminium under geothermal conditions were published during this study (Benezeth, 2000) and could further be used to recalculate the Al content in the fluid.

Finally the plausible concentrations of Na, K, Ca, Fe, SiO_2, Cl, C, SO_4, HS have been defined for the 3.5 km reservoir formation fluid. The mineral composition of the rock in contact with the circulation fluid is better known from the core samples analysis. The resulting system characterisation, although dependent on some assumptions, was satisfactory to set up the fluid-rock interaction modelling, with the exception of aluminosilicate minerals.

8.1.3 Thermodynamic model

The specificities of the system allowed to build a model for the calculation of the activity coefficients of the aqueous species that combines Pitzer formalism with a quick calculation method. Mostly based on calculation performed with TEQUIL and on some assumptions, this model can provide the activity coefficients for the system H_2O, Na^+, K^+, Ca^{++}, Mg^{++}, Fe^{++}, $Ca(HCO_3)^+$, H^+, Cl^-, OH^-, HCO_3^-, CO_3^{--}, SO_4^{--}, HS^-, $CaCO_{3(aq)}$, $CO_{2(aq)}$, H_4SiO_4 and $CaSO_{4(aq)}$ from 50 to 200 °C. The model assumes that no

SO_4/HS^- reactions occur in the fluid, which is reasonable due to the short period of time during which the fluid remains cooled and due to the absence of oxygen producing reaction.

The model can calculate the saturation indexes of the fluid in regard to calcite, dolomite, anhydrite, pyrite, quartz and gaseous CO_2. No accurate way of modelling iron oxides and oxy-hydroxides solubility has been set up yet, due to the absence of a sound model of iron redox reactions in the fluid. The possibility of modelling solid solutions such as magnesian calcite has been postponed due to its excessive numerical complexity.

The maximum potential amount of reaction was calculated with this model for one year of production in the conditions of the 1997 circulation test: near the bottom of the injection well, a dissolution of more than 300 m^3 of carbonates is obtained along with a precipitation of less than 40 m^3 of quartz and pyrite.

8.1.4 Kinetic reaction model

The kinetic model integrates dissolution and precipitation rates for calcite, dolomite, quartz and pyrite. These rates come from published works about studies performed in conditions as close as possible to the Soultz reservoir. Some uncertainties remain due to the necessary estimation of some unknown parameters like the relative importance of surface reaction versus diffusion for carbonate dissolution or the Fe^{2+}/Fe^{3+} ratio for pyrite dissolution.

The remaining unknown parameters needed for the simulation, the existent mineral surface available for reactions and the permeability changes, were linked to the chemical model via a simple geometrical representation of the fracture clusters. This geometrical model can be calibrated knowing only the porosity and permeability of the fracture cluster. Nevertheless the distribution of the different minerals between fracture and grain matrix has to be estimated based on the description of the core samples.

8.1.5 Available tools

The model of fluid-rock interactions in the Soultz system has been integrated in two codes. First, a modified version of Chem-TOUGH2 and second a new code FRACHEM obtained by coupling of the new geochemical code with FRACTURE. The respective features of the two codes are summarized in Table 8.1.1.

Table 8.1.1 Differences between the Chem-TOUGH2 and FRACHEM codes.

Characteristics	**Chem-TOUGH2 (adapted for the Soultz system)**	**FRACHEM**
Discretisation	Finite volumes	Finite elements
Fluid flows	Darcian	Darcian and turbulent
Coupling between transport and reactions	One-step coupling	Sequential non-iterative coupling
Other features		Thermal-mechanical modelling

8.1.6 Simulation results

Some simple simulations were carried out with each code. The first one, with Chem-TOUGH2, modelled the circulation trough a 1200 m fracture, starting at thermal equilibrium, showed a linear increase of permeability in the first 10 m beyond injection point, but no significant permeability variations farther in the fracture. The second simulation with FRACHEM modelled the circulation

through a 50 m fracture, starting at 165°C and progressively cooled down to 65°C by the injected fluid. The latter showed an increase of the permeability up to 350% in the first 30 m, followed by a decrease up to 25% in the last 10 m. In the third simulation, still with FRACHEM and representing the evolution of a model with a similar size to the upper Soultz reservoir, the fluid flowed through two pathways, a direct small fracture and a wider but longer one. This simulation showed a 350 % increase of the permeability at the injection point like the previous one but the subsequent decrease of permeability reached 60 %. The three simulations highlight the predominance of the carbonates reactions effect during a time step of several years.

8.1.7 Further work

Some upgrading work should be performed to the geochemical code. The thermodynamic model should be adapted to the fluid in the 5 km deep reservoir. As expected the fluid collected between 4.5 and 5 km shows a similar composition compared to the 3.5 km fluid. The iron oxides and oxi-hydroxides, as well as some aluminosilicate minerals, especially K-feldspar and clay phases, should be integrated in the thermodynamic and kinetic model. The observed minerals precipitation in the former casing of GPK2 well will be simulated in order to calibrate the geochemical model.

Some more complex coupled simulations have to be performed and finally, the upgraded FRACHEM code should be used to simulate the evolution of the future deep reservoir under exploitation.

8.2 Conclusions

This study allowed to bring decisive steps towards the understanding of fluid-rock interactions between a hot saline brine and a hydrothermalised fractured granite, as well as geochemical modelling and simulation of the 3.8-km deep geothermal reservoir in Soultz-sous-Forêts.

- First approach to model the fluid-rock interaction by means of the Pitzer formalism, used to calculate the activity coefficient of brines. To the exception of the aluminium, the lack of parameters has been circumvented. The specificity of the Soultz system allowed to reduce the number of calculations for the activity coefficients to a simple equation. The chosen method requires a first step of modelling aimed toward the specific problem. This approach leads to the building of a simplified but reliable model that can be introduced in a reactive transport code used for the simulation of a system composed by some thousands of volume elements without requiring too much computer capacity.
- Improvement of the geochemical characterisation of the formation fluid present in the fractured granite.
- Deciphering of the respective importance of the geochemical processes linked to the geothermal loop: (1) fluid raising through the production well, (2) rapid cooling through the surface heat exchanger, (3) return to the reservoir through the injection well, (4) flow into the reservoir and (5) warming up in the fractured reservoir. These processes are schematised in Figure 8.2.1.

  Based on the thermodynamic model the only significant reaction that can occur in the production well is the precipitation of carbonates in case of CO_2 degassing. During the cooling of the fluid quartz and sulphides can potentially precipitate. This precipitation can also happen in the injection well and in the reservoir near to the injection zone. This zone is also a site of potential carbonates dissolution. Finally, when the fluid warms up in the reservoir, it can precipitate carbonates and dissolve quartz and sulphides.

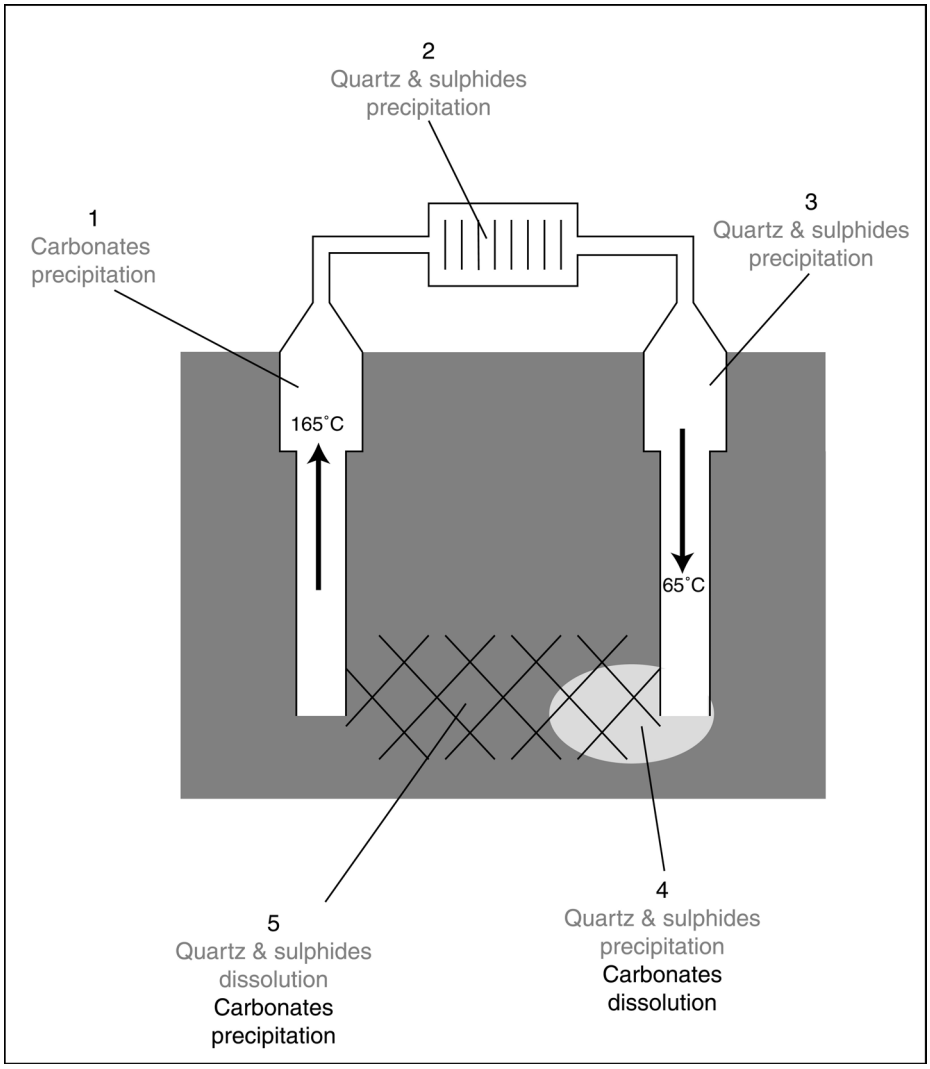

Figure 8.2.1 Potential reactions during the reservoir exploitation. Reactions indicated in bold are significantly more important than the others

- Quantitative comparison of the thermodynamic model with the kinetic model. The reaction rates obtained show that the precipitation or dissolution of quartz and pyrite are not significant in the time scale of the reservoir exploitation, especially in the heat exchanger and the injection well where the low temperature decrease these rates. However, for the deep reservoir, the silica concentration is three time higher and therefore the risk of quartz or amorphous silica precipitation in the heat exchanger should become real.
- Creation of a new combined simulation tool FRACHEM, using the code FRACTure and a geochemical module developed from the code Chem-TOUGH2. Both the simple thermodynamic calculation method and the averaging of the reaction rates during one time step allow the simulation of models composed by some thousands of elements for more than ten years of circulation on a Pentium II workstation. Using a faster computer should permit the simulation of a more complex and realistic reservoir.
- First attempts to simulate geochemical processes with a coupled model taking into account thermal, hydraulic, mechanical and geochemical processes. These simulations confirm the geochemical behaviour within the reservoir. The carbonates are dissolved in the vicinity of the injection zone and the calcite re-precipitates farther in the reservoir.

- First contribution to the permeability evolution during a long-term exploitation of the reservoir, indicating a significant increase of the permeability around the injection, followed by a more diffuse decrease at the border of the cooled zone.

8.3 Recommendations

8.3.1 Geochemical aspects

Laboratory experiments could be useful for a better definition of the model:

- A percolation test through a core sample from Soultz granite, like the experiments presently performed at the BRGM (Orléans), will help to calibrate the model, even if the experiment is limited to a small pathway and a short duration.
- Precipitation/dissolution tests in a reactor between 50 and 200°C for selected minerals interacting with brines at 100 g/l could lead to either validation or correction of the thermodynamic and kinetic models.

Field work tests carried out before the exploitation of the pilot plant:

- The difficulty to obtain a good definition of the reservoir fluid and the limited occasions to obtain fluid samples stress the importance to execute complete wellhead fluid and gas chemical analyses during the planned short production tests.

8.3.2 Modelling aspects

The theoretical model would require additional work in order to consider all possible relevant processes occurring during the exploitation of the Soultz reservoir:

- The model should be tested and modified if necessary for the conditions and the fluid of the 5-km depth reservoir.
- A model for iron oxides and oxi-hydroxides, including redox state of aqueous iron should be developed.
- A way to model the behaviour of the clay phases present in the system should be found and introduced in the model. With the addition of the aluminium in the thermodynamic model, the clays could on a first approximation be simulated by selected pure phases.

8.3.3 Coupling aspects

The coupled code FRACHEM should be used to simulate the evolution of a system closer to the real Soultz system, with dimensions and complexity corresponding to the whole reservoir and multiple flow paths.

8.3.4 Computing aspects

The programme itself could be improved in some ways:

- The code will be optimised for calculation speed.
- The comfort of the code users should be improved.

8.3.5 Reservoir production aspects

The building of the pilot plant in Soultz and the start of the first industrial production should also provide more information leading to an improved and more useful tool:

- It will provide a real validation of the model results.

- On-line tests during the circulation with bypasses containing metal coupons, as well as rock and cement samples could allow a better calibration of the model.
- Regular and complete fluid and gas analyses at the production wellheads during the first year of production should be conducted, as well as a preliminary bacteriological tests on produced and injected fluids.
- A sampling and analysis programme should be set up and realised for the whole exploitation period of the pilot plant.

The possible scaling problems in the wells and on the heat exchanger should be avoided. The attention should focus on:

- Maintaining a high enough pressure in the surface installation to avoid CO_2 degassing and turbulence zones should be kept to the minimum before the cooling of the fluid, in order to avoid carbonates precipitation.
- Designing of the heat exchanger and setting of the ideal final temperature after cooling, in order to avoid silica scaling.

9. References

Aagaard, P. and Helgeson, H.C., 1982. Thermodynamic and kinetic constraints on reaction rates among minerals and aqueous solutions; I, Theoretical considerations. American Journal of Science, 282(3): 237-285.

Althaus, E., 1982. Geochemical Problems in Fluid-Rock Interaction. In: R. Haenel (Editor), The Urach Geothermal Project (Swabian Alb. Germany). E. Schweitzerbart'sche Verlagsbuchhandlung (Naegele und Obermiller), Stuttgart, pp. 123-133.

Aquilina, L., Pauwels, H., Genter, A. and Fouillac, C., 1997. Water-rock interaction processes in the Triassic sandstone and the granitic basement of the Rhine Graben; geochemical investigation of a geothermal reservoir. Geochimica et Cosmochimica Acta, 61(20): 4281-4295.

Aquilina, L., Genter, A., Elsass, P. and Pribnow, D., 2000. Evolution of fluid circulation in the Rhine Graben; constraints from the chemistry of present fluids. Hydrogeology of crystalline rocks. In: I. Stober and K. Bucher (Editors), Hydrogeology of crystalline rocks. Kluwer Acad. Publ., Dordrecht, pp. 177-203.

Arvidson, R.S. and Mackenzie, F.T., 1999. The dolomite problem; control of precipitation kinetics by temperature and saturation state. American Journal of Science, 299(4): 257-288.

Azaroual, M., 1994.Modélisation des interactions solutions hydrothermales-granite. Application au furtur échangeur géothermique de type roche chaudes sèches de Soultz-sous-Forêts, Alsace, France. Document du BRGM N° 232, Ed. BRGM, Orléans, France, 233p.

Baechler, D., Evans, K., Hopkirk, R., Kohl T., Mégel, T. and Rybach, L., 2001. Data analysis and controls towards understanding reservoir behaviour and the creation of a conceptual reservoir model. Federal Office for Education and Science, final report, project 98.0008-1, ETH-Zurich, Switzerland, 203p.

Baria, R., Garnish, J., Baumgärtner, J., Gérard, A. and Jung, R., 1995. Recent development in the European HDR research programme at Soultz-sous-Forêts (France). World Geothermal Congress 1995, Florence, Italy, pp. 2631-2637.

Baria, R., Baumgärtner, J., Gérard, A. and Jung, R. (eds), 1998. European Hot Dry Rock geothermal research programme 1996-1997. Final report. Contract N° JOR3-CT95-0054 of the EC (Joule III), 151 pp, unpubl. report.

Baria, R., Baumgärtner, J., Gérard, A. and Garnish, J., 2000. The European HDR programme: Main targets and results of the deepening of the well GPK2 to 5000 m. World Geothermal Congress 2000, Kyushu-Tohoku, Japan, pp. 3643-3652.

Barrett, T.J. and Anderson, G.M., 1988. The solubility of sphalerite and galena in 1-5 m NaCl solutions to 300 °C. Geochimica et Cosmochimica Acta, 52(4): 813-820.

Batzle, M.L. and Wang, Z., 1992. Seismic properties of pore fluids. Geophysics, 57(11): 1396-1408.

Baumgärtner, J., Gérard, A., Baria, R., Jung, R., Tran-Viet, T., Gandy, T., Aquilina, L. and Garnish, J., 1998. Circulating the HDR reservoir at Soultz: Maintaining production and injection flow in complete balance, initial results of 1997 experiment. 23rd Workshop on Geothermal Reservoir Engineering, Stanford Univ., Stanford, USA, pp. 11-20.

Baumgärtner, J., Gérard, A. and Baria, R., 2000. Soultz-sous-Forêts: Main technical aspects of deepening the well GPK2. World Geothermal Congress 2000, Kyushu-Tohoku, Japan, pp. 3653-3663.

Bénézeth, P., Palmer, D., Wesolowski D., and Anovitz, L., 2000. Solubility and reaction rates of aluminum solid phases under geothermal conditions World Geothermal Congress 2000, Kyushu-Tohoku, Japan, pp. 2533-2537.

Berner, R.A., 1978. Rate control of mineral dissolution under Earth surface conditions. American Journal of Science, 278(9): 1235-1252.

Bolton, E.W., Lasaga, A.C. and Rye, D.M., 1996. A model for the kinetic control of quartz dissolution and precipitation in porous media flow with spatially variable permeability; formulation and examples of thermal convection. Journal of Geophysical Research, B, Solid Earth and Planets, 101(10): 22,157-22,187.

Bresee, J.C.(ed.), 1992. Geothermal energy in Europe. The Soultz Hot Dry Rock project. Gordon and Brach Science Publishers, Philadelphia, USA, 308 pp.

Darot, M., Gueguen, Y. and Baratin, M.-L., 1992. Permeability of thermally cracked granite. Geophysical Research Letters, 19(9): 869-872.

Davies, C.W., 1962. Ion Association. Butterworths, London.

Dietrich, H.G., 1982. Geological Results from the Urach 3 Borehole and the correlation with Other Boreholes. In: R. Haenel (Editor), The Urach Geothermal Project (Swabian Alb. Germany). E. Schweitzerbart'sche Verlagsbuchhandlung (Naegele und Obermiller), Stuttgart, pp. 49-58.

Dove, P.M., 1994. The dissolution kinetics of quartz in sodium chloride solutions at 25 to 300 °C. American Journal of Science, 294(6): 665-712.

Duan, Z., Moller, N., DeRocher, T. and Weare, J.H., 1996. Prediction of boiling, scaling and formation conditions in geothermal reservoirs using computer programs TEQUIL and GEOFLUIDS. Geothermics, 25(6): 663-678.

Durst, P. and Vuataz, F.-D., 2000. Fluid-rock interactions in hot dry rock reservoirs. A review of HDR sites and detailed investigations of the Soultz-sous-Forêts system. World Geothermal Congress 2000, Kyushu-Tohoku, Japan, pp. 3677-3682.

Durst, P., 2000. Review of the papers on geochemistry at the World Geothermal Congress 2000 in Japan. CHYN, Neuchatel, Switzerland, unpubl. report.

Durst, P. and Vuataz, F.-D., 2001a. Geochemical modelling of the Soultz-sous-Forêts Hor Dry Rock system. Brine-rock interactions in a deep hot fractured granite reservoir. 26th Workshop on Geothermal Reservoir Engineering, Stanford Univ., Stanford, USA, pp. 11-20.

Durst, P. and Vuataz, F.-D., 2001b. Fluid-rock interactions and geochemical modelling of the formation brine in the fissured reservoir of the Soultz-sous-Forêts Hor Dry Rock test site. Federal Office for Education and Science, final report, project 98.0008-3, CHYN, Neuchatel, Switzerland, 149p.

Gautelier, M., Oelkers, E.H. and Schott, J., 1999. An experimental study of dolomite dissolution rates as a function of pH from -0.5 to 5 and temperature from 25 to 80 °C. Chemical Geology, 157(1-2): 13-26.

Genter, A., 1990. Géothermie roche chaudes sèches. Le granite de Soultz-sous-Forêts (Bas-Rhin, France). Fracturation naturelle, altérations hydrothermales et interaction eau-roche. Document du BRGM N° 185, Ed. BRGM, Orléan, France, 201p.

Genter, A., Dezayes, C., Gentier, S., Ledésert, B. and Sausse, J., 1998. Conceptual fracture model at Soultz based on geological data. 4th HDR Forum, Strasbourg, France.

Genter, A. and Traineau, H., 1996. Analysis of macroscopic fractures in the HDR geothermal well EPS-1, Soultz-sous-Forêt, France. J. of Volc. and Geoth. Res., 72: 121-141

Gérard, A., Baumgärtner, J. and Baria, R., 1997. An attempt towards a conceptual model derived from 1993-1996 hydraulic operations at Soultz. NEDO Int. Geothermal Symp., Sendai, Japan, pp. 329-341.

Gérard, A., Baria, R. and Baumgärtner, J., 1999. Soultz-sous-Forêts: main targets and preliminary scientific results of deepening of the well GPK2. European Geothermal Conf. Basel'99, Basel, Switzerland, pp. 119-130.

Greenberg, J.P. and Moller, N., 1989. The prediction of mineral solubilities in natural waters; a chemical equilibrium model for the Na-K-Ca-Cl-SO_4-H_2O system to high concentration from 0 to 250 °C. Geochimica et Cosmochimica Acta, 53(10): 2503-2518.

Harvie, C.E., Moller, N.E. and Weare, J.H., 1984. The prediction in mineral solubilities in natural waters; the Na-K-Mg-Ca-H-Cl-SO_4-OH-HCO_3-CO_3-CO_2-H_2O system to high ionic strengths at 25 °C. Geochimica et Cosmochimica Acta, 48(4): 723-751.

Helgeson, H.C., 1969. Thermodynamics of hydrothermal systems at elevated temperatures and pressures. American Journal of Science, 267(7): 729-804.

Helgeson, H.C., Garrels, R.M. and Mackenzie, F.T., 1969. Evaluation of irreversible reactions in geochemical processes involving minerals and aqueous solutions; II, Applications. Geochimica et Cosmochimica Acta, 33(4): 455-481.

Helgeson, H.C., Kirkham, D.H. and Flowers, G.C., 1981. Theoretical prediction of the thermodynamic behavior of aqueous electrolytes by high pressures and temperatures; IV, Calculation of activity coefficients, osmotic coefficients, and apparent molal and standard and relative partial molal properties to 600 °C and 5kb. American Journal of Science, 281(10): 1249-1516.

Jacquot, E., 1998. Description of the geothermal HDR site of Soultz-sous-Forêts (Bas-Rhin, France) based on data collected during previous stimulation and circulation experiments for a modelling purpose. Proceed. 4th Int. HDR Forum, Strasbourg, Sept. 1998.

Jacquot, E., 2000. Modélisation thermodynamique et cinétique des réactions géochimiques entre fluides de bassin et socle cristallin. Application au site expérimental du programme européen de recherche en géothermie profonde (Soultz-sous-Forêts, Bas Rhin, France). Ph.D. Thesis, Univ. Louis Pasteur, Strasbourg, 202 pp.

Johnson, J., W., Oelkers, E., H., Helgeson, H., C., 1992. SUPCRT92; a software package for calculating the standard molal thermodynamic properties of minerals, gases, aqueous species, and reactions from 1 to 5000 bar and 0 to 1000 degrees C. Computers and Geosciences. 18(7), pp 899-947.

Kiho, K. and Mambo, V., 1995. Reservoir Characterisation by Geochemical Method at the Ogachi HDR Site, Japan. World Geothermal Congress 1995, Florence, Italy, pp. 2707-2711.

Kohl, T. and Hopkirk, R., J., 1995. "FRACTURE" – A simulation code for forced fluid flow and transport in fractured, porous rock. Geothermics, 24(3): 333-343.

Kohl, T., Baechler, D. and Rybach, L., 2000. Steps towards a comprehensive thermo-hydraulic analysis of the HDR test site Soultz-sous-Forêts. World Geothermal Congress 2000, Kyushu-Tohoku, Japan, pp. 2671-2676.

Komninou, A. and Yardley, B.W.D., 1997. Fluid-rock interactions in the Rhine Graben: A thermodynamic model of the hydrothermal alterationobserved in deep drilling. Geochimica et Cosmochimica Acta, 61(3): 515-531

Lasaga, A.C., 1981. Transition state theory. In: Kinetics of geochemical processes. Lasaga, A. C. and Kirkpatrick, R. J. editors. Reviews in Mineralogy, 8: 135-168.

Ledésert, B., 1993. Fracturation et paléocirculation hydrothermales. Application au granite de Soultz-sous-Forêts. Ph.D. Thesis, Univ. of Poitiers, Poitiers.

Matsunaga, I., Miyazaki, A. and Tao, H., 1995. Water-Rock Interactions During a Three Month Circulation Test at the Hot Dry Rock Test Site in Hijori, Japan. World Geothermal Congress 1995, Florence, Italy, pp. 2679-2683.

Moller, N., 1988. The prediction of mineral solubilities in natural waters; a chemical equilibrium model for the Na-Ca-Cl-SO_4-H_2O system, to high temperature and concentration. Geochimica et Cosmochimica Acta, 52(4): 821-837.

Moller, N., Greenberg, J.P. and Weare, J.H., 1998. Computer modeling for geothermal systems; predicting carbonate and silica scale formation, CO_2 breakout and H_2S exchange. Geothermal energy. Transport in Porous Media, 33(1-2): 173-204.

Norton, D. and Knapp, R., 1977. Transport phenomena in hydrothermal systems; the nature of porosity. American Journal of Science, 277(8): 913-936.

Pape, H., Clauser, C. and Iffland, J., 1999. Permeability prediction based on fractal pore-space geometry. Geophysics, 64(5): 1447-1460.

Parkhurst, D.L.R.-p., 1995. User's guide to PHREEQC--A computer program for speciation, reaction-path, advective-transport, and inverse geochemical calculations. 95-4227, U.S. Geological Survey, Water-Resources Investigations.

Pauwels, H., Fouillac, C. and Fouillac, A.-M., 1993. Chemistry and isotopes of deep geothermal saline fluids in the Upper Rhine Graben; origin of compounds and water-rock interactions. Geochimica et Cosmochimica Acta, 57(12): 2737-2749.

Pitzer, K.S., 1973. Thermodynamics of electrolytes. I. Theorethical basis and general equations. Journal of Physical Chemistry, 12: 268-277.

Pitzer, K.S., 1975. Thermodynamics of electrolytes. V. Effects of higher-order electrostatic terms. Journal of Solution Chemistry, 4: 249-265.

Pribnow, D. and Clauser, C., 2000. Heat and fluid flow at the Soutz Hot Dry Rock system in the Rhine graben. World Geothermal Congress 2000, Kyushu-Tohoku, Japan, pp. 3885-3840.

Pruess, K., 1991. TOUGH2 - A general-Purpose Numericla Simulator for Multiphase Fluid and Heat Flow. LBL-29400, Lawrence Berkeley Laboratory, Berkeley.

Richards, H.G., Savage, D. and Andrews, J.N., 1992. Granite-water reactions in an experimental hot dry rock geothermal reservoir, Rosemanowes test site, Cornwall, U.K. Applied Geochemistry, 7(3): 193-222.

Rickard, D., 1997. Kinetics of pyrite formation by the H_2S oxidation of iron (II) monosulfide in aqueous solutions between 25 and 125 °C; the rate equation. Geochimica et Cosmochimica Acta, 61(1): 115-134.

Rickard, D. and Luther, G.W., 1997. Kinetics of pyrite formation by the H_2S oxidation of iron (II) monosulfide in aqueous solutions between 25 and 125 °C; the mechanism. Geochimica et Cosmochimica Acta, 61(1): 135-147.

Rimstidt, J.D. and Barnes, H.L., 1980. The kinetics of silica-water reactions. Geochimica et Cosmochimica Acta, 44(11): 1683-1700.

Schellschmidt, R. and Pribnow, D., 2001. GGA Temperature Logs from the HDR Site in Soultz-sous-Forêts. In: Baria, R., Baumgärtner, J,. Gérard, A., Weidler, R. and Hopkirk R. (Editors). European Hot Dry Rock Geothermal Research Programme 1998-2001. European Commission Final Report, contract no. JOR3-CT98-0313, Annex 7, 15p.

Schoonen, M.A.A. and Barnes, H.L., 1991. Reactions forming pyrite and marcasite from solution; I, Nucleation of FeS_2 below 100 °C. Geochimica et Cosmochimica Acta, 55(6): 1495-1504.

Schoonen, M.A.A. and Barnes, H.L., 1991. Reactions forming pyrite and marcasite from solution; II, Via FeS precursors below 100 °C. Geochimica et Cosmochimica Acta, 55(6): 1505-1514.

Schoonen, M.A.A. and Barnes, H.L., 1991. Mechanisms of pyrite and marcasite formation from solution; III, Hydrothermal processes. Geochimica et Cosmochimica Acta, 55(12): 3491-3504.

Shiraki, R. and Brantley, S.L., 1995. Kinetics of near-equilibrium calcite precipitation at 100 degrees C; an evaluation of elementary reaction-based and affinity-based rate laws. Geochimica et Cosmochimica Acta, 59(8): 1457-1471.

Sjoeberg, E.L. and Rickard, D.T., 1984. Temperature dependence of calcite dissolution kinetics between 1 and 62 °C at pH 2.7 to 8.4 in aqueous solutions. Geochimica et Cosmochimica Acta, 48(3): 485-493.

Steefel, C.I. and Lasaga, A.C., 1994. A coupled model for transport of multiple chemical species and kinetic precipitation/dissolution reactions with application to reactive flow in single phase hydrothermal systems. American Journal of Science, 294(5): 529-592.

Steefel, C.I., MacQuarrie, K.T.B., 1996. Approaches to modeling of reactive transport in porous media. In: Lichtner, P.C., Steefel, C.I., Oelkers, E.H. (EDS.), Reactive transport in porous media. Reviews in Mineralogy. 34, pp. 83-129.

Stenger, R., 1982. Petrology and Geochemistry of the Basement Rocks of the Research Drilling Project Urach 3. In: R. Haenel (Editor), The Urach Geothermal Project (Swabian Alb. Germany). E. Schweitzerbart'sche Verlagsbuchhandlung (Naegele und Obermiller), Stuttgart, pp. 41-48.

Traineau, H., Genter, A., Cautru, J.P., Fabriol, H. and Chevremont, P., 1991. Petrography of the granite massif from drill cutting analysis and well log interpretation in the geothermal HDR borehole GPK1 (Soultz, Alsace, France). Geothermal Science and Technology, 3(1-4): 1-29.

Vuataz, F.-D. and Kohl, T., 2000. World Geothermal Congress 2000 and the status of geothermal energy. Bulletin Géothermie-CH, 28: 2-8.

Vuataz, F.-D., 2001. Review of the papers on HDR and Enhanced Geothermal System presented at the World Geothermal Congress 2000 in Japan. CHYN, Neuchatel, Switzerland, unpubl. report.

White, S.P., 1995. Multiphase nonisothermal transport of systems of reacting chemicals. Water resources research, 31(7): 1761-1772.

Williamson, M.A. and Rimstidt, J.D., 1994. The kinetics and electrochemical rate-determining step of aqueous pyrite oxidation. Geochimica et Cosmochimica Acta, 58(24): 5443-5454.

Winchester, W.W., 1993. Hot Dry Rock Energy. Progress Report. Fiscal year 1992. LA-UR-93-1678, Los Alamos Nat. Lab.

Wolery, T., J., 1992. EQ3NR, A Computer Program for Geochemical Aqueous Speciation Solubility Calculations: Theorethical Manual User's Guide, and Related Documentation (Version 7.0). Lawrence Livermore Nat. Lab. report, UCRL-MA-110662 PT III. 246 pp.

Zhang, Y. and Dawe, R.A., 2000. Influence of Mg^{++} on the kinetics of calcite precipitation and calcite crystal morphology. Chemical Geology, 163(1-4): 129-138.

Annexes

List of symbols

A	Arrhenius preexponential factor
A(T)	empirical coefficient dependent on the temperature
a_i	activity of the species i
a^0	solute hard-core diameter dependent on temperature and pressure
a_i^0	empirical parameter related to the ionic radius of the specie i
A_i	the surface area of a mineral i
A_{F0}	the initial fracture surface area
$A_{F0,i}$	the initial fracture surface area of a mineral i
$A_{F,,i}$	the fracture surface area of a mineral i
$A_{G,,i}$	the grain surface area of a mineral i
B(T)	empirical coefficient dependent on the temperature
$\dot{B}(T)$	empirical coefficient dependent on the temperature
B_{ij}^{ϕ}	parameter dependent on ionic strength and temperature
Ct_i	total concentration of element i ($mol.kg^{-1}$)
C_{ij}	are interaction parameters dependent on ionic strength and temperature
E_a	activation energy in $J.mol^{-1}$
El	number of chemical elements in the system
$f(a^*_i)$	function of the activity of the species involved in the creation and the destruction of the activated complex
from	number of the origin volume element
$\nabla.F_{in}$	variation of Qt_{in} due to transport
G	Gibbs free energy (J)
ΔG	variation of free energy ($J.mol^{-1}$)
ΔG^0	standard free energy variation associated to the reaction ($J.mol^{-1}$)
ΔG_k	variation of free energy for the reaction k ($J.mol^{-1}$)
I	ionic strength
K	equilibrium constant of the reaction (dimensionless)
K_k	equilibrium constant of the reaction k (dimensionless)
k	permeability in m^2
k_c	kinetic constant of the reaction in $mol.m^{-2}.s^{-1}$
k_{c0}	an constant independent of the conditions in $mol.m^{-2}.s^{-1}$
k_F	fracture permeability in m^2
k_G	grain permeability in m^2
m_i	molality of component i in the system ($mol.kg^{-1}$)

m_{ik}	molality of component i from reaction k in the system (mol.kg^{-1})
N	number of components of the system
n_f	fracture frequency in m^{-1}
o	empirical exponential factor
p	empirical exponential factor
p_i	product i
Pr	total number of products in the reaction
Q	ionic activity product (dimensionless)
Q_k	ionic activity product of the reaction k (dimensionless)
q_i	quantity of component i in the system (mol)
qr_{in}	variation of Qt_{in} due to the reactions in the volume element
Qt_{in}	quantity of component i (water, steam, gas or heat) in the volume element n
R	ideal gas constant (8.31451 J.mol^{-1}.K^{-1})
r_i	reactant i
R_o^I	initial radius of closed pack spherical grains
$R_{o,i}^I$	initial radius of closed pack spherical grains for the mineral i
Re	total number of reactants in the reaction
s	reaction surface area in m^2
S.I.	saturation index
T	temperature in °K
t	time
Δt	time interval
to	number of the destination volume element
v	reaction rate in mol.s^{-1}
v_c	constant dissolution rate far from equilibrium in mol.m^{-2}.s^{-1}
V_i	volume of the mineral i
V_j^{adv}	fluid volume coming from the jth advective flow, from element 'from' to element 'to'
V_{to}^{el}	fluid volume of the destination element.
V_{tot}	total volume of rock
α_{Gi}	proportion of the amount of mineral i found in the altered granite facies and in the vein facies
δ	fracture aperture in m.
δ_0	initial fracture aperture in m
ζ_{ijk}	interaction parameters dependent on temperature
Φ	porosity (dimensionless)
Φ_F	fracture porosity (dimensionless)
Φ_{Fo}	initial fracture porosity.

Φ_G grain porosity (dimensionless)

Φ_{ij}^{ϕ} interaction parameters dependent on ionic strength and temperature

γ_i activity coefficient of component i

γ_{ik} activity coefficient of component i from reaction k

Ψ_{ijk} parameters dependent on ionic strength and temperature

κ_i the ratio between the fracture permeability and the grain permeability for the mineral i

λ_{ij} interaction parameters dependent on ionic strength and temperature

$\theta_{>SiOH}$ fraction of the total surface sites occupied by hydrogen ion as >SiOH

$\theta_{>SiO^-_{tot}}$ sum of the fractions of the total sites existing as deprotonated >SiO^- site and as a complex with sodium ion as >SiO-Na^+

σ empirical parameter defining the shape of the Gaussian distribution

τ_{ij} quantity of element i contained in species j (mol)

μ_i chemical potential of component i ($J.mol^{-1}$)

μ_{ijk} interaction parameters dependent on temperature

ν_i stoechiometric coefficients of components i

ν_{ji} stoechiometric coefficients of components i from reaction k

Ω number of mole of water in 1 kg of fluid (≈55.5)

FRACHEM user's manual

Introduction

FRACHEM is a code actually in development. Consequently, this manual presents the FRACHEM input files as they are at the end of June, 2002. The input format is susceptible to modification according to improvements that will be made in the code.

Overview of the input files

Three input files are required for running FRACHEM: 'Input.dat', 'CHEM_INPUT.dat' and 'chem.dat'.

'Input.dat' is the FRACTure input file. It can be generated by the programme Winfra developed in ETH-Z. The only difference with the standard FRACTure input is that the 'ilinh' parameter have to be set to 3 in order to indicate the coupling with the geochemical module.

'CHEM_INPUT.dat' is a file generated by Winfra that contains the geometrical information used for calculating the flow trough the surface separating to elements.

'chem.dat' contains all the information for the geochemical module. The structure of this file is detailed in the next section.

The 'CHEM.dat' file

The 'chem.dat' file must have the following structure. The parameter are underlined and are followed by their format in italic. *int* is an integer, *dbl* is a double precision real number, *character* is one character and *string* is a string of up to ten characters.

Structure of 'chem.dat'

CHEM

chem_tol *dbl* output_step *int* feedback *logical*

NoReactions *dbl* NoSpecies *dbl* NoGasReactions *dbl*

i = 1 to NoSpecies

    Species(i) *string* Charge(i) *dbl* Phase(i) *character* conc(i) *dbl* MW(i) *dbl* volmas(i) *dbl*

    Gammacoeff(j,i) for j=0 to 4

i = 1 to NoReactions

    Reaction(i) *string*

    ExtendedMatrix(j,i) *dbl* for j = 1 to NoPrimary type(i) *int*

    KCoeff(j,i) for j = 1 to 5

    If type(i) equal 5, RateData(j,i) *dbl* for j = 1 to 5

INJ

ninj *int*

i= 1 to ninj

    inj(i) *dbl* inj_rate(i) *dbl*

PROD

nprod *int*

i= 1 to nprod

prod(i) *dbl* prod_rate(i) *dbl*

SURF

volume *dbl* temperature *dbl* pressure *dbl*

DISS (optionnal)

while ENDFI

n *int*

concentration(i) *dbl* for i=1 to NoSpecies-1

ENDFI

Description of the parameters

chem_tol: maximum relative variation allowed for a chemical species.

output_step: number of chemical steps between the generation of a chemical output.

feedback: if feedback is true, the variation in porosity and permeability calculated in the geochemical module are passed to FRACTure. If not, FRACTure will not take into account these variation, allowing faster simulation if you are only interested in the evolution of the geochemisrty.

NoReactions: number of reactions.

NoSpecies: number of species

NoGasReactions: number of gas reaction. This feature is not yet operational in FRACHEM.

Species(i): name of the species

Charge(i): electrical charge of the species.

Phase(i): phase of the species L for liquid, S for solid, G for gas.

conc(i): concentration in mol/kg

MW(i): molecular weight in g/mol

volmas(i): for solids only, volume massic of the solid in kg/m^3.

Gammacoeff(j,i): coefficients for the calculation of activity coefficients for aqueous species in the form $gamma=B_{0i}+B_{1i}T+B_{2i}T^2+B_{3i}T^3+B_{4i}T^4$

Reaction(i): name of the reaction

ExtendedMatrix(j,i): stoechiometric coefficients of the basic species in the reaction

type(i): type of the reaction. 1 for aqueous species, 4 for solid species at thermodynamic equilibrium, 5 for kinetic reaction.

KCoeff(j,i): coefficient for the calculation of the logK.

$logK=A_{0i}+A_{1i}T+A_{2i}T^2+A_{3i}T^3+A_{4i}T^4$

RateData(j,i): with five parameters for non equilibrium reactions a added line is provided. The first is the reaction surface area, which will be recalculated by the code. The 2nd is the proportion of mineral in grain type porous space. The 3rd is the ratio between grain permeability and fracture permeability.

The 4th indicates which subroutine should be used (actually, 1 for quartz, 2 for calcite, 3 for dolomite and 4 for pyrite). The 5th is not used in the present version.

ninj: number of element in which the fluid is injected.

inj(i): number of the injection element.

inj_rate(i): injection rate in m^3/s. If inj_rate(i) is negative, FRACHEM will calculate the amount of fluid injected from the advective flow values.

nprod: number of element in which the fluid is produced.

prod(i): number of the production element.

prod_rate(i): production rate in m^3/s. If prod_rate(i) is negative, FRACHEM will calculate the amount of fluid produced from the advective flow values.

volume: volume of the surface element.

temperature: temperature in the surface element.

pressure: pressure in the surface element.

n: number of the element in which the concentration have to be modified

concentration(i): concentration of the species in the exception of H_2O in the element n. The species should be in the same order as they where declared previously

Example of an input file 'chem_dat'

This file was used for the single fracture simulation described in paragraph 7.1

```
CHEM
10.0 1 .T.
 10 22  0
H2O          0.00 L  5.55000E+01  1.80000E+01  0.00000E+00
  0.955608E+00 -0.268621E-04  0.389146E-06 -0.125171E-08  0.257202E-11
Na+          1.00 L  .993         23.0000E+00  0.00000E+00
  0.180993E+01 -0.411519E-01  0.544797E-03 -0.298645E-05  0.568416E-08
K+           1.00 L  80.8E-3      39.0000E+00  0.00000E+00
  0.148302E+01 -0.316001E-01  0.419182E-03 -0.229938E-05  0.437243E-08
Ca++         2.00 L  .160         40.0000E+00  0.00000E+00
  0.137038E+01 -0.424256E-01  0.543639E-03 -0.292164E-05  0.552984E-08
H+           1.00 L  2.05E-5      1.00000E+00  0.00000E+00
  0.294133E+01 -0.744534E-01  0.949630E-03 -0.508025E-05  0.956790E-08
Cl-         -1.00 L  1.460       35.45000E+00  0.00000E+00
  0.171669E+01 -0.449296E-01  0.574913E-03 -0.308265E-05  0.581276E-08
HCO3-       -1.00 L  2.020E-3     61.0000E+00  0.00000E+00
  0.149635E+01 -0.444200E-01  0.571479E-03 -0.308008E-05  0.583848E-08
SO4--       -2.00 L  1.47E-3      96.0000E+00  0.00000E+00
  0.313601E+00 -0.104143E-01  0.131810E-03 -0.703870E-06  0.133359E-08

H4SiO4       0.00 L  2.17E-3      96.0000E+00  0.00000E+00
```

```
  0.193092E+01 -0.268539E-01  0.337269E-03 -0.178498E-05  0.334362E-08
FE++          2.00 L  .501E-3       55.8500E+00  0.00000E+00
  0.343449E+00 -0.201020E-02  0.448980E-05  0.000000E+00  0.000000E+00
MG++          2.00 L  5.42E-3       24.3000E+00  0.00000E+00
  0.396939E+00 -0.314796E-02  0.108163E-04  0.000000E+00  0.000000E+00
HS-          -1.00 L  .72E-3        33.0000E+00  0.00000E+00
  0.210969E-03 -0.507186E-05  0.877067E-07 -0.609429E-09  0.136579E-11
CO3--        -2.00 L  0.00000E-05  60.0000E+00  0.00000E+00
  0.205858E+00 -0.681574E-02  0.854205E-04 -0.452599E-06  0.852881E-09
OH-          -1.00 L  0.00000E-05  17.0000E+00  0.00000E+00
  0.163025E+01 -0.481896E-01  0.619779E-03 -0.333916E-05  0.632716E-08
Ca(HCO3)+     1.00 L  0.00000E-16  101.000E+00  0.00000E+00
  0.137701E+01 -0.345803E-01  0.446597E-03 -0.240895E-05  0.455247E-08
CO2(aq)       0.00 L  38.1E-3       44.0000E+00  0.00000E+00
  0.167784E+01 -0.131991E-01  0.170756E-03 -0.931070E-06  0.180041E-08
CaCO3(aq)     0.00 L  0.00000E-04  100.000E+00  0.00000E+00
  0.100000E+01  0.000000E+00  0.000000E+00  0.000000E+00  0.000000E+00
CASO4(AQ)     0.00 L  0.00000E-02  136.000E+00  0.00000E+00
  0.100000E+01  0.000000E+00  0.000000E+00  0.000000E+00  0.000000E+00
QUARTZ        0.00 S  167.0E+00     60.0000E+00  2.65000E+03
  0.100000E+01  0.000000E+00  0.000000E+00  0.000000E+00  0.000000E+00
CALCITE       0.00 S  12.1E+00     100.0000E+00  2.71000E+03
  0.100000E+01  0.000000E+00  0.000000E+00  0.000000E+00  0.000000E+00
DOLOMITE      0.00 S   1.63E+00   184.3000E+00  2.71000E+03
  0.100000E+01  0.000000E+00  0.000000E+00  0.000000E+00  0.000000E+00
PYRITE        0.00 S  .83E+00      119.8500E+00  5.00000E+03
  0.100000E+01  0.000000E+00  0.000000E+00  0.000000E+00  0.000000E+00
CO3--
 0.00 0.00 0.00 0.00  -1.00 0.00 1.00 0.00 0.00 0.00 0.00 0.00 1
  0.106210E+02 -0.141799E-01  0.119948E-03 -0.377598E-06  0.563170E-09
OH-
 1.00 0.00 0.00 0.00  -1.00 0.00 0.00 0.00 0.00 0.00 0.00 0.00 1
  0.149397E+02 -0.427928E-01  0.221928E-03 -0.752711E-06  0.129450E-08
Ca(HCO3)+
 0.00 0.00 0.00 1.00 0.00 0.00 1.00 0.00 0.00 0.00 0.00 0.00 1
 -0.109172E+01  0.377718E-02 -0.100084E-03  0.355916E-06 -0.566154E-09
CO2(aq)
  -1.00 0.00 0.00 0.00 1.00 0.00 1.00 0.00 0.00 0.00 0.00 0.00 1
 -0.657655E+01  0.122524E-01 -0.143343E-03  0.466424E-06 -0.666853E-09
CaCO3(aq)
 0.00 0.00 0.00 1.00  -1.00 0.00 1.00 0.00 0.00 0.00 0.00 0.00 1
  0.750075E+01 -0.218770E-01  0.865748E-04 -0.237638E-06  0.206620E-09
```

```
CASO4(AQ)
 0.00 0.00 0.00 1.00 0.00 0.00 0.00 1.00 0.00 0.00 0.00 0.00 1
 -0.207040E+01 -0.255960E-03 -0.654052E-04  0.314719E-06 -0.770838E-09
QUARTZ
  -2.00 0.00 0.00 0.00 0.00 0.00 0.00 0.00 1.00 0.00 0.00 0.00 5
 -0.450127E+01  0.230740E-01 -0.136254E-03  0.554763E-06 -0.955384E-09
0 .1 .1 1 0
CALCITE
 0.00 0.00 0.00 1.00  -1.00 0.00 1.00 0.00 0.00 0.00 0.00 0.00 5
  0.222690E+01 -0.154277E-01  0.866480E-05  0.164848E-07 -0.126807E-09
0 .1 .1 2 0
DOLOMITE
 0.00 0.00 0.00 1.00  -2.00 0.00 2.00 0.00 0.00 0.00 1.00 0.00 5
  0.340778E+01 -0.370318E-01  0.430942E-04 -0.191080E-07 -0.215571E-09
0 .1 .1 3 0
PYRITE
  -1.00 0.00 0.00 0.00 0.25 0.00 0.00 0.25 0.00 1.00 0.00 1.75 5
 -0.265025E+02  0.836345E-01 -0.427566E-03  0.142557E-05 -0.247958E-08
0 .1 .1 4 0
INJ
1
12 -1
PROD
1
13 -1
SURF
400.0  65.0d0  40.0e6
ENDFI
```

Output files

Different output files are generated by FRACHEM.

The first four types came from FRACture:

- 'output.dat' contains informations about the of the simulation.
- 'adv??.dat' files contain informations about the advective flows.
- 'dis??.dat' files contain informations about the pressure and temperature at the nodes.
- 'hfl??.dat' files contain informations about the heat flows and the thermal gradient in the elements. These files also contains the coordinates of the centres of the elements that can not be found elsewhere.
- 'result.dat' contains information about the advective flows during the last time step.

The last file contains the chemical ouptut:

- 'chem_outpout.dat' have the following format for each timestep

  time in second, time in day, number of chemical iterations, number of transport iterations

  and for each volume element:

  Element number, temperature (°C), pressure (pa), porosity, permeability (m^2), pH, Ca concentration in mol/kg, Mg concentration in mol/kg, quartz reaction rate ($mol/m^3/s$), calcite reaction rate ($mol/m^3/s$), dolomite reaction rate ($mol/m^3/s$), pyrite reaction rate ($mol/m^3/s$)

At the present state, all modification of the 'chem_output format have to be done in the code in the 'Chem_output' subroutine.

Thermodynamic data

The equilibrium constants used in this study come from the database compiled by Johnson et al. (1992) for the software SUPCRT92.

Reactions	**Coefficients of the equation** $\log K = A_0 + A_1 T + A_2 T^2 + A_3 T^3 + A_4 T^4$				
	A_0	A_1	A_2	A_3	A_4
$CO_3^{--} + H^+ \rightarrow HCO_3^-$	$0.106 \cdot 10^{+2}$	$-0.142 \cdot 10^{-1}$	$0.120 \cdot 10^{-3}$	$-0.378 \cdot 10^{-6}$	$0.563 \cdot 10^{-9}$
$OH^- + H^+ \rightarrow H_2O$	$0.149 \cdot 10^{+2}$	$-0.428 \cdot 10^{-1}$	$0.222 \cdot 10^{-3}$	$-0.753 \cdot 10^{-6}$	$0.129 \cdot 10^{-8}$
$CaHCO_3^+ \rightarrow Ca^{++} + HCO_3^-$	$-0.109 \cdot 10^{+1}$	$0.378 \cdot 10^{-2}$	$-0.100 \cdot 10^{-3}$	$0.356 \cdot 10^{-6}$	$-0.566 \cdot 10^{-9}$
$CO_{2(aq)} + H_2O \rightarrow H^+ + HCO_3^-$	$-0.658 \cdot 10^{+1}$	$0.123 \cdot 10^{-1}$	$-0.143 \cdot 10^{-3}$	$0.466 \cdot 10^{-6}$	$-0.667 \cdot 10^{-9}$
$CaCO_{3(aq)} + H^+ \rightarrow Ca^{++} + HCO_3^-$	$0.750 \cdot 10^{+1}$	$-0.219 \cdot 10^{-1}$	$0.866 \cdot 10^{-4}$	$-0.238 \cdot 10^{-6}$	$0.207 \cdot 10^{-9}$
$CaSO_{4(aq)} \rightarrow Ca^{++} + SO_4^{--}$	$-0.207 \cdot 10^{+1}$	$-0.256 \cdot 10^{-3}$	$-0.654 \cdot 10^{-4}$	$0.315 \cdot 10^{-6}$	$-0.771 \cdot 10^{-9}$
$Quartz + 2H_2O \rightarrow H_4SiO_4$	$-0.450 \cdot 10^{+1}$	$0.231 \cdot 10^{-1}$	$-0.136 \cdot 10^{-3}$	$0.555 \cdot 10^{-6}$	$-0.955 \cdot 10^{-9}$
$Calcite + H^+ \rightarrow Ca^{++} + HCO_3^-$	$0.222 \cdot 10^{+1}$	$-0.154 \cdot 10^{-1}$	$0.866 \cdot 10^{-5}$	$0.165 \cdot 10^{-7}$	$-0.127 \cdot 10^{-9}$
$Dolomite + 2H^+ \rightarrow Ca^{++} + Mg^{++} + 2HCO_3^-$	$0.340 \cdot 10^{+1}$	$-0.370 \cdot 10^{-1}$	$0.431 \cdot 10^{-4}$	$-0.191 \cdot 10^{-7}$	$-0.216 \cdot 10^{-9}$
$Pyrite + H_2O \rightarrow Fe^{++} + .25H^+ + .25SO_4^{--} + 1.75HS^-$	$-0.265 \cdot 10^{+2}$	$0.836 \cdot 10^{-1}$	$-0.428 \cdot 10^{-3}$	$0.143 \cdot 10^{-5}$	$-0.248 \cdot 10^{-8}$